EAGLE 2006

EAGLE Netherlands Multi-purpose, Multi-Angle and Multi-sensor In-situ, Airborne and Space Borne Campaigns over Grassland and Forest

Final Report

(Edited by W. Timmermans, R. Dost, Z. Su)

January 2008

Table of Content

1 Introduction

1.1 Campaign overview

The understanding of bio-geophysical parameter retrieval from multi-parameter optical and SAR data as well as the direct modelling of the underlying physical processes in forests and grassland remain challenging due to lack of appropriate observation data. In EAGLE2006 an intensive filed campaign is carried out using different airborne sensors - an optical imaging sensor, an imaging microwave radiometer, and a flux airplane - for data acquisition and to collect extensive ground measurements simultaneously over one grassland (Cabauw) and two forest sites (Loobos & Speulderbos), in addition to acquisition of multi-angle and multi-sensor satellite data. As such the dataset is both unique and urgently needed for the development and validation of models and inversion algorithms for quantitative surface parameter estimation and process studies.

The understanding and quantification of bio-geophysical parameters of different vegetated surfaces are essential in the development of validated, global, interactive Earth system models for the prediction of global change accurately enough to assist policy makers in making sound decisions concerning the planning, sustainable use and management as well as conservation of water resources and environment. Multi-sensor remote sensing monitoring (using radar & optical data) are essential for the development and validation of models and retrieval algorithms for the above stated purposes.

The EAGLE2006 activities are performed over central parts of the Netherlands (the grassland site at Cabauw and two forest sites at Loobos & Speulderbos; with yearly precipitation around 750 mm and yearly average temperature about 10° Celsius) from the 8th until the 18th of June 2006. EAGLE2006 originated from the combination of a number of initiatives coming under different funding. As such, the objectives of the EAGLE2006 campaign were closely related to the objectives of other ESA Campaigns (SPARC04, Sen2Flex2005 and especially AGRISAR2006).

One important objective of the campaign is to build up a data base for the investigation and validation of the retrieval of bio-geophysical parameters, obtained at different radar frequencies (X-, C- and L-Band) and at hyperspectral optical and thermal bands acquired over vegetated fields (forest and grassland). All activities were related to algorithm development for future satellite missions such as Sentinels and for validations of products of CHRIS, MODIS and MERIS data, with activities also related to validation of AATSR and ASTER thermal data, as well as the retrievals of soil moisture and biomass from active microwave sensors (ASAR) on board ESA’s Envisat platform and those on EPS/MetOp and SMOS. Most of the activities in the campaign are highly relevant to the EU FP6 GMES EAGLE project, especially issues related to retrieval of biophysical parameters from CHRIS and MERIS as well as AATSR and ASTER, and scaling issues and complementary characteristics between these sensors (covering only local sites) and global sensors such as MERIS/SEVIRI, EPS/MetOP and SMOS are also key elements.

1.2 Campaign objectives

The general purposes of the EAGLE2006 campaign are:

1. Acquisition of simultaneous multi-angular and multi-sensor (from visible to microwave domain) data over a grassland and a forest.
2. Advancement of process understanding in description of radiative and turbulent processes in land-atmosphere interactions.

3. Validation of primary bio-geophysical parameters derived from satellite data using in-situ and airborne data.
4. Improvement of soil moisture retrieval accuracy by synergy of multi-angular (L-band) SMOS and multi-angular C-band SAR/Optical-thermal observations.
5. Development of operational algorithms to extract land surface parameters and heat fluxes from the future EPS/MetOp mission.
6. Development of physically based drought monitoring and prediction method (Hydro-climatologic modeling) on the basis of EPS/MetOp observations.

In particular, the EAGLE2006 campaign addressed important specific programmatic needs of Sentinel-1 and -2:

1. To assess the impact of Sentinel-1 and Sentinel-2 sensor and mission characteristics for land applications (land use mapping, parameter retrieval) over forest and grassland.
2. To provide a basis for the quantitative assessment of sensor or mission trade-off studies, e.g. spatial and radiometric resolution.
3. Simulate Sentinel-1 and Sentinel-2 image products over the land (forest and grassland).

In the context of Sentinel-1, EAGLE2006 aimed primarily at the investigation of radar signatures over forest and grassland simultaneously which is currently not addressed. An important dataset of coordinated in-situ and airborne SAR measurements is collected which provides support both to studies of the Sentinel-1 technical concept, as well as contributing to studies of future mission concepts involving parameter retrieval at L-band.

As part of the refinement and verification of the Sentinel-1 technical concept, EAGLE2006 data will be used for the assessment of land use classification using the proposed nominal operating configuration (i.e. IW mode, VV + HH polarisation plus co-polarisation). Simulation of Sentinel-1 image products is planned.

By including an optical data acquisition component, the campaign also provides feedback on key issues relating to definition of the ESA Sentinel-2 multi-spectral mission requirements. Attention focuses on the investigation of the optimum position and width of spectral bands for land cover/change classification and retrieval of bio-geophysical parameters (e.g. improved surface classification, quantitative assessment of vegetation status – forest and grassland). The imaging spectrometer data acquired as part of EAGLE2006 will be used to simulate Sentinel-2 L1b products using the proposed different configurations, and to investigate compatibility with the envisaged L2/L3 products.

1.3 Campaign Institutions

EAGLE2006 involved 16 different institutions coming from 6 different countries. During the intensive ground campaign in total 67 people from 16 different countries were involved.

European Space Agency (ESA/ESRIN)

Via Galileo Galilei

I-00044 Frascati, Italy

In the following referred to as ESA

FUGRO-Inpark B.V.

Dillenburgsingel 69

2263 HW Leidschendam

The Netherlands

In the following referred to as FUGRO

German Aerospace Center (DLR), Microwaves and Radar Institute (HR)

P.O. Box 11 16, D-82230 Wessling, Germany

In the following referred to as DLR-HR

German Aerospace Center (DLR), Flight Operations (FB)

P.O. Box 11 16, D-82230 Wessling, Germany

In the following referred to as DLR-FB

Instituto Nacional de Técnica Aeroespacial (INTA)

Area de Teledetección, Dpto. de Observ. de la Tierra, Teledetección y Atmósfera

Carretera de Ajalvir, p.k. 4 – 28850 Torrejón de Ardoz (Madrid), Spain

In the following referred to as INTA

International Institute for Geo-Information Science and Earth Observation (ITC), Dept. of Natural Resources (NRS)

P.O. Box 6, 7500 AA

Enschede, The Netherlands

In the following referred to as ITC-NRS

International Institute for Geo-Information Science and Earth Observation (ITC), Dept. of Water Resources (WRS)

P.O. Box 6, 7500 AA

Enschede, The Netherlands

In the following referred to as ITC-WRS

ITRES Research Limited

Suite 110, 3553 – 31st Street NW

Calgary, Alberta, Canada T2L 2K7

In the following referred to as ITRES

MIRAMAP, ESA/ESTEC (TEC-ST)

P.O. Box 299, 2200 AG

Noordwijk, The Netherlands

In the following referred to as MIRAMAP

National Institute for Public Health and the Environment (RIVM)

PO Box 1, 3720 BA

Bilthoven, The Netherlands

In the following referred to as RIVM

National Research Council (CNR), Institute for mediterranean agriculture and forest systems (ISAFoM)

Via Patacca 85

80056 Ercolano (NA), Italy

In the following referred to as ISAFoM

Royal Dutch Meteorological Institute (KNMI)

P.O. Box 201, 3730 AE

De Bilt, The Netherlands

In the following referred to as KNMI

Staatsbosbeheer

Princenhof Park 1

P.O. Box 1300, 3970 BH

Driebergen, The Netherlands

In the following referred to as SBB

Universidad de Valencia (UV)

Faculty of Physics, Department of Thermodynamics, Global Change Unit (GCU)

c/Dr. Moliner, 50

46100 Burjassot, Spain

In the following referred to as UV-GCU

University of South Carolina

Department of Geological Sciences

Columbia, SC 29208, United States of America

In the following referred to as USC

University of Washington

Dept of Earth and Space Sciences
Seattle, WA 98195-1310, United States of America
In the following referred to as UW

Utrecht University
Department of Physical Geography, Faculty of Geosciences
P.O. Box 80.115, 3508 TC
Utrecht, The Netherlands
In the following referred to as UU

Wageningen University and Research Center (WUR)
Green World Research (ALTERRA)
P.O. Box 47, 6700 AA
Wageningen, The Netherlands
In the following referred to as ALTERRA

Wageningen University and Reseach Center (WUR)
Meteorology and Air Quality Group (MAQG)
P.O. Box 47, 6700 AA
Wageningen, The Netherlands
In the following referred to as WUR-MAQG

1.4 Campaign participants

Organisation Team:	
ESA:	Remo Bianchi
ITC-WRS:	Remco Dost
	Bob Su
	Wim Timmermans
Airborne Team:	
DLR-FB:	Heinz Finkenzeller
	Andrea Hausold
DLR-HR:	Irena Hajnsek
	Ralf Horn
	Rolf Scheiber

INTA:	Alix Fernandez-Renau
	José Antonio Gómez
	Óscar Gutiérrez-de-la-Cámara
	Eduardo de Miguel
	Elena Prado
	Ricardo Puente Robles
ITRES:	Jason Howse
	Andrew House
	Steve Mah
ISAFoM:	Marco Esposito
	Vicenzo Magliulo
	Massimo Menenti

Ground/Atmosphere Team:

FUGRO:	Erik Claassen
	Ron Rozema
ITC-NRS:	Kwabena Asubonteng
	Nilam Kayastha
	Badri Karki
	Patrick van Laake
	Jan de Leeuw
	Joan Looijen
ITC-WRS:	Ali Abkar
	Ard Blenke
	Remco Dost
	Fang Huang
	Fouad Khaier
	Chris Mannaerts
	Jeniffer Kinoti Mutiga
	Gabriel Parodi
	Bob Su
	Joris Timmermans
	Wim Timmermans
	Christiaan van der Tol
	Zoltan Vekerdy
	Kitsiri Weligepolage
MIRAMAP:	Roland Haarbrink

RIVM:	Ton van der Meulen
	Ariën Stolk
KNMI:	Fred Bosveld
	Richard Rothe
	Andre Swinkels
	Sjaak Warmer
	Ed Worrel
SBB:	Dhr. Boonen
	Jan de Wilde
UV-GCU:	Mariam Atitar
	Anaïs Barella
	Juan Cuenca
	Monica Gómez
	Juan Carlos Jiménez-Muñoz
	Yves Julien
	Mireia Romaguera
	Jose Sobrino
	Guillem Sòria
	Malena Zaragoza
USC:	Rahul Kanwar Venkataraman Lakshmi
UW:	Alan Gillespie
UU:	Hans van der Kwast
ALTERRA:	Jan Elbers
	Eddy Moors
	Li Jia
WUR-MAQG:	Oscar Hartogensis

2 Description of the study area

Simultaneous measurements took place at three sites (Fig. 1):

Cabauw, grassland, 51°58’00” N, 04°54’00” E, -0.7 m. a.m.s.l.

Loobos, forest, 52°10’02.8” N, 05°44’38” E, 23 m. a.m.s.l.

Speulderbos, forest, 52°15’08.1” N, 05°41’25.8” E, 52 m. a.m.s.l.

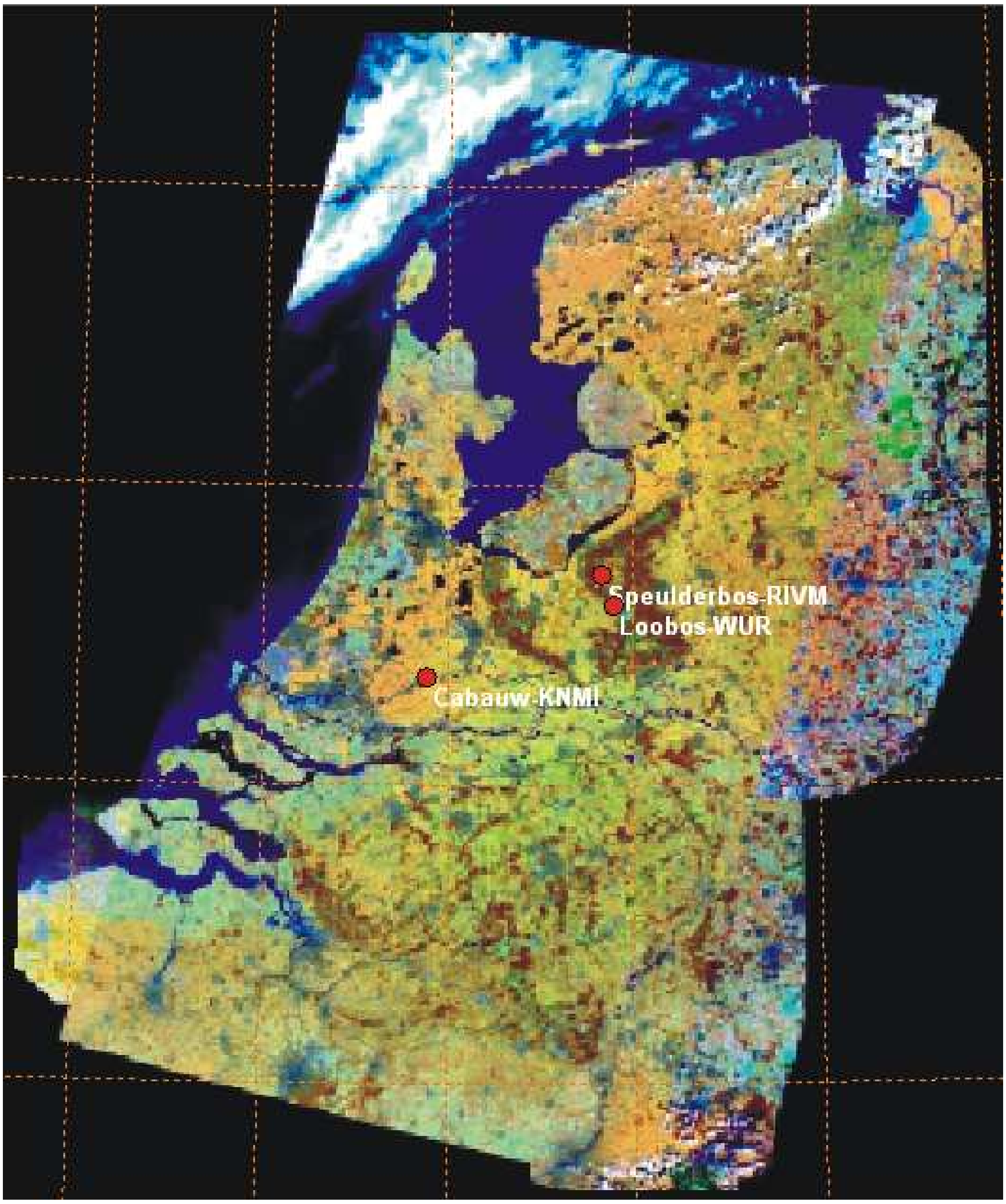

Figure 1. Overview of the study area on a resampled (1000 m) Landsat-TM false color composite of the Netherlands; red dots indicate sites described in the text.

2.1 Cabauw

The Cabauw site (Fig. 2) is located approximately at the central western part of the Netherlands near the village of Cabauw. In 1972 at Cabauw a 213 m high mast was built by the Koninklijk Nederlands Meteorologisch Instituut (KNMI). This tower was built to establish relations between the state of the atmospheric boundary layer (ABL), land surface conditions and the general weather situation for all seasons. The Cabauw mast is located in a polder 0.7 m below average sea level.

Figure 2. The 213 meter high Cabauw tower as seen during different weather conditions.

The instruments are mounted on a 213 m tower placed in an extensive grassland area. In the immediate surroundings of the tower (corresponding to an area of 1 ha) the grass is kept at a height of 8 cm by frequent mowing. Apart from scattered villages, roads and trees the landscape within a radius of at least 20 km consist of flat grassland. Approximately 1.5 km south of the tower runs the river Lek, which is one of the main branches of the Rhine river. The river is a few hundred meters broad. The water holding capacity of the soil at the site is high, the soil is fine grained with a high content of organic matter. The ground water level in the whole catchment area, within which the field tower is located, is artificially managed through narrow, parallel ditches spaced 40 m apart from each other. The water level in the ditches is always kept at 40 cm below the surface level maintaining the level of the ground water table near the surface. Due to the rich supply of water and the fine grained soil, the evaporative fraction rarely falls below 0.6.

More detailed information is provided in (Ulden & Wieringa, 1996).

An overview of recorded data is provided on the web at:

http://www.knmi.nl/kodac/ground_based_observations_climate/cabauw.html

2.2 Loobos

The Loobos site (Fig. 3) is located two kilometers south-west of the village Kootwijk. Continuous micrometeorological measurements are carried out since 1997 at a height of 23 m above the surface. In a radius of 500 m, 89% of the vegetation consists of pine trees with an average height of about 16 meter, 3.5% is open vegetation e.g. heather and the remainder is a mixture of coniferous and deciduous trees.

Figure 3. The Loobos forest (left panel) and the ALTERRA flux tower (right panel)

Some more detailed information is available from the ALTERRA research web-site at: http://www.loobos.alterra.nl

2.3 Speulderbos

The Speulderbos site (Fig. 4), operated by the National Institute for Public Health and the Environment (RIVM), is located approximately 60 km northeast from Cabauw within a large forested area in the Netherlands. The tower is placed within a dense 2.5 ha Douglas fir stand planted in 1962. The tree density is 785 trees per hectare and the tree height in 1995 was approximately 22 m, which has grown till 32 meter in 2006! The tower, which is currently used for research (not operational routine) measurements, is 46 meter high and has electric power supply. The single-sided leaf area index varies between 8 and 11 throughout the year. The surrounding forest stands have typical dimensions of a few hectares and varying tree heights. Dominant species in the neighbourhood of the Douglas fir stand are Japanese Lark, Beech, Scotch Pine and Hemlock. At a distance of 1.5 km east from the tower the forest is bordered by a large heather area. In all other directions the vegetation consists of forest at distances of several kilometers. The topography is slightly undulating with height variations of 10 to 20 m within distances of 1 km.

Figure 4. Forester tower site at Drie, Speulderbos (upper panels) and the RIVM tower site (lower panels), where the lower right panel shows a view from the top (46 m) of the tower in the direction of the forester tower.

Another tower in the area, currently used by foresters of SBB, is located in Drie at about 2 km distance at 52°15’54.8” N latitude and 5°40’39.4” E longitude. A Large Aperture Scintillometer (LAS) is installed between this and the previous tower to obtain spatially averaged sensible heat fluxes.

2.4 Topographic data

Topographical data for the entire study area is digitally available, originating from scale 1:50,000 and scale 1:10,000 topographical maps. For an index of the different sheets and their numbering, see Fig. 5.

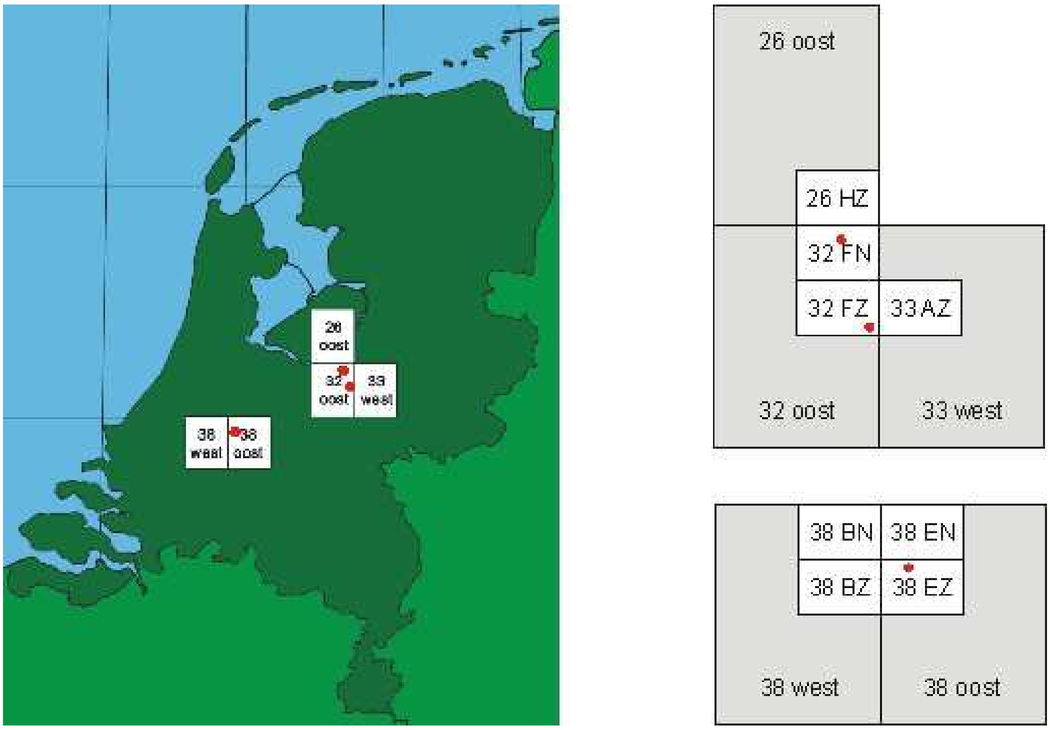

Figure 5. Overview of the map-sheets covering the areas of interest; the red dots indicate the positions of the three observation towers.

Scale 1:50,000

Maps are in stereographic projection, origin at Amersfoort, Bessel Spheroid 1842. The numbered grid lines indicate the national reference rectangular coordinate system. The origin at Amersfoort has the false coordinates X=155000 m and Y=463000 m. The coordinate values are given in kilometers. The geographical coordinate system is indicated by intersections of meridians and parallels with an interval of 5’ and a one minute graduation of the neat line.

Elevation data is in meters and are based on Amsterdam Ordnance Datum (N.A.P.) with contour interval 5 m.

Scale 1:10,000

Maps are in stereographic projection, origin at Amersfoort, Bessel Spheroid 1842. The numbered grid lines indicate the national reference rectangular coordinate system. The origin at Amersfoort has the false coordinates X=155000 m and Y=463000 m. Elevation data is in meters and are based on Amsterdam Zero (N.A.P.) with contour interval 2.5 m.

2.5 Digital Elevation Model data (AHN)

Digital elevation data from the Actual Height model of the Netherlands (AHN) is available for the areas of interest. The AHN is a detailed elevation model of the entire country obtained from Airborne Laser Altimetry. The Actual Elevation Model is an initiative of three layers of authorities in the Netherlands, i.e. "Rijkswaterstaat" (Ministry of Transport, Public Works and Water Management), the water boards, and the provinces. As such, it consists of a uniform, country-covering dataset that is commercially available to third parties.

Basically two data formats are available; the so-called "base database", which contains filtered elevation points, with X, Y and Z coordinates of the RD (triangulation of national grid) and NAP (Amsterdam Ordnance Datum, the Dutch National leveling reference system), and the grid databases, consisting of three different grid formats with grid cells of the sizes 5x5, 25x25 and 100x100 m. In the current campaign we have disposal of the base database files as well as the 5x5 m resolution raster data in three different formats; ArcInfo Export (.E00), Arc-Info ASCII-Grid (.agr), and in ASCII-XYZ (.xyz) data format.

Table 1. AHN products overview.

Product	Unit	Format	Extension	Max. size (Mb)
Base database	meter	ASCII	.adf	36
5x5 m DEM	cm	ARC/INFO export	.e00	17.8
	cm	ARC/INFO ASCII Grid	.agr	10.5
	cm	ASCII-XYZ	.xyz	32.2
25x25 m DEM	cm	ARC/INFO export	.e00	3
	cm	ARC/INFO ASCII Grid	.agr	0.8
	cm	ASCII-XYZ	.xyz	6
100x100 m DEM	cm	ARC/INFO export	.e00	0.6
	cm	ARC/INFO ASCII Grid	.agr	0.1
	cm	ASCII-XYZ	.xyz	0.8

The AHN raster data in the 5 meter resolution have their elevation data stored in centimeters. The value is calculated from surrounding laserpoints of the filtered base database, using a weighted average interpolation. If no laser points are available neighbouring the gridcell, a "no-data" value is assigned. Generally, however, one grid cell value is calculated from several laser points. The number herein depends on the density of the base database at the location under consideration, which originates form different sources; reason for the density to be variable.

Horizontal coordinates originate from the "Rijksdriehoekstelsel", which is the national Dutch reference rectangular coordinate system, RD. For vertical coordinates, the datum used is Amersfoort, Bessel 1841 Ellipsoid in a double stereographic projection, where the reference system is again the NAP.

The products are divided into map sheets, following the same numbering system as the 1:10,000 topographic mapsheets, section 2.4. The base database and 5x5 meter grid DEM's are stored in half-size 10:10,000 sheets, using a 1 for the western half and a 2 for the eastern half, and a N for the northern half and a Z for the southern half. In the current campaign, a total of 80 sheets (Fig. 6) are available originating from the following 20 1:10,000 mapsheets: 26f, 27a, 26g, 26h, 27c, 32a, 32b, 32e, 32f, 33a, 31g, 31h, 32c, 32d, 32g, 32h, 33c, 38b, 38e, 38f. The north-eastern sheet of mapsheet 27a, for example, would be indicated as "27an2".

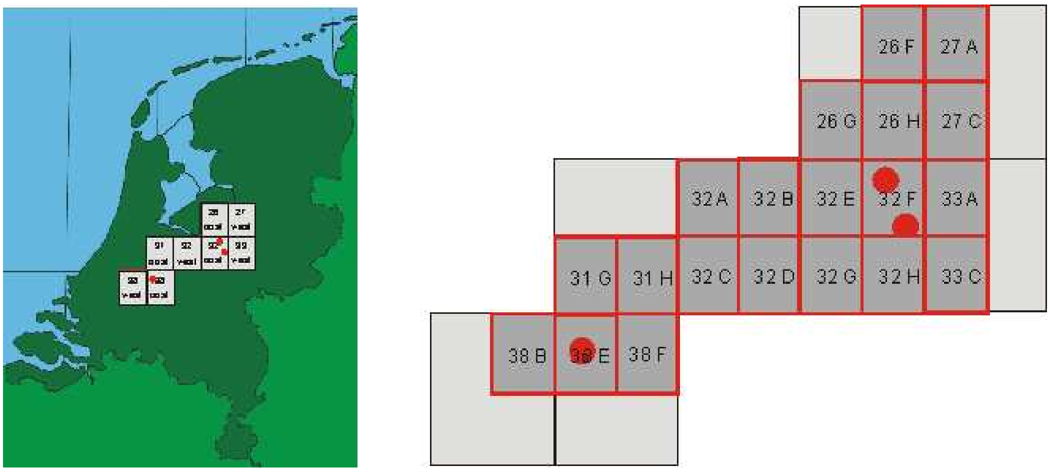

Figure 6. Overview of the 20 available AHN-sheets (which in turn are divided into 4 sub-sheets each) covering the areas of interest; the red dots indicate the positions of the three observation towers.

The accuracy of the elevation data depends strongly on the amount of vegetation and topography in the area. Here, for the accuracy of solid topography (such as roads and parking lots) as well as flat or soft topography (such as beaches and grass-fields) applies a standard deviation of 15 cm maximum with a systematic error of 5 cm maximum. In wooded areas this degree of accuracy is not feasible. In this case one accepts a minimum point density of one point per 36 m^2, a standard deviation of 20 cm maximum and a systematic error of 10 cm maximum, see Table 2.

Table 2. AHN error overview.

Landcover	RMS error (m)	Systematic error (m)	Point density (/m^2)
Coastal area	0.15	+/- 0.05	1
Grassland, short	0.15	+ 0.05	1/16
Grassland, natural	0.20	+ 0.20	1/16
Riparian area, crops	0.20	Vegetation height	1/16
Bushland	0.20	+ 0.20	1/16
Bare and smooth	0.15	+ 0.05	1/16
Forest	0.20	+ 0.10	1/36
Urban	N.A.	N.A.	1/16

2.6 National data

Digital data on a national level is also made available within the project. This concerns general data taken from external sources but made available to the EAGLE2006 Campaign Participants through the EAGLE2006 database. Basically three data types are available, they are:

1. General data, taken from the Pennsylvania State University, University Libraries, Pattee Maproom, where typical features such as boundaries, (rail) roads, drainage network, etcetera are available. They are in the ARC/INFO .e00 format.
2. Digital Elevation Model data, originating from the SRTM mission, available in the ARC-GIS .IMG format
3. Landcover data, originating from the Corine Landcover database, available in the Arc-View shape format.

3 Satellite data acquisitions

3.1 CHRIS-PROBA acquisitions

Due to severe cloud conditions over the study area in the time window of CHRIS overpasses, no CHRIS-PROBA observations of the surface could be made. Hence, no CHRIS-PROBA imagery is available.

3.2 MERIS acquisitions

The MERIS sensor is a programmable, medium-spectral resolution, imaging spectrometer operating in the solar reflective spectral range installed on board of ESA's Earth Observation satellite ENVISAT. Fifteen spectral bands can be selected by ground command, each of which has a programmable width and a programmable location in the 390 nm to 1040 nm spectral range.

The instrument scans the Earth's surface by the so-called 'push broom' method. CCDs arrays provide spatial sampling in the cross track direction, while the satellite's motion provides scanning in the along-track direction. MERIS is designed so that it can acquire data over the Earth whenever illumination conditions are suitable. The instrument's 68.5^{o} field of view around nadir covers a swath width of 1150 km. This wide field of view is shared between five identical optical modules arranged in a fan shape configuration. In the calibration mode, correction parameters such as offset and gain are generated, which are then used to correct the recorded spectra. This correction can be carried out either on board or on the ground. The Earth is imaged with a spatial resolution of 300 m (at nadir). This resolution is reduced to 1200 m by the on board combination of four adjacent samples across track over four successive lines.

The scene is imaged simultaneously across the entire spectral range, through a dispersing system, onto the CCD array. Signals read out from the CCD pass through several processing steps in order to achieve the required image quality. These CCD processing tasks include dumping of spectral information from unwanted bands, and spectral integration to obtain the required bandwidth. On-board analogue electronics perform pre-amplification of the signal and correlated double sampling and gain adjustment before digitisation. The on-board digital electronics has three major functions: it completes the spectral integration, performs offset and gain corrections in full processed mode, and creates the reduced resolution data when required. The calibration of MERIS is performed at the orbital south pole, where the calibration diffuser is illuminated by the sun by rotating a calibration mechanism.

The engineering requirements on the instrument, which have been derived from the ENVISAT mission requirements, are provided in Table 3.

Table 3. Key characteristics of MERIS

Spectral range	390 nm to 1040 nm
Spectral resolution	1.8 nm
Band transmission capability	Up to 15 bands, programmable in position and width
Band-to-band registration	Less than 0.1 pixel
Band-centre knowledge accuracy	Less than 1 nm

Polarisation sensitività	Less than 0.3 %
Radiometric accuracy	Less than 2% of detected signal, relative to sun
Band-to-band accuracy	Less than 0.1%
Dynamic range	Up to albedo 1.0
Field of view	68.5°
Spatial resolution	300 m at nadir

For the campaign the following overpasses and characteristics are available (Table 4), one MERIS image is shown in Fig. 7.

Table 4. MERIS observations during the EAGLE2006 Campaign.

Orbit	Frame	Date	DOY	Quality	Start time	Scene center	
22335	237	08-06-2006	159	Good	10:16:03	52°12’33”N	05°09’56”E
22364	266	10-06-2006	161	Good	10:52:53	52°25’42”N	04°18’39”E
22378	280	11-06-2006	162	Good	10:21:41	52°12’25”N	05°10’47”E
22421	323	14-06-2006	165	Cloudy	10:27:22	52°12’54”N	05°09’00”E
22464	366	17-06-2006	168	Good	10:33:06	52°12’59”N	05°09’45”E
22478	380	18-06-2006	169	Cloudy	10:01:48	52°12’37”N	05°10’51”E

Figure 7. Part of MERIS scene as acquired on 11th of June 2006 over the study area (RGB: 3-2-1).

3.3 MODIS acquisitions

The Moderate Resolution Imaging Spectroradiometer (MODIS) is a key instrument aboard the Terra (EOS AM) and Aqua (EOS PM) satellites. Terra's orbit around the Earth is timed so that it passes from north to south across the equator in the morning, while Aqua passes south to north over the equator in the afternoon. Terra MODIS and Aqua MODIS are viewing the entire Earth's surface every 1 to 2 days, acquiring data in 36 spectral bands, or groups of wavelengths (see MODIS Technical Specifications). These data will improve our understanding of global dynamics and processes occurring on the land, in the oceans, and in the lower atmosphere. MODIS is playing a vital role in the development of validated, global, interactive Earth system models able to predict global change accurately enough to assist policy makers in making sound decisions concerning the protection of our environment.

The MODIS instrument provides high radiometric sensitivity (12 bit) in 36 spectral bands ranging in wavelength from 0.4 µm to 14.4 µm. The responses are custom tailored to the individual needs of the user community and provide exceptionally low out-of-band response. Two bands are imaged at a nominal resolution of 250 m at nadir, with five bands at 500 m, and the remaining 29 bands at 1 km. A ±55-degree scanning pattern at the EOS orbit of 705 km achieves a 2,330-km swath and provides global coverage every one to two days. The Scan Mirror Assembly uses a continuously rotating double-sided scan mirror to scan ±55-degrees and is driven by a motor encoder built to operate at 100 percent duty cycle throughout the 6-year instrument design life. The optical system consists of a two-mirror off-axis afocal telescope, which directs energy to four refractive objective assemblies; one for each of the VIS, NIR, SWIR/MWIR and LWIR spectral regions to cover a total spectral range of 0.4 to 14.4 µm. A high performance passive radiative cooler provides cooling to 83K for the 20 infrared spectral bands on two HgCdTe Focal Plane Assemblies (FPAs). Novel photodiode-silicon readout technology for the visible and near infrared provide unsurpassed quantum efficiency and low-noise readout with exceptional dynamic range. Analog programmable gain and offset and FPA clock and bias electronics are located near the FPAs in two dedicated electronics modules, the Space-viewing Analog Module (SAM) and the Forward-viewing Analog Module (FAM). A third module, the Main Electronics Module (MEM) provides power, control systems, command and telemetry, and calibration electronics. The system also includes four on-board calibrators as well as a view to space: a Solar Diffuser (SD), a v-groove Blackbody (BB), a Spectroradiometric calibration assembly (SRCA), and a Solar Diffuser Stability Monitor (SDSM).

Table 5. MODIS technical specifications

Orbit	705 km altitude, sun-synchronous, near-polar, circular
Descending node (TERRA)	10:30 am
Ascending node (AQUA)	1:30 pm
Scan rate	20.3 rpm, cross track
Swath dimensions	2330 km (cross track) by 10 km (along track at nadir)
Telescope	17.78 cm diam. Off-axis, afocal (collimated)
Size	1.0 x 1.6 x 1.0 m
Weight	228.7 kg
Power	162.5 W (single orbit average)
Data rate	10.6 Mbps (peak daytime); 6.1 Mbps (orbital average)
Quantization	12 bits
Spatial resolution	250 m (bands 1-2), 500 m (bands 3-7), 1000 m (bands 8-36)

The first MODIS Flight Instrument, ProtoFlight Model or PFM, is integrated on the TERRA (EOS AM-1) spacecraft. Terra was successfully launched on 18 December 1999. The second MODIS flight instrument, Flight Model 1 or FM1, is integrated on the AQUA (EOS PM-1) spacecraft; it was successfully launched on 4 May 2002. These MODIS instruments offer an unprecedented look at terrestrial, atmospheric, and ocean phenomenology for a wide and diverse community of users throughout the world. For the period of the campaign (8th until 18th of June) level 1B data is available, at 250 m, 500 m and at 1000 m resolution, from both the AQUA and TERRA platforms, Table 6.

Table 6. MODIS acquisitions during the EAGLE2006 Campaign.

Date	Platform	DOY	Acquisition time (utc)	Quality
08-06-2006	TERRA	159	10:40	Good
08-06-2006	AQUA	159	12:25	Good
09-06-2006	TERRA	160	09:45	Cloudy/hazy
09-06-2006	TERRA	160	11:25	Light clouds
09-06-2006	AQUA	160	11:30	Light clouds
09-06-2006	AQUA	160	13:10	Cloudy/hazy
10-06-2006	TERRA	161	10:30	Good
10-06-2006	AQUA	161	12:15	(Almost) Cloud-free
11-06-2006	TERRA	162	11:15	Good
11-06-2006	AQUA	162	11:20	Cloud-fee, scene-edge
11-06-2006	AQUA	162	13:00	Cloud-fee, scene-edge
12-06-2006	TERRA	163	10:15	Good
12-06-2006	TERRA	163	10:20	Good
12-06-2006	AQUA	163	11:55	Cloud-fee, scene-edge
12-06-2006	AQUA	163	12:05	Good, scene-edge
13-06-2006	TERRA	164	11:00	Good
13-06-2006	AQUA	164	12:45	Partly cloudy
17-06-2006	TERRA	168	10:35	Partly cloudy
17-06-2006	AQUA	168	12:20	Good
18-06-2006	TERRA	169	11:20	Clouds

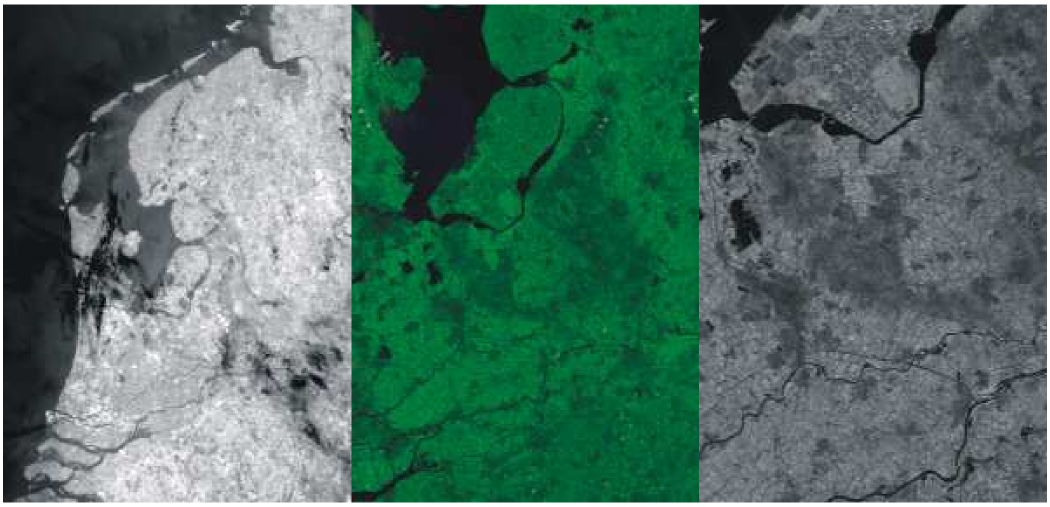

Figure 8. MODIS acquisitions on 13th of June 2006 at 11:00 utc. From left to right; Brightness temperature (Ch. 31) at 1000 m resolution, R-G-B Ch. 3-2-1 at 500 m and Channel 2 reflectance at 250 m resolution.

3.4 AATSR acquisitions

The AATSR (Advanced Along Track Scanning Radiometer) instrument is an imaging radiometer primarily designed to measure global Sea Surface Temperature (SST) to the high levels of accuracy and stability required for climate research and modelling. Like its predecessors, ATSR 1 & 2 it will also produce high quality visible and thermal images. AATSR is the third in the ATSR series, and is a payload instrument on ESA's ENVISAT-1 polar orbiting mission. It is primarily funded by the UK Department of Environment, Transport and the Regions (DETR) with contributions from the Natural Environment Research Council and from Australia. On behalf of the DETR, the Principal Investigator is Professor David Llewellyn Jones of the University of Leicester.

The first ATSR instrument, ATSR-1, was launched on board the European Space Agency's (ESA) European Remote Sensing Satellite (ERS-1) in July 1991, as part of their Earth Observation Programme. An enhanced version of ATSR, ATSR-2, was successfully launched on board ESA's ERS-2 spacecraft on 21 April 1995. ATSR-2 is equipped with additional visible channels for vegetation monitoring. The AATSR (Advanced Along Track Scanning Radiometer) instrument has been successfully launched on board the ENVISAT spacecraft on 1 March 2002 at 01:07 GMT from the Kourou spaceport in French Guiana

AATSR has the same signal channels and embodies exactly the same viewing principle as ATSR-2. These are: thermal channels at 3.7, 10.8, and 12 microns wavelength; and reflected visible/near infrared channels at 0.555, 0.659, 0.865, and 1.61 microns wavelength. The main objective of AATSR is to contribute to the long-term climate record of global Sea Surface Temperature by extending the current ATSR-1 and -2 global data-sets well into the next decade. This could eventually provide the climate research community with uniformly high quality global SST data over a period of 12-15 years (depending on the lifetime of AATSR).

Like its predecessors, ATSR-1 and ATSR-2, AATSR carries on-board calibration systems for the thermal channels, using two black bodies, viewed every scan, and for the visible channels a sample of solar radiation scattered from a diffuser plate is viewed once per orbit. Unlike ATSR-2 it maintains full digitisation of all channels all the time and has no limited-data-rate operating modes.

The AATSR instrument, in contrast to its predecessors (funded by SERC/NERC), is primarily funded by the DETR's Global Atmosphere Division, in order to complete a data-set of accurate global SST, lasting over ten years, which will contribute to the Climate Record and help provide quantitative assessments of possible climate change. The DETR is funding AATSR as a potential operational user of the data - the first environment ministry in Europe to take such a step - as part of a UK Government drive to direct the development and deployment of Earth Observation satellite missions more specifically towards the requirements of end-users of the data.

Like the predecessors onboard the ERS-1/2 (ATSR-1/2), AATSR can provide observations of the surface reflectance spectra in the visible and surface emission spectra in the thermal part of the electromagnetic spectrum, and observes the earth' surface at two viewing angles; at nadir and at a 55 degrees forward looking view. The resolution of the forward and nadir looking channels are approximately 2.0 and 1.0 km, respectively. The combination of optical and thermal observations provided by the AATSR sensor is especially appropriate for the application of remote sensing based energy budget modeling approaches. In addition, AATSR's dual angle configuration allows the potential extraction of component vegetation and soil temperatures.

Table 7. Out of 6 programmed AATSR acquisitions for the EAGLE2006 campaign 4 were successful.

Orbit	Frame	Date	DOY	Time	Available
22335	237	08-06-2006	159	10:15:43	Yes
22356	258	09-06-2006	160	21:07:22	Failed
22378	280	11-06-2006	162	10:21:24	Yes
22413	315	13-06-2006	164	20:41:49	Failed
22421	323	14-06-2006	165	10:27:05	Severe clouds
22464	366	17-06-2006	168	10:32:45	Yes

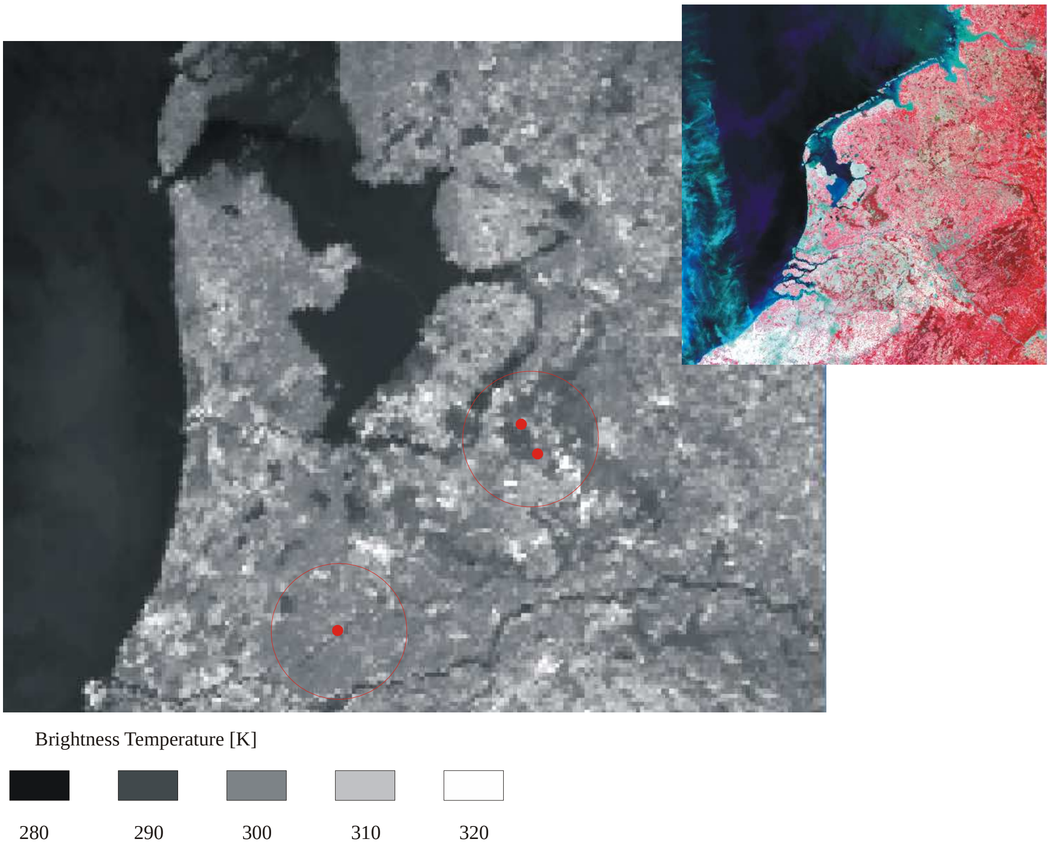

Figure 9. AATSR acquisitions on 11th of June 2006 (RGB-3-2-1) and Brightness temperature @ 12µm as acquired on 8th of June 2006.

3.5 ASTER acquisitions

The ASTER products are provided in hierarchical data format (HDF), and are defined by level:

Level 1B: at-sensor radiance (geometric and radiometric coefficients applied)

Level 2 (AST09): at-surface radiance in the VNIR and SWIR regions

Level 2 (AST09T): at-surface radiance in the TIR region

Level 2 (AST08): land surface temperature (obtained with the TES algorithm)

Level 2 (AST05): land surface emissivity (obtained with the TES algorithm)

Figure 10. Cabauw grassland site as acquired by ASTER channels 3,2,1 on 08 June 2006.

The ASTER observations acquired within the EAGLE campaign over the study area correspond to June 8th, 2006 and are level 1B data. They comprise of two scenes, one covering the forest areas and another one covering the grassland areas.

3.6 ASAR acquisitions

The ASAR sensor on board of the Envisat platform, operates at C-band, ensuring continuity with the image mode (SAR) and the wave mode of the ERS-1/2 AMI. It features enhanced capability in terms of coverage, range of incidence angles, polarisation, and modes of operation. This enhanced capability is provided by significant differences in the instrument design: a full active array antenna equipped with distributed transmit/receive modules which provides distinct transmit and receive beams, a digital waveform generation for pulse "chirp" generation, a block adaptive quantisation scheme, and a ScanSAR mode of operation by beam scanning in elevation.

The Advanced SAR is built up on the experience gained with the ERS-1/2 active microwave instrument (AMI) to continue and extend Earth observation with SAR. Compared to ERS AMI, ASAR is a significantly advanced instrument employing a number of new technological developments which allow extended performance. The replacement of the centralized high-power amplifier combined with the passive waveguide slot array antenna of the AMI by an active phased array antenna system using distributed elements is the most challenging development. The resulting improvements in image and wave mode beam elevation steerage allow the selection of different swaths, providing a swath coverage of over 400-km wide using ScanSAR techniques. In alternating polarisation mode, transmit and receive polarisation can be selected allowing scenes to be imaged simultaneously in two polarisations.

Table 8. ASAR acquisitions during EAGLE2006.

Orbit	Frame	Date	DOY	Direction	Acquisition Time (utc)
22356	258	09-06-2006	160	A	21:07:57
22392	294	12-06-2006	163	D	09:50:45
22399	301	12-06-2006	163	A	21:13:28
22442	344	15-06-2006	166	A	21:19:11
22442	344	15-06-2006	166	A	21:19:22
22485	387	18-06-2006	165	A	21:24:55
22521	423	21-06-2006	168	A	21:30:38
22578	480	25-06-2006	172	D	09:42:04
22578	480	25-06-2006	172	D	09:42:13

The ERS high resolution products PRI, SLC, and GEC will be continued for image mode, and generated for alternating polarisation mode on user request. The wave mode products are continued and their quality improved thanks to cross spectra algorithms.

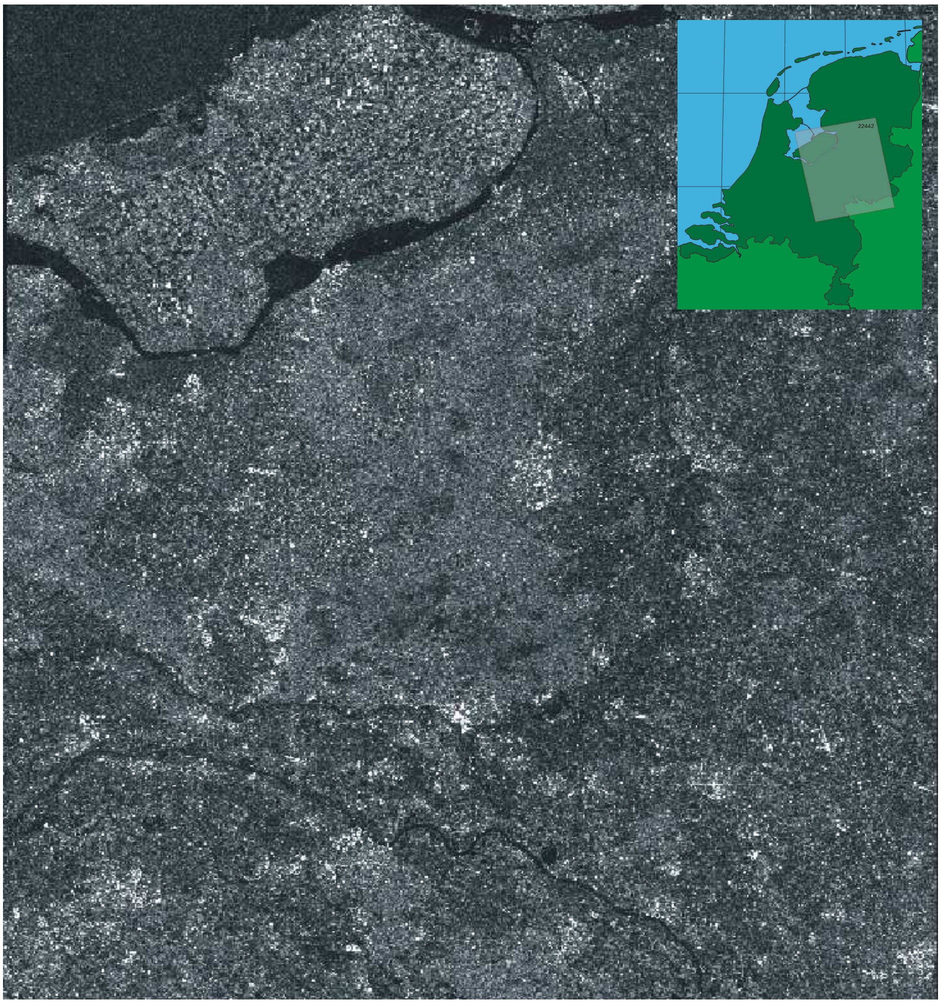

Figure 11. ASAR scene acquired from the ENVISAT platform on 15th of June 2006 over both forest sites, acquisition time 21:19:22 G.M.T.

3.7 SEVIRI acquisitions

The images are received as a series of wavelet compressed segments (e.g. 8 segments for bands 1-11 and 24 segments for band 12, the High Resolution Visible, HRV). There are also Epilogue (*.epi) and Prologue files (*.pro) which contain important information with regard to the SEVIRI settings. These epilogues and prologue files are in binary format but not compressed. The compressed segment files are in fact made up of two parts: first, a header which contains information with regard to coordinates and radiometric settings and which is not compressed, and second the actual wavelet compressed image segment.

After decompression, the segments have to be combined and provided with a coordinate and a georeference system. After that, radiometric calibration coefficients have to be used to transform the two-byte per integer pixel values into radiances. For bands 1 to 3, radiances can be converted into TOA albedo and the thermal bands 4 to 11, radiances can also be converted into brightness (TOA) temperature.

The SEVIRI radiometric characteristics are displayed in Table 9. The noise is expressed in Signal to Noise Ratio (SNR) at a referenced target for the solar channels (MDR standing for Maximum of the Dynamic Range) and in Kelvin for the IR channels at a referenced source brightness temperature (Noise Equivalent Temperature difference or NEdT). The specified radiometric SNR or NEdT is the one between parentheses.

Table 9. SEVIRI radiometric specifications.

Channel	Bandwidth (µm)	Center wavelength (µm)	In-flight radiometric noise results
HRV	Broad band – 0.6 to 0.9		2.84 (1.20) at 0.28% MDR
VIS 0.6	0.56 to 0.71	0.6	159 (10.1) at 1% MDR
VIS 0.8	0.74 to 0.88	0.8	53 (7.28) at 1% MDR
NIR1.6	1.50 to 1.78	1.6	10 (3.00) at 1% MDR
IR 3.9	3.48 to 4.36	3.9	0.105 K (0.35) at 300 K
WV 6.2	5.35 to 7.15	6.2	0.05 K (0.75) at 250 K
WV 7.3	6.85 to 7.85	7.3	0.060 K (0.75) at 250 K
IR 8.7	8.30 to 9.10	8.7	0.07 K (0.28) at 300 K
IR 9.7	9.38 to 9.94	9.7	0.11 K (1.50) at 255 K
IR10.8	9.80 to 11.80	10.8	0.074 K (0.25) at 300 K
IR12.0	11.00 to 13.00	12.0	0.11 K (0.37) at 300 K
IR13.4	12.40 to 14.40	13.4	0.295 K (1.80) at 270 K

The data for the period of the campaign is recorded at ITC's receiving station and as such available. For the EAGLE2006 Campaign database SEVIRI images are made available directly. Due to size limitations a window has been cut from the full globe scene covering latitudes 46 to 56 North and Longitudes 0 to 10 East (Fig. 12), and stored in the ENVI HDR-format. At sensor radiances, as well as at-sensor reflectances and at-sensor temperatures (where applicable) have been stored from all timeslots.

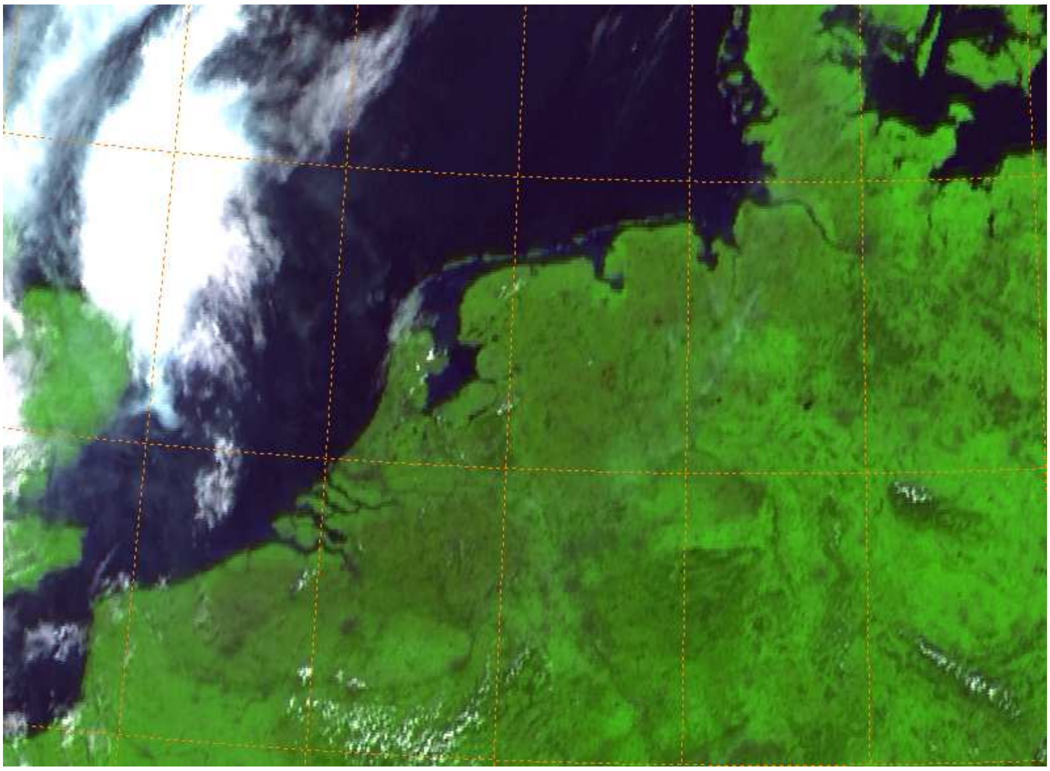

Figure 12. SEVIRI observation over The Netherlands of 13 June 2006, 1200 GMT.

3.8 ALOS PALSAR acquisitions

Due to the experimental character of these data during the period of the campaign no data is recorded over the area of interest.

4 Airborne data acquisitions

Four airborne sensors have been operated during the EAGLE 2006 campaign to acquire unique data for bio-/geo-physical parameter estimation over the grassland and forest sites. The AHS from INTA and the CASI sensor of ITRES were both mounted on the CASA 212-200 N/S 270 “Paternina” airplane of INTA, Fig 13. Because the objective of the campaign was primarily aiming at AHS acquisitions the configuration was designed such that if conflicting criteria between AHS and CASI occurred preference was given to AHS. Furthermore, DLR-HR flew a Do228 aircraft that carried their multi-frequency and multi-polarisation Synthetic Aperture Radar system, and ISAFoM operated a Sky-Arrow airplane for flux measurements. In addition one sensor (MIRAMAP L-band) was mounted at 100 meters height at the Cabauw grassland site.

4.1 AHS-INTA acquisitions

The AHS is an imaging 80-band line-scanner radiometer, built by Sensytech Inc (currently Argon ST, and formerly Daedalus inc.) and purchased by INTA in 2003. AHS is based on previous airborne hyperspectral scanners, such as the MIVIS (Multispectral Infrared and Visible Imaging Spectrometer) and MAS (MODIS Airborne Simulator). The instrument has been installed in the INTA´s aircraft (CASA C-212), and integrated with an INS/GPS POS-AV 410 from Applanix, see Fernandez-Renau et.al. (2006) for details. The AHS was first flown by INTA in September 2003. During 2004 the instrument was validated during a number of flight campaigns which included extensive ground surveys (SPARC-2004 and others). It has been fully operational from the beginning of 2005.

It has a design which has very distinct spectral performances depending on the spectral range considered. In the VIS/NIR range, bands are relatively broad (28-30 nm): the coverage is continuous from 0.43 up to 1.0 microns. In the SWIR range, there is an isolated band at 1.6, useful to simulate the corresponding band found in a number of satellite missions. Next, there are a number of continuous, fairly narrow bands (13 nm) between 2.0 and 2.5 microns, which are well suited for soil/geologic studies. In the MIR and TIR ranges, spectral resolution is again high (30 to 50 nm), and the atmospheric windows (3 to 5 microns and 8 to 13 microns) are fully covered.

Figure 13. AHS sensor and INTA plane.

4.1.1 AHS Characteristics

The main characteristics of AHS are:

- Optical design: scan mirror plus reflective optics with a single IFOV determining field stop.

- FOV (Field Of View) / IFOV (Instantaneous Field Of View): 90º / 2.5 mrad.

- GSD (Ground Sampling Distance): 2.1 mrad (0.12 degrees).

- Scan rates: 6.25, 12.5, 18.75, 25, 31.25 and 35 r.p.s., providing GSD's from 7 to 2.5 m@72ms^{-1}

- Digitization precision: 12 bits to sample the analog signal, with gain level from x0.25 to x10.

- Samples per scan line: 750 pixels/line.

- Reference sources: two controllable thermal black bodies within the field of view, set to a temperature range from -15ºC to +25ºC with respect to scan heat sink temperature.

- Spectrometer: four dichroic filters to split radiation in four optical ports, and diffraction gratings within each port.

- Detectors: Si array for VIS/NIR port; InGaAs, InSb and MCT arrays, cooled in N_2 dewars, for SWIR, MIR and TIR ports.

- Spectral bands: continuous coverage in four spectral regions + one single band at 1.5 micrometers, as shown in Table 10.

- Data recording media: Removable SCSI magnetic hard disks.

Table 10. AHS spectral configuration

Optical port	Detector	Bands	Spectral range (nm)	Band width (FWHM)	NΔλ (minimum)
Port 1 - VNIR	Si-not cooled	20	442 – 1019	27 – 30 nm	≈ 17
Port 2A – SWIR	InGaAs-cooled	1	1491 – 1650	159 nm	≈ 10
Port 2 – SWIR	InSb-LN2 cooled	42	2024 – 2498	12 – 13 nm	≈ 156
Port 3 – MWIR	InSb-LN2 cooled	7	3030 – 5410	260 – 420 nm	≈ 9
Port 4 – LWIR	HgCdTe-LN2 cooled	10	7950 – 13700	400 – 550 nm	≈ 17

The spectral bands in the narrower ports (Port 1 and Port 2) have a gaussian distribution with FWHM equal to bandpeak-to-bandpeak spacing, as assumed by processing tools (typically ENVI). Bands in the thermal ports (3 and 4) are also well approximated by the gaussian curve, but their broader size would require the use of the spectral responsitivity for detailed analysis. Band AHS-21 (port 2A) is the less regular one, and band center, peak response and FWHM have a singular relation. More details are given in Table 11.

Table 11. AHS technical specifications

FOV	90°
IFOV	2.5 mrad
GFOV	2 ÷ 6 m at 140 kt cruise speed
Scan rate	6.25, 12.5, 18.75, 25, 31.25, 35 rps

Quantization	12 bits		
Sampling	750 samples per line		
Pixel size	2.5 m @ 3200 ft Above Ground Level		
Calibration	Black body thermal reference		
Spectral characteristics:	80 bands in 5 ports:		
Optical ports	Number of bands	Spectral region	Band width
VIS	20	430 to 1030 nm	30 nm
NIR	1	1.550 to 1.750 µm	200 nm
SWIR	42	1.994 to 2.540 µm	13 nm
MWIR	7	3.3 to 5.4 µm	300 nm
LWIR	10	8.20 to 12.7 µm	400 nm

4.1.2 AHS Flight data and settings

The flight lines were designed to match the most likely expected areas to be included in all the views for the different CHRIS-PROBA acquisitions during the campaign. The main flights as such were scheduled for June 14th and the 15th, with a backup flight at the 13th. Due to cloudiness there were no CHRIS-PROBA acquisitions and also no AHS acquisitions on 14 and 15 of June. Therefore there was only one day in the possible time frame suitable for acquisition, which was on the 13th of June. Other characteristics are given in Table 12.

Table 12. AHS flight characteristics.

Flight data	
Aircraft	CASA 212-200 N/S 270, *"Paternina"*
Nominal aircraft ground speed	GS 140kts (72ms^{-1})
Altitude above ground level	2.4m AHS survey AGL3200ft (975m)
	6.9m AHS survey AGL9000ft (2743m)
AHS settings	
AHS installation	On main cabin floor front window
AHS positioning & orientation	INS/GPS Applanix POS/AV 410 V4
AHS-IMU installation	On AHS scan head. ACTIVE
AHS boresight calibration flight	Performed on April 20, 2006 over "Tirez" site.
AHS scan rate	35rps @ AGL975m (3200ft)
	12.5rps @ AGL2743m (9000ft)
AHS IFOV/FOV	2.5mrad / 90degrees
Number of pixels per scan-line	750 pixels
AHS pixel size / GSD @ nadir	2.4m / 2.1m @ AGL975m
	6.9m / 5.8m @ AGL2743m
AHS along-track scan-line overlap	16% @ GS72ms^{-1}, AGL975m, 35rps

	16% @ GS72ms^{-1}, AGL2743m, 12,5rps
AHS across-track scan-line overlap	~54% @ AGL975m (3200ft)
	N/A @ AGL2743m (9000ft)
AHS swath	1965m @ AGL975m (3200ft)
	5502m @ AGL2743m (9000ft)
AHS internal thermal reference sources	T_{BB1}= 20°C & T_{BB2} = 45°C/50°C
AHS spectral configuration	80 spectral channels. VNIR, SWIR, MWIR & LWIR
	Port 1+ Port 2A + Port 2 + Port 3 + Port 4
AHS calibration date	February 2006

One complete survey is carried out on Tuesday the 13th of June. Weather conditions were a hazy atmosphere and some clouds at the end of the survey. The flight lines are shown in Figs 14-15 and Tables 13-14. The quicklooks are shown in Fig. 16.

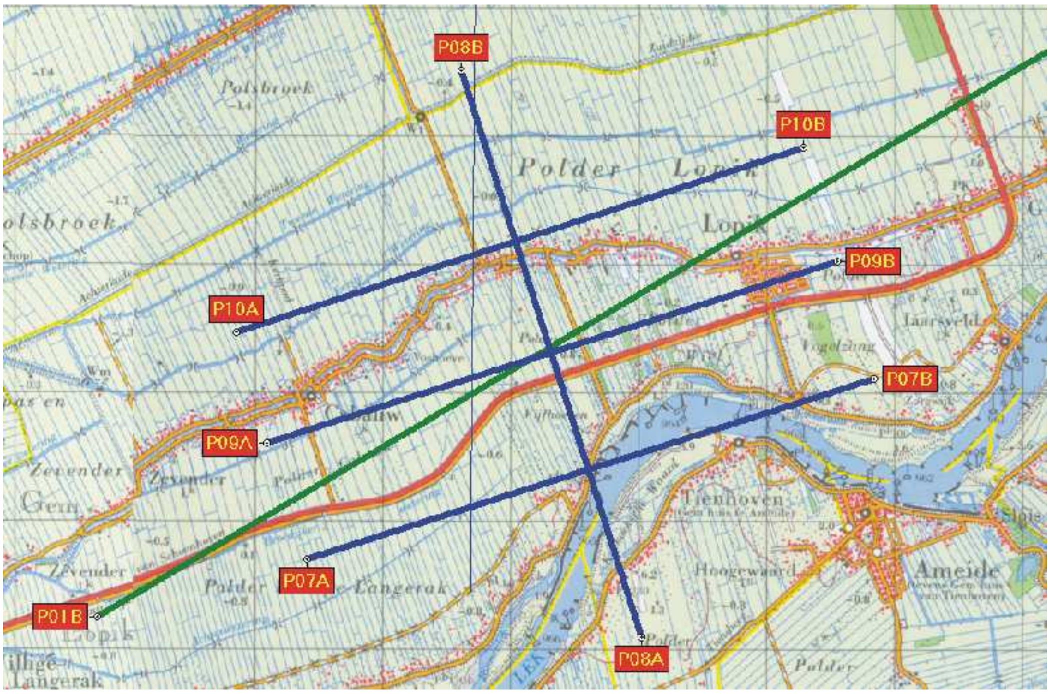

Figure 14. EAGLE2006 Cabauw grassland flight line pattern for AHS GSD2.1m (lines in blue) and GSD6.9 m (lines in green) surveys.

Table 13. UTM WGS84/ETRS89 Flight lines co-ordinates for EAGLE optical survey, June 13th 2006.

	Starting point			Ending point		
Line	Easting	Northing	Zone	Easting	Northing	Zone
P01	686 129	5 794 169	31U	628 780	5 757 073	31U
P02	688 660	5 781 019	31U	678 511	5 806 749	31U
P03	688 055	5 781 925	31U	682 378	5 794 641	31U
P04	681 004	5 792 091	31U	685 265	5 793 996	31U
P05	681 342	5 791 319	31U	685 597	5 793 220	31U
P06	681 765	5 790 631	31U	685 877	5 792 491	31U
P07	630 405	5 757 578	31U	634 798	5 759 129	31U
P08	633 048	5 757 059	31U	631 481	5 761 417	31U

P09	630 058	5 758 465	31U	634 479	5 760 026	31U
P10	629 795	5 759 324	31U	634 179	5 760 906	31U
P11	689 641	5 780 443	31U	687 192	5 785 919	31U

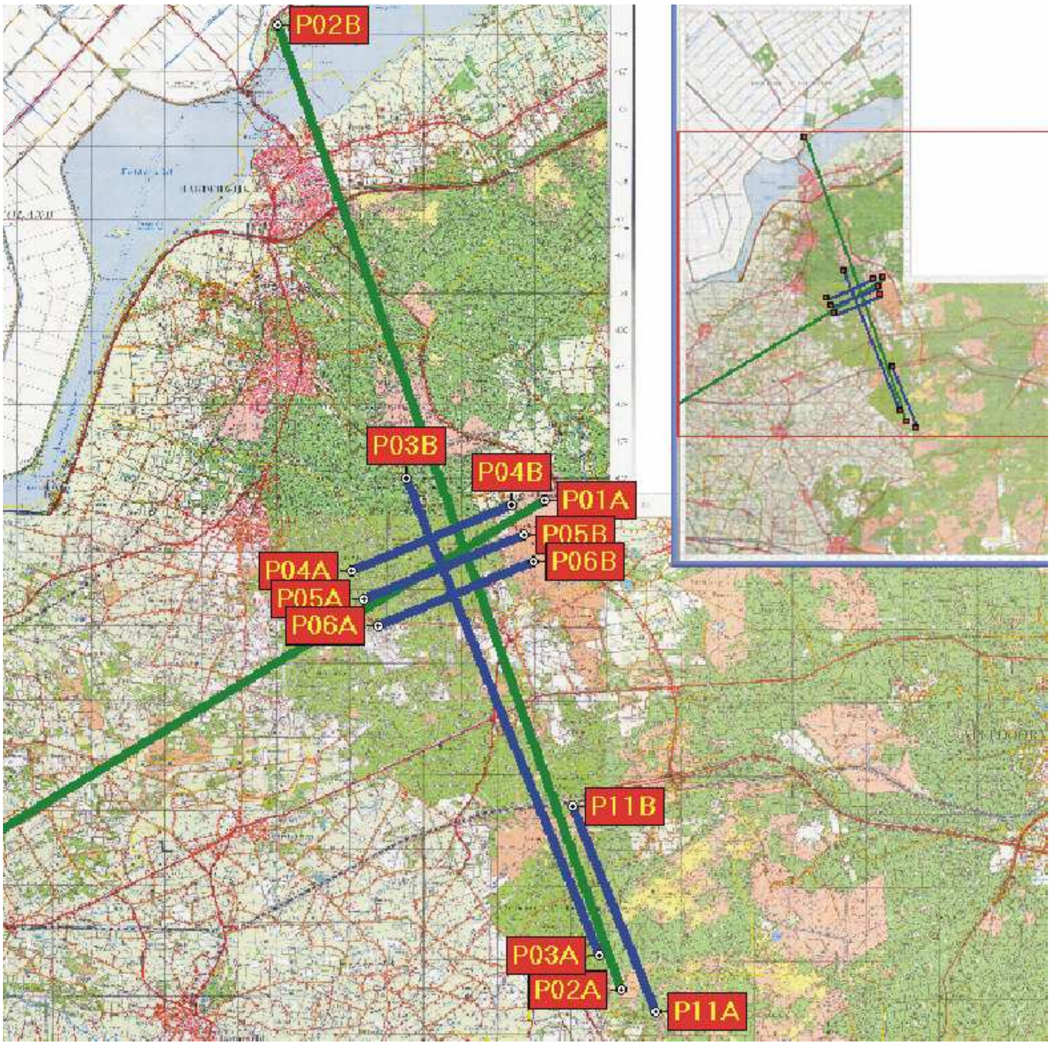

Figure 15. EAGLE2006 Speuld- and Loo-bos forest flight line pattern for AHS GSD2.1m (lines in blue) and GSD6.9 m (lines in green) surveys.

Since the Air Traffic Control (ATC) did not allow line P03 to be completed at side A, because this area is an active military terrain. Another attempt was made but again the ATC did not allow the line to be completed. In addition, line 7 was repeated setting the internal thermal reference source T_{BB2} to 50°C.

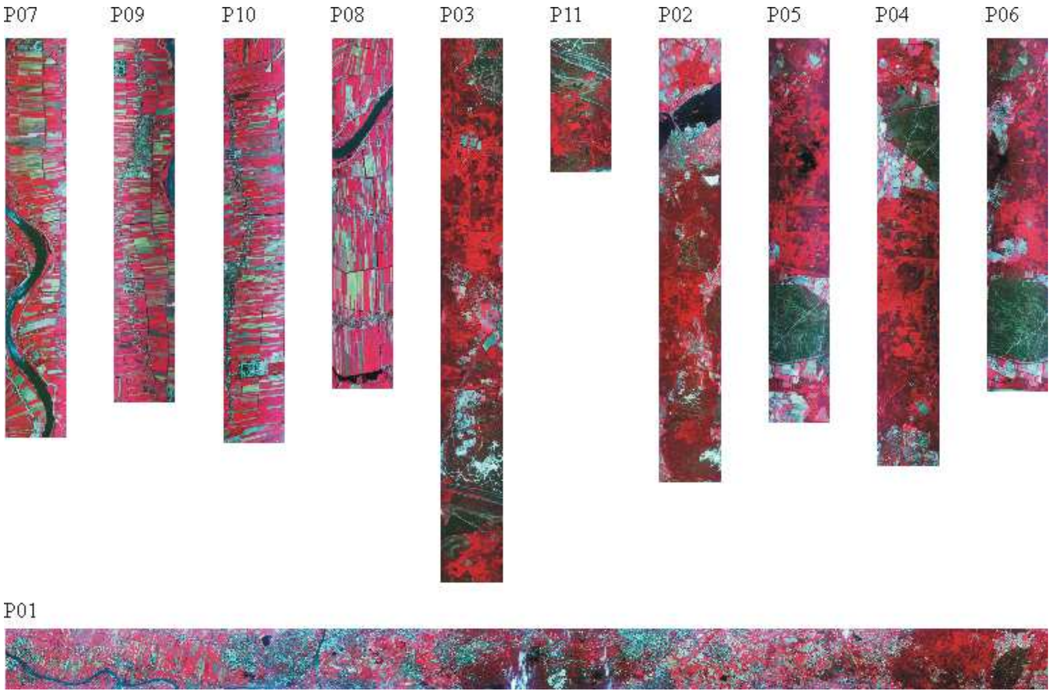

Figure 16. Quicklooks reported by INTA of AHS channels 4-8-15 (R-G-B) acquired on 13-06-2006

Table 14. Flight lines characteristics. * Indicates that the line is not included in Figure 16. Speed in knots, and altitude in feet above ground level.

Line	P07	P09	P10	P07*	P08	P03	P03*	P11	P02	P01	P05	P04	P06
Heading	072	252	072	072	342	158	158	158	161	240	068	248	068
Time	09:57	10:06	10:13	10:24	10:34	10:51	11:03	11:13	11:34	11:50	12:24	12:32	12:41
Speed	142	137	140	140	138	137	135	140	142	140	139	136	140
Altitude	3237	3234	3225	3205	3217	3384	3420	3400	9300	9248	3365	3317	3441

4.1.3 AHS Data processing

Table 15 provides a list of the standard products potentially produced by INTA. Table 16 lists the data specifications.

Table 15. INTA AHS standard data products.

Identification	Radiometric correction	Geometric correction
L0/L1a raw data	No processing	No processing
L1b At-sensor radiance	From DN to Ls using test bench + Labsphere data for VIS-NIR-SWIR and sensor black-bodies for TIR bands	No processing
L1c Geo-referenced at-sensor radiance	From DN to Ls using test bench + Labsphere data for VIS-NIR-SWIR and sensor black-bodies for TIR bands	Direct geo-referencing using PARGE
L2c Geo-referenced reflectance & apparent temperature	From Ls to ρ and Tb using ATCOR 4	Direct geo-referencing using PARGE

For EAGLE2006 the data levels produced are L1a, L1b and L1c.

Table 16. INTA AHS data specifications.

Port	Radiometric resolution	Radiometric accuracy
1. VIS/NIR	NedL< 0.25 w/(m2 sr um) (in 90% of the bands) *NedL = stdev NDbb in image*	< 2% (at sensor radiance)
2. SWIR, including AHS21	NedL< 0.4 w/(m2 sr um) (in 90% of the bands) *NedL = stdev NDbb in image*	< 5% (at sensor radiance)
3. MIR	N/A	N/A
4. TIR	NedT < 0.33 ºC in at least 5 bands *NedL = stdev NDbb for a 32 lines moving window in datafile*	< 0.5ºC (at sensor apparent temperature)

No radiometric or spectral specification is given for Port 3 (3 to 5 micrometers). Two separate files are per scene in ENVI format, with filenames:

AHS_YYMMDD_ZONEX_PNNHD_L10020_PT12.raw / .hdr (Port 1 & 2)

AHS_YYMMDD_ZONEX_PNNHD_L00120_PT34.raw / .hdr (Port 3 & 4)

Example: AHS_060613_EAGLE_PA3BD_L10020_PT12.raw

In addition, Applanix AV410 attitude and position per scanline computed by POSPAC, in ZI-Imaging format, cartographic system UTM, datum WGS84; orthometric height computed with POSPAC using EGM96 is delivered. The attitude and position data accuracy is better than 1 pixel. There is one file per scene, with example filename: "AHS_060613_EAGLE_PB7BD_L0R000_PTT.csv". The repetitions of P03 and P07 are also processed and delivered, so that finally 13 image files are available.

Furthermore, Image Geometry Files (IGM), describing the ground UTM position of each imaged pixel, in ENVI format are available. There will be an IGM file for each scene (the same IGM file is used for PT12 and PT34 files). The IGM files are then used in ENVI to generate georeferenced products from L1b data using GLT or SuperGLT tools.

Auxiliary files are a text file containing radiometric performance (NedL/NedT and SNR) and calibration coefficients (slope, gain and offset per scene and per spectral band). Furthermore Metadata for the AHS image files is provided in one XML file per scene and processing level, INTA profile (according to ISO19115:2003). No metadata is provided for the Applanix data or the auxiliary files.

4.2 CASI-1500 acquisitions

The commercial CASI-1500 (Compact Airborne Spectrographic Imager) system (Fig. 17) developed by ITRES is a calibrated remote sensing instrument designed to measure and record spectral reflectance differences across a specified wavelength region. The CASI-1500 generates a digital image in the chosen spectral wavelengths along a swath representing an individual flight line.

Figure 17. From left to right; ITRES CASI-1500 sensor, operating system and calibration unit (Not to scale).

The CASI-1500 is typically installed for operational use on a variety of fixed wing or rotor-based aircraft. This instrument is integrated with an Inertial Measurement Unit (IMU) that records aircraft motion (roll, pitch and heading) using gyroscopes and accelerometers and also records aircraft position using differential GPS. A geometric calibration flight was conducted before acquisition to determine the offsets between the CASI-1500 sensor and the IMU. This allows measurements made by the IMU and GPS to be referenced to the CASI-1500 sensor head.

4.2.1 CASI-1500 Characteristics

The characteristics of the sensor are such that a full calibration of the system enables data to be provided in spectral radiance values. The system has a free spectral range of 650nm, adjustable between 400 and 1050nm of which the spectral programmability can be adjusted as to suit various applications. The sensor has a high spatial (25cm to 1.5m) and spectral resolution (288 bands), with long dwell times yielding high signal-to-noise ratios.

Table 17. CASI-1500 Characteristics

Field of View	40.5 degrees across-track over 1490 pixels
Spectral Range	650nm between 400 and 1050nm
Spectral Samples	288 at 2.2nm intervals (2.5 nominal)
Aperture	F/3.5 to F/18.0
Dynamic Range	16384:1 (14 bits)
Noise Floor	3.0 DN
Signal to Noise Ratio	800:1 Peak
Calibration Accuracy	To Be Determined
Data Throughput	5 Megapixel/sec

4.2.2 CASI Flight data and settings

The CASI sensor was put on board of the INTA plane and therefore, as described before, the flight characteristics (coordinates and timings) are identical to those mentioned in Paragraph 4.1.2 (see also Table 18).

Table 18. CASI flight characteristics and settings.

Flight data	
Aircraft	CASA 212-200 N/S 270, *"Paternina"*
Nominal aircraft ground speed	GS 140kts (72ms^{-1})
Altitude above ground level	2.4m Survey AGL3200ft (975m)
	6.9m Survey AGL9000ft (2743m)
CASI settings	
CASI-1500 detector head installation	On main cabin floor rear window
CASI-1500 positioning & orientation	INS/GPS Applanix POS/AV 410 V5
CASI-1500 IMU installation	On CASI plate. ACTIVE
CASI-1500 set up lever arms	
CASI-1500 spectral config. (see note 1)	60 channels
CASI-1500 IFOV/FOV	0.49 mrad / 39.34 degrees
Number of pixels per line	1490 pixels
CASI-1500 pixel size @nadir – GSD	
Across track	0.48m @ AGL3200ft (975m)
	1.34m @ AGL9000ft (2743m)
Along track	1.29m @ 60 bands
CASI-1500 swath	697m @ AGL3200ft (975m)
	1961m @ AGL9000ft (2743m)
CASI-1500 across-track overlap	N/A
CASI-1500 calibration date	N/A

Note 1: Number of channels can be selected in order to optimise SNR depending on illumination of the site to survey. Further information about CASI-1500 can be found at www.itres.com

Due to the priority given to the AHS specifications, CASI-1500 characteristics had to be adjusted to meet the conditions induced by AHS settings. As such, the data were collected at 60 spatial bands, see Table 19. A quicklook is shown in Fig. 18.

Table 19. CASI-1500 VNIR Hyperspectral bandset.

b1	406.3nm+/-	5.8nm		b31	664.5nm+/-	3.5nm
b2	416.9nm+/-	4.6nm		b32	671.6nm+/-	3.5nm
b3	427.4nm+/-	5.8nm		b33	677.4nm+/-	2.3nm
b4	438.0nm+/-	4.6nm		b34	682.1nm+/-	2.3nm
b5	447.3nm+/-	4.6nm		b35	686.8nm+/-	2.3nm
b6	456.7nm+/-	4.6nm		b36	691.5nm+/-	2.3nm
b7	467.3nm+/-	5.8nm		b37	696.3nm+/-	2.3nm
b8	477.8nm+/-	4.6nm		b38	701.0nm+/-	2.3nm
b9	487.2nm+/-	4.6nm		b39	706.8nm+/-	3.5nm
b10	496.6nm+/-	4.6nm		b40	715.1nm+/-	4.6nm
b11	506.0nm+/-	4.6nm		b41	724.5nm+/-	4.6nm
b12	516.5nm+/-	5.8nm		b42	733.9nm+/-	4.6nm
b13	527.1nm+/-	4.6nm		b43	743.3nm+/-	4.6nm
b14	534.1nm+/-	2.3nm		b44	753.8nm+/-	5.8nm
b15	540.0nm+/-	3.4nm		b45	764.4nm+/-	4.6nm
b16	545.9nm+/-	2.3nm		b46	773.8nm+/-	4.6nm
b17	550.6nm+/-	2.3nm		b47	783.2nm+/-	4.6nm
b18	555.3nm+/-	2.3nm		b48	793.8nm+/-	5.8nm
b19	560.0nm+/-	2.3nm		b49	804.4nm+/-	4.6nm
b20	564.6nm+/-	2.3nm		b50	813.8nm+/-	4.6nm
b21	569.3nm+/-	2.3nm		b51	823.2nm+/-	4.6nm
b22	576.4nm+/-	4.6nm		b52	833.7nm+/-	5.8nm
b23	587.0nm+/-	5.8nm		b53	844.3nm+/-	4.6nm
b24	597.5nm+/-	4.6nm		b54	853.7nm+/-	4.6nm
b25	606.9nm+/-	4.6nm		b55	863.1nm+/-	4.6nm
b26	616.3nm+/-	4.6nm		b56	873.6nm+/-	5.8nm
b27	626.9nm+/-	5.8nm		b57	884.2nm+/-	4.6nm
b28	637.5nm+/-	4.6nm		b58	894.8nm+/-	5.8nm
b29	646.9nm+/-	4.6nm		b59	939.3nm+/-	10.5nm
b30	656.3nm+/-	4.6nm		b60	968.6nm+/-	11.6nm

Figure 18. Sample of CASI-1500 data as observed over the Cabauw site (Tower is clearly seen in middle left part of the image). Natural Color Composite R-G-B, channels 29-17-05, see Table 19.

4.2.3 CASI Data processing

The data is in the PCIDisk format, band interleaved by pixel, in a 16-bit unsigned integer format. All images are geocorrected to UTM coordinates (WSG84 Datum), zone 30. The imagery has not been geocoded using a DEM; instead an average terrain height was used for each flight line.

The files are named as follows; Sensor Date Project_Line#.pix. As an example, the file CASI0613_EAGLE_L10.pix indicates the file is CASI1500 data acquired on June 13th (2006) in support of the EAGLE project. Each file is accompanied by an identically named Geographic Lookup (.glu) file containing UTM coordinates for each pixel in the image file. A sample .glu header file is provided below.

Sample Header of Geographic Look Up (.glu) File

CASI0613_EAGLE_L10.glu.hdr
:::::::::::::
ENVI
description = {
Ground coordinates Lookup Channels for CASI0613_EAGLE_L10.pix, size: 157080000, [Fri Oct 27 17:38:27 2006] }
samples = 1500
lines = 6545
bands = 2
header offset = 0
file type = ENVI Standard
data type = 5
interleave = BIP
sensor type = ITRES
byte order = 0
pixel size = { 1.000, 1.000, units=meters }

band names = {
EASTING_CHANNEL: Easting coordinate of image pixel,
NORTHING_CHANNEL: Northing coordinate of image pixel }
default bands = { 1 }

However, the bandset description of Table 20 below, supercedes the band values in the CASI1500 image header, if different.

Table 20. CASI-1500 bandset description overview.

Geo-corrected File name	Image dimensions	File size
	Rows x Cols x Channels	(Giga-Byte)
CASI0613_EAGLE_L10.glu	6545 x 1500 x 2	0.16
CASI0613_EAGLE_L10.pix	6545 x 1500 x 60	1.18
CASI0613_EAGLE_L11.glu	7520 x 1500 x 2	0.18
CASI0613_EAGLE_L11.pix	7520 x 1500 x 60	1.36
CASI0613_EAGLE_L1.glu	31156 x 1500 x 2	0.75
CASI0613_EAGLE_L1.pix	31156 x 1500 x 60	5.62
CASI0613_EAGLE_L2.glu	12703 x 1500 x 2	0.30
CASI0613_EAGLE_L2.pix	12703 x 1500 x 60	2.29
CASI0613_EAGLE_L3b.glu	9607 x 1500 x 2	0.23
CASI0613_EAGLE_L3b.pix	9607 x 1500 x 60	1.73
CASI0613_EAGLE_L3.glu	9503 x 1500 x 2	0.23
CASI0613_EAGLE_L3.pix	9503 x 1500 x 60	1.71
CASI0613_EAGLE_L4.glu	6605 x 1500 x 2	0.16
CASI0613_EAGLE_L4.pix	6605 x 1500 x 60	1.19
CASI0613_EAGLE_L5.glu	6796 x 1500 x 2	0.16
CASI0613_EAGLE_L5.pix	6796 x 1500 x 60	1.22
CASI0613_EAGLE_L6.glu	6410 x 1500 x 2	0.15
CASI0613_EAGLE_L6.pix	6410 x 1500 x 60	1.16
CASI0613_EAGLE_L7.glu	7184 x 1500 x 2	0.17
CASI0613_EAGLE_L7.pix	7184 x 1500 x 60	1.29
CASI0613_EAGLE_L8.glu	5342 x 1500 x 2	0.13
CASI0613_EAGLE_L8.pix	5342 x 1500 x 60	0.96
CASI0613_EAGLE_L9.glu	6734 x 1500 x 2	0.16
CASI0613_EAGLE_L9.pix	6734 x 1500 x 60	1.21

4.3 ESAR-DLR acquisitions

DLR-HR operates the experimental multi-frequency, multi-polarisation Synthetic Aperture Radar (SAR) system E-SAR onboard a Do228 aircraft. The aircraft Do 228 is operated by the DLR's flight operation institute; they are contributing with the full maintenance of the aircraft, with pilots and one technician. The incidence angle range for all frequencies is ranging between 25 and 55 degrees.

4.3.1 ESAR Characteristics

E-SAR features across track SAR interferometry capabilities at X-band (VV polarisation). Single channel operation in X-band takes place with VV and HH polarisations switched from pass to pass. C-Band data can be acquired either in single channel mode (VV, HH polarisations, pass to pass) or in dual-channel mode with combinations of VV/VH and HH/HV polarisations switched from pass to pass. Fully polarimetric data acquisition is possible in L- and P-bands only. Technical specifications for each of the RF bands are shown in Table 21. The SAR processing ground segment, adapted to E-SAR data at DLR-HR, includes operational modules for DEM generation and geo-coding amongst others. The data products fulfill high quality standards in terms of calibration and geometric accuracy. Aircraft navigation and SAR motion compensation are based on a modern combined DGPS/INS system.

Table 21. E-SAR Technical Parameters.

RF-Band	X Band	C Band	L Band	P Band
RF-centre frequency	9.6 GHz	5.3 GHz	1.3 GHz	350 MHz
Transmit peak power	2.5 kW	750 W	400 W	1000 W
Receiver noise figure	4.0 dB	4.0 dB	8.5 dB	6.0 dB
Antenna gain	17.5 dB	17 dB	15 dB	10 dB
Azimuth beamwidth	17°	17°	18°	30°
Elevation beamwidth	30°	33°	35°	40°
Antenna Polarization	H and V	H and V	H and V	H and V
Acquisition Mode	single pol	dual pol	quad pol.	quad pol.
IF-centre frequency	300 MHz	300 MHz	300 MHz	300 MHz
Max. Signal bandwidth	100 MHz	100 MHz	100 MHz	100 MHz
System bandwidth	120 MHz	120 MHz	100 MHz	100 MHz

4.3.2 ESAR Flight data and settings

Two radar flight tracks were originally designed to cover the sites of interest, which took place on the 15th of June 2006. They were carried out following the original schedule. No additional flights were carried out due to the constraints in budget and the stable phenological conditions over the campaigns period.
However, for the EAGLE2006 Campaign the idea was to fly X-, C-, and L-band configurations, as well as to obtain an X-band DEM. To cover both the grassland and the forest sites a total of 11 tracks had to be flown, cutting the forest as originally planned into a Northern and a Southern section, Table 22.

Table 22. ESAR Flight overview.

#	Tape ID	Site	Band Freq.	Polarisation
1	I06EAGLES0109X1_T01	Cabauw	X	VV
2	I06EAGLES0141X1_T01	Cabauw	C	Syn. PM
3	I06EAGLES0103X1_T01	Cabauw	L	PM
	Southern segment			
4	I06EAGLES0108X1_T01	Loobos	X	VV
5	I06EAGLES0146X1_T01	Loobos	C	Syn. PM
6	I06EAGLES0104X1_T01	Loobos	L	PM
7	I06EAGLES0105X1_T01	Loobos	L	PM
	Northern segment			
8	I06EAGLES0108X1_T02	Speulderbos	X	VV
9	I06EAGLES0146X1_T02	Speulderbos	C	Syn. PM
10	I06EAGLES0104X1_T02	Speulderbos	L	PM
11	I06EAGLES0105X1_T02	Speulderbos	L	PM

The quicklooks of the 11 tracks are provided in Fig. 19a. Fig. 20 shows an image for the Cabauw site.

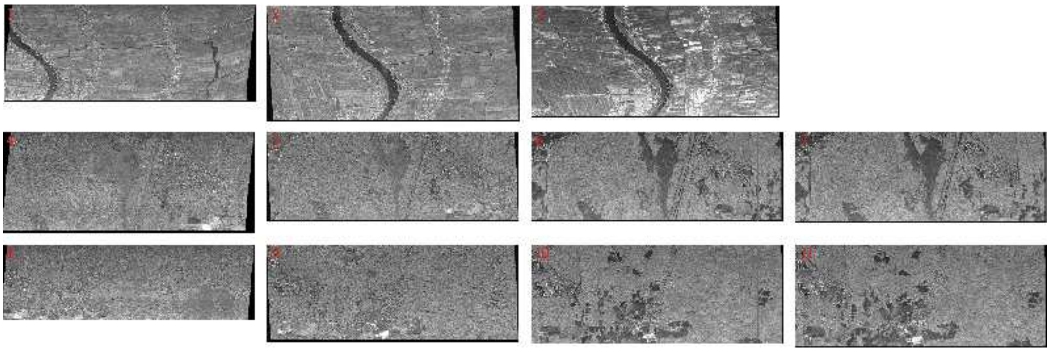

Figure 19. ESAR quicklooks acquired by DLR-HR over the sites of interest on 15th of June 2006. Scne # refers to Table 22.

4.3.3 ESAR Data processing

The E-SAR processing is described herein as subsequent steps with well-defined interfaces, most of which are fully automated. The procedure is divided into the following functional blocks:

- Track-point generation
- Transcription
- Survey-Processing
- Navigation Data Processing
- Tie-point Data Processing (i.e. Corner Reflector Positions)
- Generation of Processing-Setup-Table (Excel-Sheet)
- Full Performance SAR Processing
- Archiving
- Delivery

DLR-HR provided the following radar data products:

Radar Geometry Image Products (RGI)
- Multilook (slant & ground range) & SLC data
- L- & P-band full polarimetric, C-band 2xdual polarimetric, X-band VV-pol.

Geocoded Terrain Corrected Products (GTC)
- WGS-84, UTM projection, zone 50
- Horizontal posting: 2 m
- Incl. DEM (except MAWAS) & Incidence angle map

Geocoded Digital Elevation Products (DEM)
- For each segment with 2m posting (used as input for GTC)
- Mosaic for complete test-site with 5m posting

Repeat-pass interferometric products
- Master & Slave data sets as RGI products
- Including resampled SLC data of slave
- With coherence, interferometric phase, tracks & kz-matrix

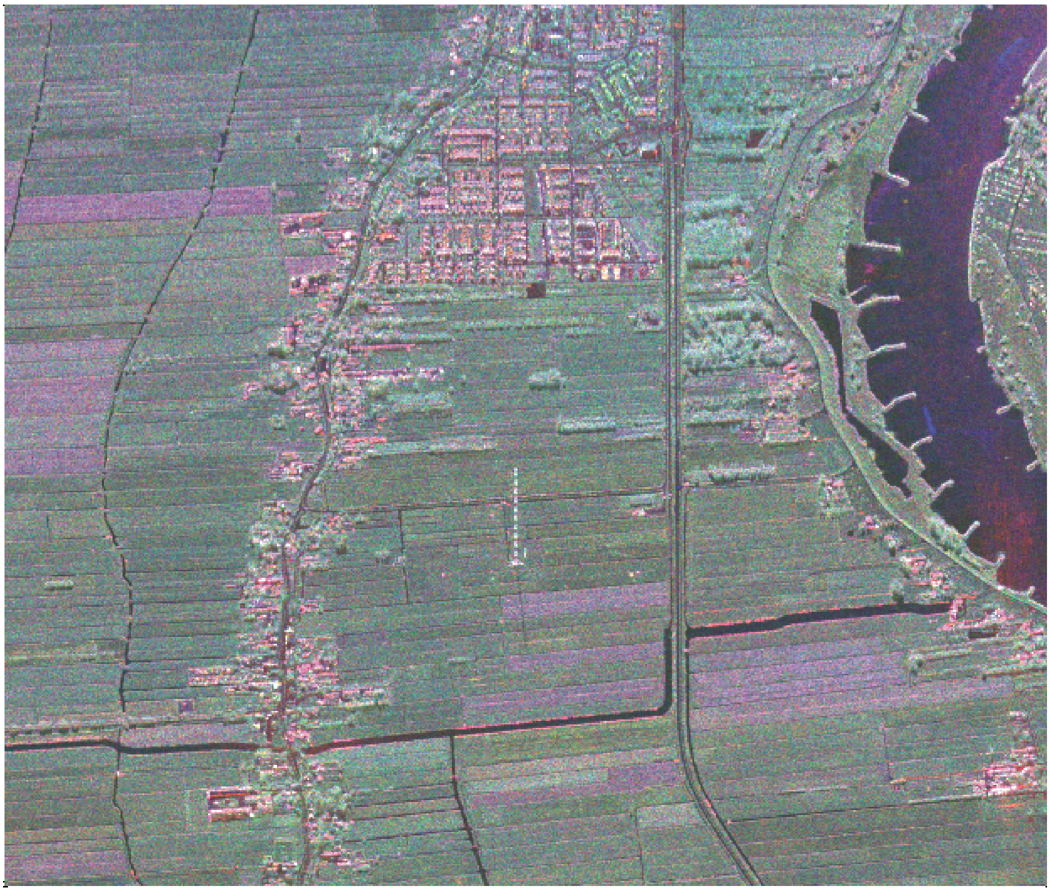

Figure 20. Example zoom over the Cabauw tower site, track # 2, C-band, acquired at June 15th, 2006.

4.4 FLUXES-ISAFoM acquisitions

ISAFoM-CNR is currently operating a flux airplane, the Sky Arrow ERA, which was operated from Teugen Airport during the EAGLE 2006 campaign, Fig. 21.

Figure 21. ISAFoM-CNR Skye Arrow ERA airplane on Teugen airport during the EAGLE Campaign.

The purpose of using these airborne flux measurements here was to develop alternatives to ground-based measurements in order to obtain information required to predict the effects of soil and land use on the surface energy balance and the water balance. Satellite-based algorithms have been developed via flux measurements from an aircraft to estimate vegetation and soil conditions on a regional scale. These flights made measurements in the planetary boundary layer of the fluxes of sensible and latent heat, momentum, and carbon dioxide, plus supporting meteorological parameters such as temperature, humidity, wind speed, and wind direction. Aircraft position, heading, and altitude were also recorded.

Measurements in the Planetary boundary layer (PBL) are the main subject for the use of the Sky Arrow Environmental Research Aircraft. The PBL is the part of the atmosphere that is mostly influenced by the earth's surface and so responds to surface forcing with a timescale of less than one hour. Within the PBL the air flow during the day-time can be assumed as permanently turbulent with vertical and horizontal wind components, enabling a transport of heat and gases. With the measurement of temperature, humidity and gas concentrations in the PBL it is possible to calculate sensible and latent heat fluxes, momentum and carbon dioxide fluxes of the underlying surface. Wind components are vital for calculating any atmospheric fluxes as well as the location of the measurement with its specific vegetation conditions.

4.4.1 ISAFoM Skye Arrow ERA Characteristics and Sensors

Aircraft description

The Sky Arrow 650 TCNS ERA aircraft allows steady flight trajectories at low airspeed down to levels less than 10 m above the ground. Critical in the development of this type of aircraft is exactly its capability to fly at low altitude and low speed, thereby allowing comparisons between flux estimates from ground sites and from the aircraft, and allowing flux estimates at high spatial resolution. The aircraft has been developed to host the Mobile Flux Platform (MFP) which consists of a set of sensors for atmospheric measurements (Fig. 22). A more detailed description of ISAFoM and the Sky Arrow ERA system is provided in Esposito et.al. (2007).

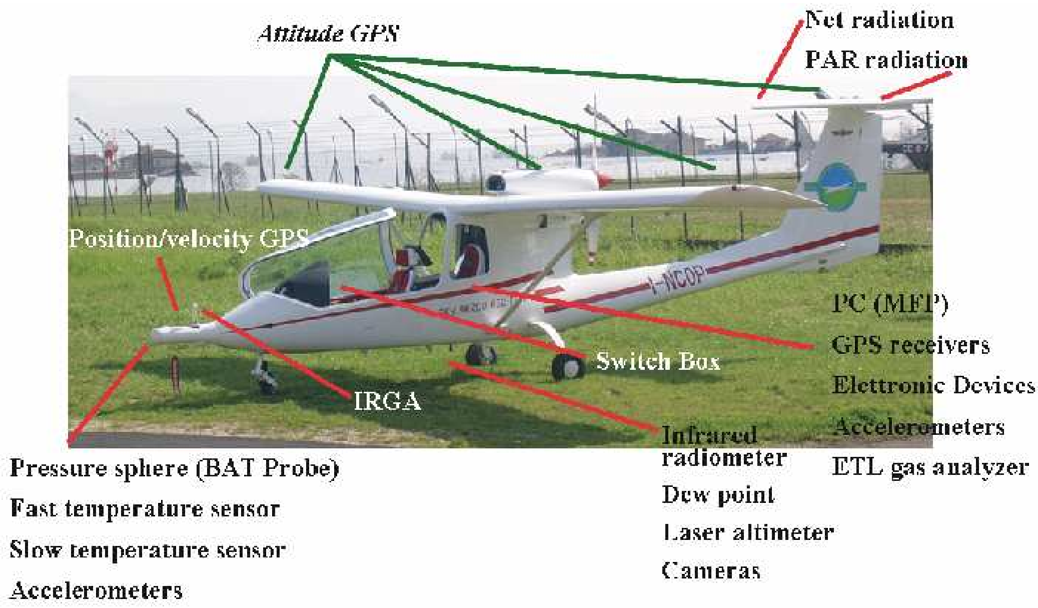

Figure 22. Sky Arrow ERA with sensors and instruments mounted onboard.

The pusher engine configuration is ideal for turbulence measurements, because it allows instruments to be mounted on the nose of the fuselage where they can project into the relatively undisturbed air ahead of the aircraft. In addition, the high wing configuration results in a high vertical separation between the probe and the wing, minimizing flow distortion effects in the probe region due to air circulation around the wing, the so called 'upwash' effect. With its clean aerodynamics due to the pusher configuration, the Sky Arrow is thus able to perform low-and-slow air-surface-exchange measurements.

Sensors on board

The Mobile Flux Platform (MFP) has an onboard computer which is purchased from off-the-shelf components to aid in replacement and troubleshooting if any part of the computer should fail in service. The computer itself consists of a single-board computer and industrial chassis from American Portwell Technologies. Two PCI serial cards from Quatech and a custom ISA card finish the system. This computer operates the following sensors:

Best Aircraft Turbulence Probe (BAT): The BAT probe, see Fig. 23, assembly is a system of circuit boards and electronic hardware encased in a weatherproof fiberglass/carbon fiber housing that is mounted on the nose of an aircraft. The probe assembly consists of a pressure sphere with 9 holes used to measure the magnitude and direction of the incident wind vector on the hemisphere. A tapered cone afterbody houses a BAT-REM module that is used for digitizing the analog signals and providing a serial data stream to the host MFP computer, much like the BAT-REM module in the auxiliary box. In addition to pressure measurements, a set of three orthogonal accelerometers is also installed in the pressure sphere to measure high frequency motion of the hemisphere in three dimensions. High and low frequency air temperature measurements are made utilizing a PRT probe and a micro-bead thermister. Static pressure measurements from the pressure sphere round out the BAT probe instrument suite.

Figure 23. Left: The BAT probe. Middle panel shows the laser altimeter whereas on the right the operational diagram of the altimeter is shown.

Laser Altimeter Riegl Ld90-3: This is a laser range finder that is mounted so that is looks downward from the bottom of the aircraft. The laser reports distance at programmable time intervals (up to 100 Hz) via an RS-232 serial port. Data is acquired through one of the eight serial ports on the Quatech ESC-100-D9 eight-port serial card in the MFP computer. An electrical pulse generator periodically drives a semiconductor laser diode sending out infrared light pulses, which are collimated by the transmitter lens. Via the receiver lens, part of the echo signal reflected by the target hits a photodiode which generates an electrical receiver signal. The time interval between the transmitted and received pulses is counted by means of a quartz-stabilised clock frequency. The calculated range value is fed into the internal microcomputer which processes the measured data and prepares it for range (and speed) display as well as for data output.

Accelerometers (IC Sensors): The accelerometer consists of a silicon micro machined accelerometer with signal conditioning electronics in a lightweight housing that can be easily attached to a mounting surface. On the aircraft are mounted two three dimensional set of accelerometers, on the nose of the aircraft and in the back seat in the auxiliary box near the centre of gravity (Fig. 24).

Figure 24. Accelerometer (left) and GPS's for aircraft position (middle) and pitch, roll and heading angle (right) with respect to the Earth.

Satellite positioning systems: The NovAtel OEM4-G2 RT-20 GPS system is used to measure the position and velocity of the aircraft using differential corrections at 10 Hz. The antenna for this system is mounted on the top of the BAT probe assembly. Data is acquired through one of the eight serial ports on the Quatech ESC-100 eight-port serial card in the MFP computer.

Javad AT4 GPS attitude system is used to measure the pitch, roll, and heading angle of the aircraft with respect to Earth at 20 Hz. The system utilizes four antennas to make its attitude measurement. The first antenna is mounted on top of the Sky Arrow just behind the cabin. The second is mounted on top of the vertical fin and horizontal stabilizer. The third is mounted on top of the left wing near the wing/strut junction, and the fourth is mounted on top of the right wing near the wing/strut junction. Data is acquired through one of the eight serial ports on the Quatech ESC-100 eight-port serial card in the MFP computer.

Open-path analyzer IRGA Licor-7500: The LI-7500 is a high performance, non-dispersive, open path infrared CO2/H2O analyzer designed for use in eddy covariance flux measurement systems (Fig. 24). Some of the LI-7500's important features include:

Simultaneous measurements of CO2 and H2O in the free atmosphere.

High speed measurements. Internal 150 Hz measurements are digitally filtered to provide a true 5, 10, or 20 Hz bandwidth.

Withstands exposure to rain or snow without damage or calibration shift.

Figure 19. the open path gas analyzer (left) and it's electronics (middle). right panel shows the EdgeTech 200 DewTrack.

EdgeTech 200 DewTrack (Tdew): The model 200 DewTrack® Humidity transmitter is a low power, blind transmitter which consists of a sensor probe and an electronic control unit. The control unit is housed in a plastic or aluminium enclosure. This instrument combines the inherent accuracy, reliability, and long term stability of optical chilled mirror technology with an advanced electro-optic sensing scheme. The model 200 provides continuous and repeatable humidity measurements.

Radiation sensors (Fig. 25):

Radiation Energy Balance Systems (REBS) Q*7: The Q7 is an high-output thermopile sensor that generates a millivolt signal proportional to the net radiation level, that is the algebraic sum of incoming and outgoing all-wave radiation (i.e. short-wave and long-wave components). Incoming radiation consists of direct (beam) and diffuse solar radiation plus long-wave irradiance from the sky. Outgoing radiation consists of reflected solar radiation plus the reflected long-wave component. The sensor is mounted in a glass-reinforced plastic frame with a built-in level. A ball joint is supplied on the stem to facilitate leveling. The sensor surface and surrounding surfaces are painted flat black to reduce reflections within the instrument and to achieve uniform performance over reflective and non-reflective surfaces. Sensor surfaces are protected from excessive convective cooling by hemispherical polyethylene windshields. Polyethylene is used for the windshield material because it is transparent to both long and shortwave energy. The windshields are open to the atmosphere through a desiccated breather tube to prevent the domes from collapsing at night. A mounting stake located away from the tower to decrease shading and interference is recommended. Net radiation measurement height is typically between 1 and 3 m.

Figure 20. From left to right the net radiometer, the Licor 190SA and the Everest radiometers are shown.

Licor 190SA: In the photosynthesis process plants use energy in the region of the electromagnetic spectrum from 400-700 nm. The radiation in this range, referred to as Photosynthetically Active Radiation (PAR), can be measured in energy units (watts m-2) or as Photosynthetic Photon Flux Density (PPFD), which has units of quanta (photons) per unit time per unit surface area. The units most commonly used are micromoles of quanta per second per square meter (mmol s-1 m-2).

Infrared thermometer Everest Interscience 4000.4 ZL: The infrared thermometer measures the radiant energy in “thermal infrared” portion of the spectrum, from where is possible to recover the target temperature. The sensor allows temperatures measured from -40°C to 100°C, with the accuracy of 0.1°C.

Thermal camera FLIR Thermovision A40M (Fig. 26): The FLIR A40M thermal infrared camera is FLIR long wave, handheld, Focal Plane Array cameras that are capable of temperature measurement. It is based on “bolometer” technology, and allows measurements of electromagnetic radiation relative at the spectrum form 7500 to 13000 nm.

Figure 21. Flir thermal camera and the Duncantech multispectral camera.

Multispectral camera Duncantech MS4100: The Sky Arrow ERA aircraft can operate with two different three-CCD multispectral cameras, the RGB and CIR camera. DuncanTech's MS4100 high-resolution, progressive-scan digital camera for remote sensing, aerial photogrammetry, and high-end color imaging acquires data with a resolution of 1,920 x 1,080 pixels at a rate of 10 frames per second. The RGB camera employs a color-separating prism and three charge-coupled device (CCD) sensors to support red-green-blue. The multispectral “CIR” cameras capture 3 bands of imagery Green, Red, and NIR. Multispectral Images are saved in TIFF image file format with 3 bands per image.

4.4.2 ISAFoM Skye Arrow ERA Flight mission data

The Sky Arrow flux flights were performed over the three sites where towers are present, to compare the airborne fluxes measurements with the towers fluxes measurements, and also to quantify the exchange of carbon dioxide, sensible and latent heat, momentum fluxes between the atmosphere and different vegetated surfaces.

The three sites are respectively:

- Cabauw, with a 213m towers on grassland land-use
- Loobos , with a 23 m tower on forest land-use
- Speulderbos, with a 46 m tower on forest land-use.

The Sky Arrow aircraft performed three missions, the first two on the 13th of June, and the last on the 14th. The first mission was intended to collect data over all the three sites, to have the possibility to evaluate the net exchange of latent and sensible heat fluxes, carbon dioxide and momentum fluxes over different vegetation cover.

The mission plan (Fig. 27) and timing were chosen to have the possibility to merge fluxes data with the hyperspectral data collected by the INTA group.

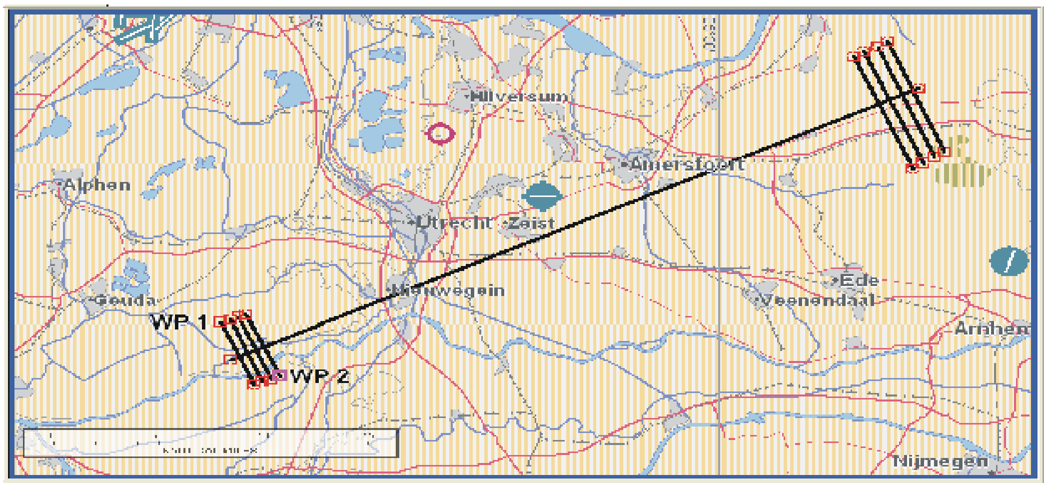

Figure 22. Mission plan.

The second mission was performed on the Speulderbos site, and is composed of flux legs at different levels to evaluate the vertical divergence of fluxes.

The third mission was performed the day after, to have information about the fluxes in very different conditions, since between the 13th and the 14th there were strong differences in ambient temperature and humidity. In Table 23 the flights performed with auxiliary information are reported.

Table 23. Sky ERA flight overview.

Mission ID	**Date**	**Target**	**(UTC)**	**Site**
1	13/06/2006	Fluxes	11:41	Speulderbos, Loobos, Cabauw
2	13/06/2006	Fluxes and divergence	16:00	Speulderbos, Loobos
3	14/06/2006	Fluxes	11:56	Speulderbos, Loobos

Golden day mission;

As in the previous section, the flight on 13th of June 2006 was performed at the same time as the INTA CASA aircraft mission, to collect fluxes information and hyperspectral data simultaneously. The flight tracks are given in Figs. 28-29, where it is also visible the ferry flight between the two principal sites. Problems raised that dial not allow to fly over the Loobos site at low altitude, since the tower is located in a military zone. Therefore the legs flown were not long enough to cover the Loobos tower, but reached until the southern reaches of the Speulderbos.

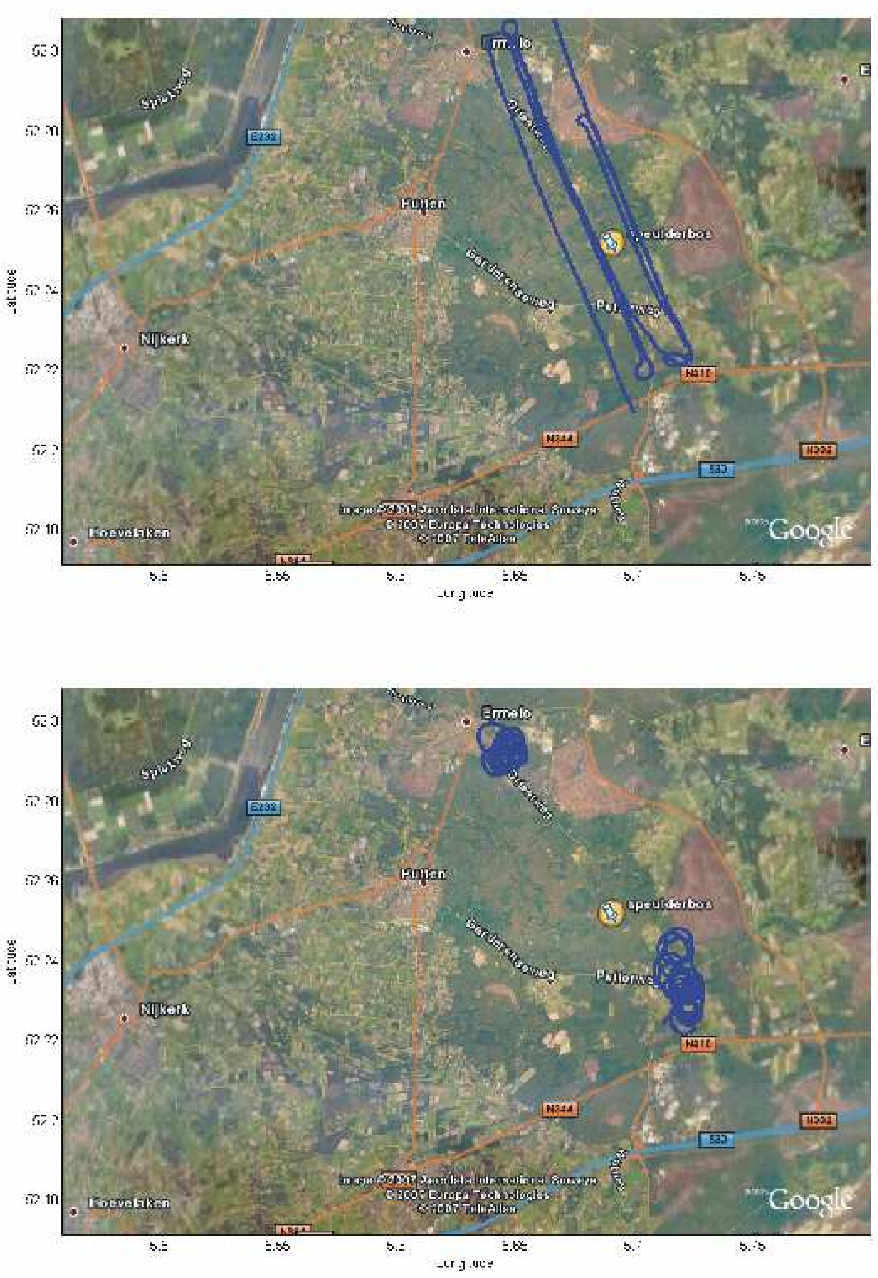

Figure 28. Mission # 1: Speulderbos Northen and Southern transect (upper panel) and profiles (lower panel) flown.

Three PBL profiles were made, the first two close to Speulderbos tower (up to 1000 m; Figure 31, left and middle panels), and the third close to the Cabauw tower (up to 460 m; Figure 31 right panels).

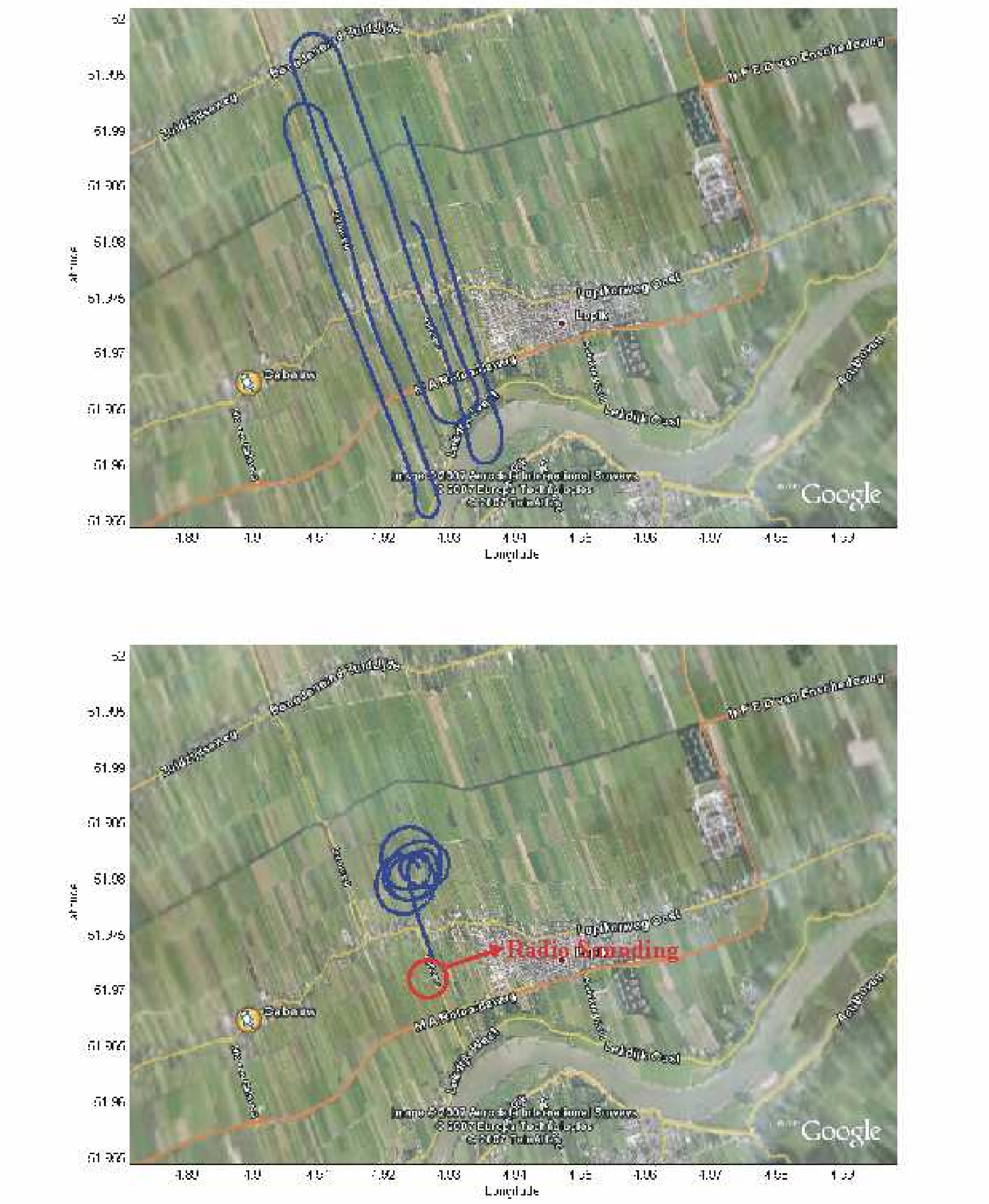

Figure 29. Mission # 1 Cabauw transects (upper panel) and profiles (lower panel) flown.

In the lower panel of Fig. 30 also the location of the Cabauw tower is shown, as well as the location of the radio-sounding performed by the ITC group twin at 9:44 and 14:35 UTC.

4.4.3 ISAFoM Skye Arrow ERA Preliminary results

The first results of the profiles flown in the first mission over the different areas are shown in Figure 31. The left column shows the profiles over the start at the Speulderbos (North), the middle column shows profiles over the Southern part of the Speulderbos, approaching the Loobos area, whereas the right column shows profile measurements over the Cabauw site. Going from the top to the bottom, the 6 panels in each column show Carbon dioxide, air temperature, potential temperature, dewpoint temperature, water content and air density, respectively.

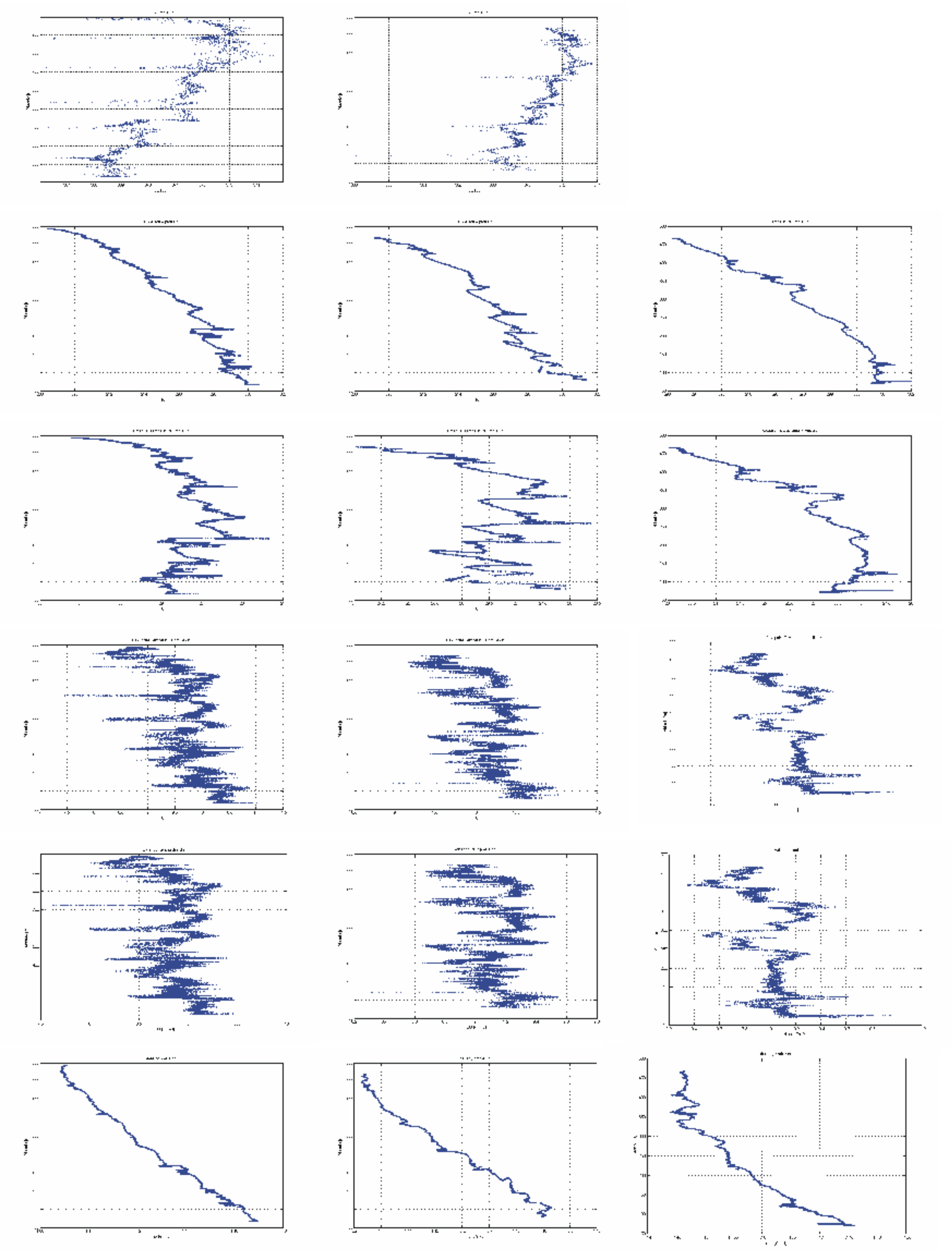

Figure 30. Profiles as measured over the three sites.

In addition, some preliminary results of the transects flown over Speulderbos are presented in Figs. 31-32.

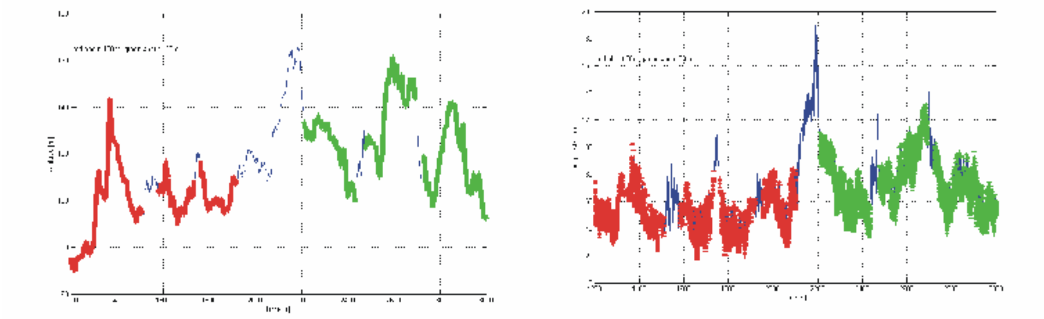

Figure 31. Aircraft altitude during the Speulderbos flight, the flux transects are highlighted.

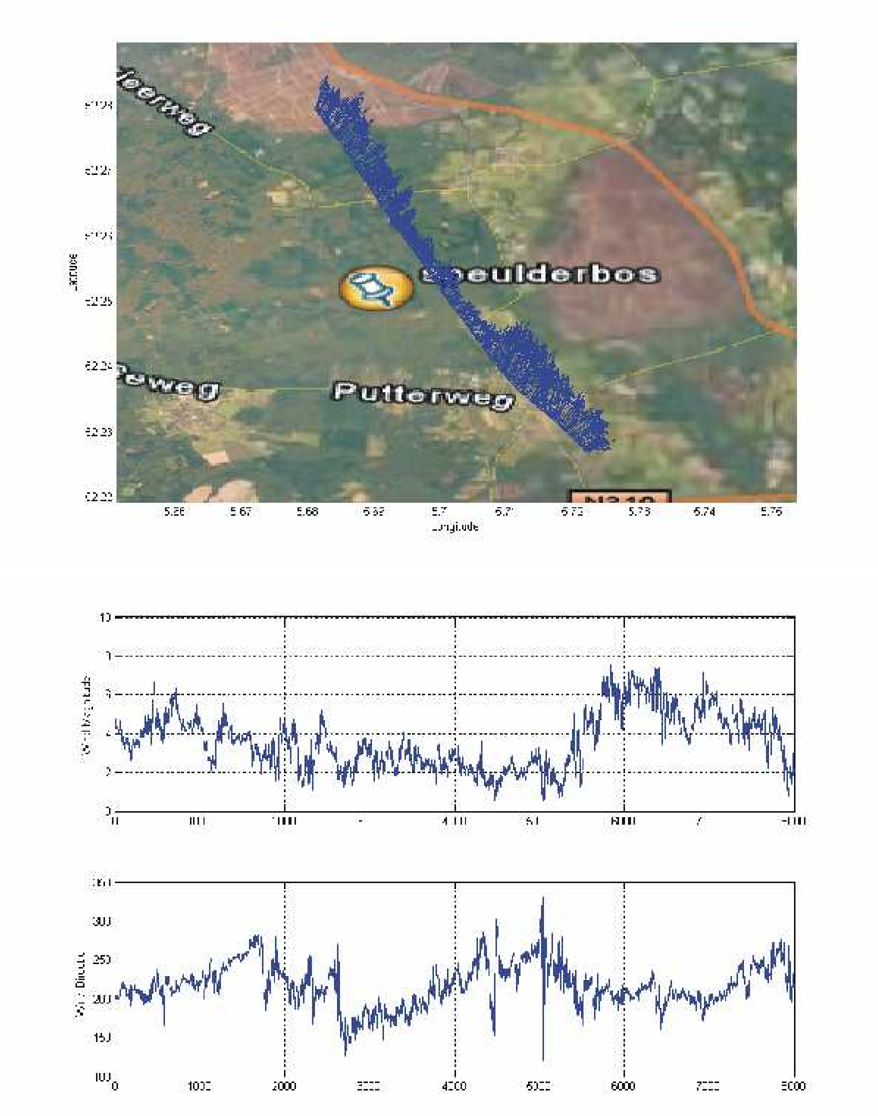

Figure 32. Horizontal windspeed (3-D representation in the upper panel, transect in the middle panel) as well as wind direction (lower panel) over the Speulderbos.

Generally, a first analysis of the airborne fluxes shows good agreement with tower fluxes. However, fluxes divergence shows a slightly unusual behavior on DOY 164 (different footprints along with higher altitude?). Therefore an attempt will still be made to:

1. Improve the data quality analysis (i.e. Integral turbulent test).
2. Carry out a deeper analysis of the footprint for each calculated flux and comparison with tower footprints.
3. Reprocess the data streams with different spatial length (for the Cabauw area).

4.5 MIRAMAP L-band acquisitions

MIRAMAP is a private earth observation company providing an affordable collection, processing and management solution to measure the water situation from the air with Airborne Passive Microwave Radiometry. This technology is capable of quickly producing soil moisture maps of the upper ground layers and in certain conditions to produce depth to water table maps down to several meters of large areas at a time.

The XCL-band Microwave radiometers are used with different wavelengths, parameter models and processing software. The end product is a geo-referenced map that clearly shows potential problem areas. This digital map can be used in combination with existing or concurrently collected digital photography, lidar elevation data and thermal infrared imagery for many different applications.

Due to a delay in the airplane for the installation of the XCL-band radiometer (two beams), MiraMap provided, installed and operated a twin-beam L-band radiometer system that continuously collected Brightness Temperature data from an elevation of 100 meters on the Cabauw tower, looking in Northern direction, antennas facing down at an angle of 10 degrees off nadir, see Fig 33. This included the fabrication of special mount for installation on tower, waterproof installation on tower, and two intermediate inspections to check system operation (was OK). It has been continuously recording from June 8th 14:47 local time until the 19th 10:13 local time, at a 1 minute interval.

The technical system specifications are given in Table 24. This specific L-band sensor was designed for airborne operations, so for this project it had to be altered (special mount, weather proof, power adaptation, etc.). A Data Acquisition System controlled the sensor, wrote the data to a removable memory card and was connected to a GPS receiver for positioning and timing information.

Figure 33. Part of the IFOV of the MIRAMAP L-band sensor, 08 June 2006.

Table 24. Miramap L-band sensor characteristics.

Parameter	Value
Band	L (twin-beam)
Frequency	1.4 GHz
Polarization	H
Sensitivity	1 K
Absolute accuracy	± 5K
3-dB Beam width	25°
Integration time	about 200 ms
Data rate	≤ 1 Hz
Band width	60 MHz
Elevation	15°
Size antenna array	60 x 70 x 20 cm^3
Proposed mounting angle	10-30°
Footprint size at H (m)	2 * H (m)

Unfortunately, the data was not usable due to heavy interference from a strong radio source on the same tower. This was not reported to Miramap prior to sensor installation. Figure 34 below shows the raw data from the sensor over about 11 days. Normally the raw data (blue line) varies between 0 and 5. Most data have value 5, which means the data was heavily saturated. The yellow line, indicating one of the temperatures in the sensor that is used for calibration, shows that the sensor itself worked fine. The variations in day, night, shadow and rainfall temperatures are clearly visible.

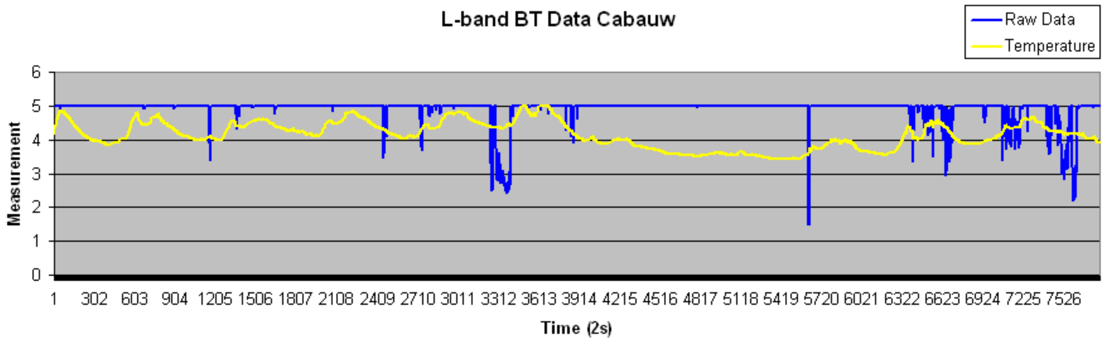

Figure 34. L-band temperature recordings made at the Cabauw tower.

Due to interference of permanent instruments installed at the Cabauw site the observations failed and the deliverables; raw Brightness Temperature data in Kelvin with location and time stamps, could not be delivered.

5 Atmospheric measurements

Knowledge of the atmospheric conditions - its vertical profile and the water content - is required to perform accurate atmospheric corrections of space and airborne observations. Two types of measurements were performed. In-situ atmospheric soundings were carried out during airborne overpasses at the Cabauw site. Furthermore routine measurements carried out at De Bilt, KNMI and at the Cabauw tower site are available as well.

5.1 In situ soundings

5.1.1 Introduction

The Vaisala radiosondes are small sensors integrated in a light box and released into the atmosphere on meteorological helium filled balloons. Pressure, temperature, and humidity are measured at regular intervals and transmitted to the surface by radio signals. The system was completed by a DigiCORA II WM15 Rawinsonde receiver. The position of the sonde can be computed using the hydrostatic equation, which is a function of the pressure. Relative humidity is calculated with the dry and wet bulb temperatures. Wind speed and direction are not directly measured but computed by the ground equipment from the GPS information about the sonde position. One balloon was released approximately a half hour before airplane overpass to characterize the condition of the atmosphere exactly at the time of overpass, since conditions can change rather rapidly.

5.1.2 Team members

Team leader/contact person: Richard Rothe, email: richard.rothe@knmi.nl

Team members: Ard Blenke, Wim Timmermans.

5.1.3 Location

The soundings were made from the Cabauw tower site. Exact coordinates of the ground station were: Cabauw tower site, main office: 51º 58’ 12” North, 04º 57’ 00” East

5.1.4 Timing

The soundings were planned to be released 1 hour before airborne overpasses of INTA and ISAFoM. For the INTA flight on the 13th of June these were at 09:44 UTC and 14:35 UTC time. The release for the ISAFoM flights (on the 14th of June at 14:23 UTC) unfortunately failed, see below.

5.1.5 Measurement protocol

Instruments (Table 25)

Table 25. Vaisala RS-80-15G radiosondes

Parameter	Sensor	Range	Resolution	Accuracy
Pressure	Barocap capacitive aneroid	3 – 1060 hPa	0.1 hPa	0.5 hPa

Temperature	Thermocap capacitive head	-90 - +60 ºC	0.1 ºC	0.2 ºC
Humidity	Humicap thin film capacitor	0 – 100 % RH	1 % RH	< 3 % RH

Procedure

The measurements are based on the use of a free flying balloon-carried radiosonde, transmitting data to the ground station at a frequency of 403 MHz. Pressure, temperature and Humidity (PTU) are measured by sensors in the radiosonde, whereas wind is determined by means of GPS navigation satellites. The sonde includes a GPS module for this purpose. The GPS wind finding data are relayed to the ground station for processing and wind vector computation (Fig. 35).

Figure 35. From left to right; inflating the balloon and connecting the sonde, release of the sounding, receiving station and graphical real-time data display.

Data level

Level 1b; Geo-referenced bio-physical data.

5.1.6 Data summary

Figure 36 shows the two sounding profiles.

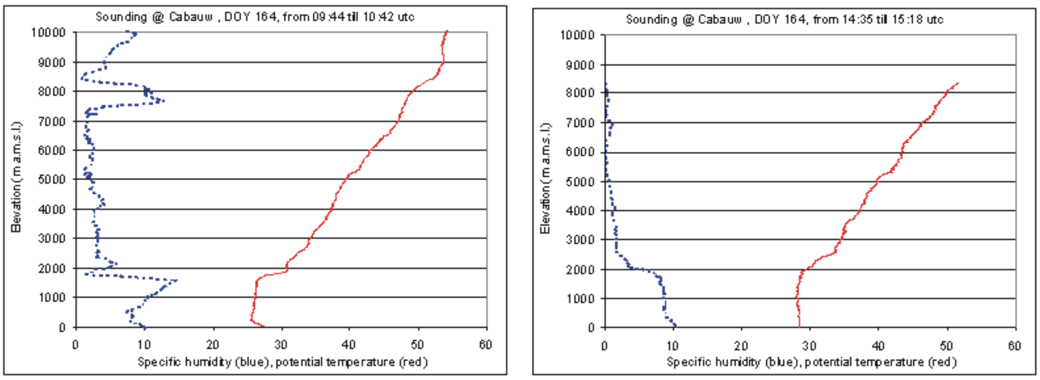

Figure 36. The processed soundings output from 13th of June 2006, Cabauw.

5.1.7 Data quality

The soundings of 13th of June are of excellent quality. The sounding on the 14th of June failed. This was due to the atmospheric stability which caused the balloon to make a drop in height, which causes the recording to stop automatically. Several attempts were undertaken, all the same result.

5.1.8 Prospects

The soundings still need be further analyzed/integrated to obtain total precipitable water values. Furthermore the windspeed and direction still needs to be calculated from the GPS data.

5.2 CESAR observations at Cabauw

5.2.1 Introduction

The KNMI Cabauw tower site is also part of the CESAR (Cabauw Experimental Site for Atmospheric Research) Consortium. This is a consortium of seven national institutes in the Netherlands working together on land-atmosphere and atmospheric research. For the duration of the EAGLE2006 Campaign we have direct access to the data recorded and they are included in the EAGLE2006 database. Additional data is available on request, see below.

5.2.2 Team members

Team leader/contact person: Henk Klein Baltink, email: henk.klein.baltink@knmi.nl

Team members: Fred Bosveld.

5.2.3 Location

The soundings were made from the Cabauw tower site. Exact coordinates of the ground station were: Cabauw tower site, main office: 51º 58’ 12” N, 04º 57’ 00” E.

5.2.4 Timing

The data that is available is recorded during the entire month of June 2006. In principle the data is recorded at 10 minute intervals.

5.2.5 Measurement protocol

Instruments

In principle the following instruments and measurements are available (Table 26):

Table 26. CESAR instruments and data overview.

Instrument	**Parameter**	**Format**
CT75 Ceilometer*	Cloud base	netCDF
	Backscatter profile	netCDF
Total Sky Imager (TSI)*	TSI images (10 minute interval)	Jpeg
	Analysed images	Png
	Cloud cover	ASCII
Radio soundings, De Bilt*	Temperature	ASCII, NASA Ames

(Twice daily)	Relative Humidity	ASCII, NASA Ames
	Wind-speed	ASCII, NASA Ames
	Wind-direction	ASCII, NASA Ames
Brewer ozone soundings	Ozone content (Twice per week)	Unknown
Wind profiler*	Wind profile	Unknown
LIDAR backscatter	Aerosol vertical structure	Unknown

Procedure

The procedure on how the observations are made is rather variable between instruments, and will not be discussed here. The procedure of obtaining the data is uniform though: if the data is in the EAGLE2006 database the data is indicated with an * and they can be directly accessed. The other data is available on request, which should be made through the team responsible for this: Henk Klein Baltink, email: henk.klein.baltink@knmi.nl while mentioning that you are an EAGLE2006 participant.

Data level

Level 1b; Geo-referenced bio-physical data.

5.2.6 Data summary

Currently no data summary is available.

5.2.7 Data quality

The measurements that are automatically logged have an automatic quality control, which consists of tests of the electronics and of the exceedance of physical limits for the parameter at hand. Some other instruments have no automatic quality control. After the data are stored in the database a manual (on-eye) check is performed and together with information from the logbook data are rejected if appropriate. As such, all data recorded is of excellent quality.

5.2.8 Prospects

There is no need for further processing.

6 Ground radiometric measurements

6.1 Solar range radiometric measurements

6.1.1 Introduction

Optical solar range radiometric measurements were performed with mainly three objectives in mind, see also Table 27, which shows how and where this was accomplished:

- Characterization or reference measurements of different surface types for calibration and validation of Remote Sensing observations.

- Angular measurements.

- Biophysical characteristics of plants and individual leaves.

Table 27. Summary of spectrometric measurement objectives.

Objective	Location	Instrument	Typical target
Reference measurements	Cabauw	GER	Water
			Grass
			Concrete
	Speulderbos	ASD	Sand
			Forest canopy
			Water
			Grass
			Heathland
Angular dependance	Cabauw	GER	Grass
			Young maize
	Speulderbos	ASD	Forest canopy
Biophysical characteristics	Speulderbos	ASD	Leaves
			Branches
Water quality	Harderwijk	ASD	Lake water

6.1.2 Team members

Team leader/contact person: Zoltan Vekerdy, email: vekerdy@itc.nl

Team members: Patrick van Laake, Fang Huang, Nilam Kayasta, Kitsiri Weligepolage, Joris Timmermans, Jose Guzman, Mohammad Abuali.

6.1.3 Location

The measurements focused on several landcover units and therefore took place at various sites, exact coordinates can be found in the EAGLE2006 database. An overview:

- Speulderbos tower (52º15'08.1"N, 5º41'25.8"E)
- Kootwijkerzand (52º10'03.7"N, 5º45'40.4"E)
- Cabauw (51º58'00.0"N, 04º54'00.4"E)
- Harderwijk (52º19'12.0"N, 05º36'12.0"E)

6.1.4 Timing

Field spectrometry is highly dependant on illumination, i.e. on cloudiness and sun angle. As a rule of thumb, measurements were not taken before 10 a.m. and after 4 p.m. to avoid low sun angle. Clouds and atmospheric haze made measurements of backscattered sunlight difficult, on many days impossible. Contact probe was tested for plant measurements, but with limited success. The reference panels were gradually deteriorating in the field due to dirt, which had to be removed. For quantifying the level of deterioration, the panels were cross calibrated in the laboratory at ITC. Details on the schedule of the spectrometry measurements are provided in Table 28.

Table 28. Field spectrometry schedule.

Date	Location	Objective	#	Weather
02-06-2006	All sites	Reconnaissance	N.A.	
10-06-2006	Speulderbos	Reference	204	Ideal
11-06-2006	Speulderbos	Reference	78	Good
12-06-2006	Cabauw	Angular	169	Good
13-06-2006	Cabauw	Reference	30	Good
13-06-2006	Speulderbos	Reference & Angular	224	Good
15-06-2006	Speulderbos	Plant (contact probe)	169	Variable clouds
16-06-2006	Speulderbos	Plant (contact probe)	47	Cloudy
17-06-2006	Speulderbos	Reference	78	Variable clouds
18-06-2006	Speulderbos	Angular	305	Partially cloudy
20-06-2006	Laboratory	Panel calibration	221	
21-06-2006	Laboratory	Panel calibration	181	
22-06-2006	Speulderbos	Plant (from crane)	65	Deteriorating illumination
04-07-2006	Harderwijk	Water quality	170	Good, windy

6.1.5 Measurement protocol

Instruments

Reflected solar spectra were measured by two groups using field spectroradiometers: ASD FieldSpec Pro (Fig. 37 left and middle panel) and GER 3700 (Fig. 37 right panel). Both instruments are sensitive in the range of 400-2500 nm, with a spectral resolution of 1-8 nm.

Figure 37. ASD and GER field spectroradiometers at Kootwijkerzand (middle) and Cabauw (right) respectively.

Procedure

Photos were taken at each measurement site. In good weather conditions, a reference panel measurement was taken and then 5-9 spectra were recorded. In quickly changing illumination conditions, a reference panel measurement was followed by a target spectrum recording and then a white panel as a target. In the spectral analysis, this second white panel measurement serves for determining whether the illumination changed during the measurement.

Attempts were made for angular measurements taken about the forest canopy from a crane. Unfortunately the weather did not make it possible to take measurements of good quality (Fig. 38).

Figure 38. A crane was used for spectral measurements from the forest canopy, the right panel shows a view from the basket of the crane.

Data level

In principle level 1b; Geo-referenced biophysical parameters. Spectral data were saved in ASCII format for providing easy access to them. The pre-processing of the results is going on in the time of the compilation of the present report using Excel, SAMS and MatLab routines.

6.1.6 Data summary

Some characteristic spectra are shown in Fig. 39. The frame of the photos represents an area of 1x1 m^2. On the graphs, the grey lines show the measured spectra, the red line is the spectrum accepted as the characteristic spectrum of the site under consideration.

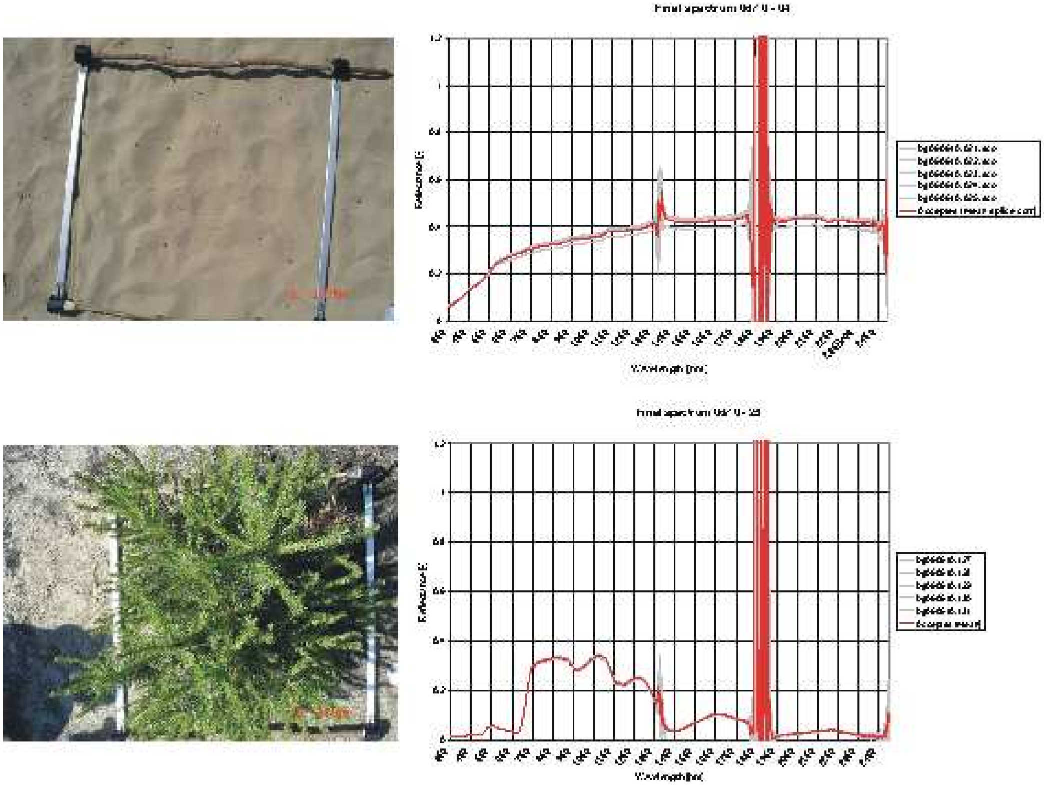

Figure 39. Example spectra of bright sand (upper panels) and of a young pine tree (lower panels).

A comment about the spectra - the weather conditions were not ideal during a large part of the field spectrometry. Special care has to be taken in the processing of the data; it is not recommended to use the raw data without consulting the Team Responsible.

As a result of pre-processing, a characteristic spectrum has to be created for each measured target. These spectra will be further analyzed for achieving the research objectives.

6.1.7 Data quality

See also above; due to weather conditions care needs be taken in further processing of the data.

6.1.8 Prospects

Further analysis is on-going for achieving the research objectives.

6.2 Thermal infrared radiometric measurements

6.2.1 Introduction

A set of thermal radiometric measurements is carried out in the framework of the EAGLE2006 experimental field campaign for the retrieval of bio-geophysical parameters such as land surface emissivity and temperature, which is the main aim of these measurements. To this end, radiometric measurements are carried out in the thermal infrared region with various instruments that include fixed FOV and single band or multi bands radiometers. Therefore, the experimental work of the Global Change Unit of the University of Valencia was the measurement of thermal radiometric temperatures, emissivities, atmospheric radiances, air temperature, temperature transects and angular measurements within the site area.

6.2.2 Team members

Team leader/contact person: J.A. Sobrino, email: sobrino@uv.es

Team members: J.C. Jiménez-Muñoz, G. Sòria, M. Romaguera, M. Gómez, M.M. Zaragoza, J. Cuenca, Y. Julien, A. Barella and M. Atitar.

6.2.3 Location

The measurements focused on the “forest” sites and as such took place at:

- Speulderbos tower (52º15'08.1"N, 5º41'25.8"E)

- Kootwijkerzand (52º10'03.7"N, 5º45'40.4"E)

6.2.4 Timing

The measurements took place at the same time as the optical airborne measurements, which is June 13th, starting at 11:00 and ending at 17:00 hrs. local time.

6.2.5 Measurement protocol

Instruments

Various instruments were used to measure in the thermal infrared domain that include multiband and single band radiometers with fixed field-of-view (FOV) (Table 29, Fig. 40).

Table 29. Technical specifications of the instruments.

Instrument	Spectral Range (micron)	Temperature Range (ºC)	Accuracy	Resolution	FOV
Cimel CE312-1	8 – 13 11.5 – 12.5 10.5 – 11.5 8.2 – 9.2	-80 to 50	0.1	8 mK 50 mK 50 mK 50 mK	10º
Cimel CE312-2	8 – 13 11 – 11.7 10.3 – 11 8.9 – 9.3 8.5 – 8.9 8.1 – 8.5	-80 to 60	0.1	8 mK 50 mK 50 mK 50 mK 50 mK 50 mK	10º
Raytek MID	8 – 14	-40 to 600	1	0.5	30º (6º)
Raytek ST	8 – 14	-32 to 400	1	0.1	7º - 2º
Optris minisight	8 – 14	-32 to 530	1	0.7	3º
NEC TH9100	8 – 14	-40 to 120	2	0.1	22ºx16º
EVEREST 1000		Fixed to ambient	0.3	0.1	

The CIMEL model CE-312-1 and CE312-2 are two radiance-based thermal-infrared radiometers composed of an optical head and a data storage unit. The CE312-1 detector includes one broad-band filter, 8-13 µm, and three narrower filters, 8.2 – 9.2 µm, 10.5 – 11.5 µm and 11.5 – 12.5 µm. The CE312-2 detector includes 6 bands, a wide one, 8-13 µm, and five narrower filters, 8.1 – 8.5 µm, 8.5 – 8.9 µm, 8.9 – 9.3 µm, 10.3 – 11 µm and 11 – 11.7 µm. Temperature of an external blackbody can be measured with a temperature probe, especially for the estimation of absolute emissivity. Different fixed scenarios can be selected to collect data.

Three Raytek Thermalert MID radiometers with FOV of 30º, 30º and 6º respectively were used. They have an infrared sensor with a single band 8–14 µm. They range from -40º up to 600ºC with a sensitivity of 0.5 K and an accuracy of 1K. Three different Licor LI-1000 dataloggers were used to store data from the radiometers set up on the masts.

A thermal camera was used during the field campaign. The NEC Thermo Tracer TH9100 Pro thermal camera has a single band 8-14 µm, with an IFOV of 21º×16º and adjustable emissivity operation mode. It ranges from -40 up to 120ºC with a sensitivity of 0.08K. A visible image can also be acquired simultaneously to the thermal image.

Figure 40. Radiometers and instruments used during the EAGLE006 Campaign.

A calibration source was used to calibrate the radiometers, a calibration source EVEREST model 1000 whose operating range is from 0ºC to 60ºC, with a sensitivity of 0.1K and an absolute accuracy of 0.3 K over entire range.

A diffuse reflectance standard plate, model Labsphere Infragold, was used to estimate the downward radiance.

Procedure

Temporal series of BT were acquired, measuring the canopy under different angles at intervals of 1 and 3 minutes, and measuring the ground at a 1 minute interval in the Speulderbos tower site (Fig. 41). At Kootwijkerzand temporal series of BT were acquired at a 3 minute interval, measuring canopy and sky radiance. The measurement schedule is listed in Table 30.

Figure 41. Instrumental setting of the CIMEL 312-1, Raytek MID 1 & 3 and Thermal Camera NEC at the Speulderbos tower (upper panels) and CIMEL 312-1, RAYTEK MID 1 & 3 and Thermal Camera NEC at the top of the Speulderbos tower and ground measurements with Raytek MID 2.

Table 30. Thermal infrared measurement schedule.

Date	Local time	Site	Instrument	Measurement
12/06/06	12	Laboratory	All	Calibration
13/06/06	11-17	Speulderbos tower	CIMEL CE312-1 measuring canopy	Temporal serie of BT. Frequency=3’
			RAYTEK MID 1 measuring canopy	Temporal serie of BT. Nadir view. Frequency=1’
			RAYTEK MID 3 measuring canopy	Temporal serie of BT. 50º view. Frequency=1’
			RAYTEK MID 2 measuring ground	Temporal serie of BT. Frequency=1’
			NEC TH9100 measuring canopy	Temporal serie of BT. Frequency=1’
13/06/06	12.30 -15.30	Sand near Loobos	CIMEL CE312-2 measuring canopy and sky radiance	Temporal serie of BT. Frequency=3’

Data level

Level 2. Geo-referenced biophysical parameters.

6.2.6 Data summary

Some example observations are shown in Figs. 42-43.

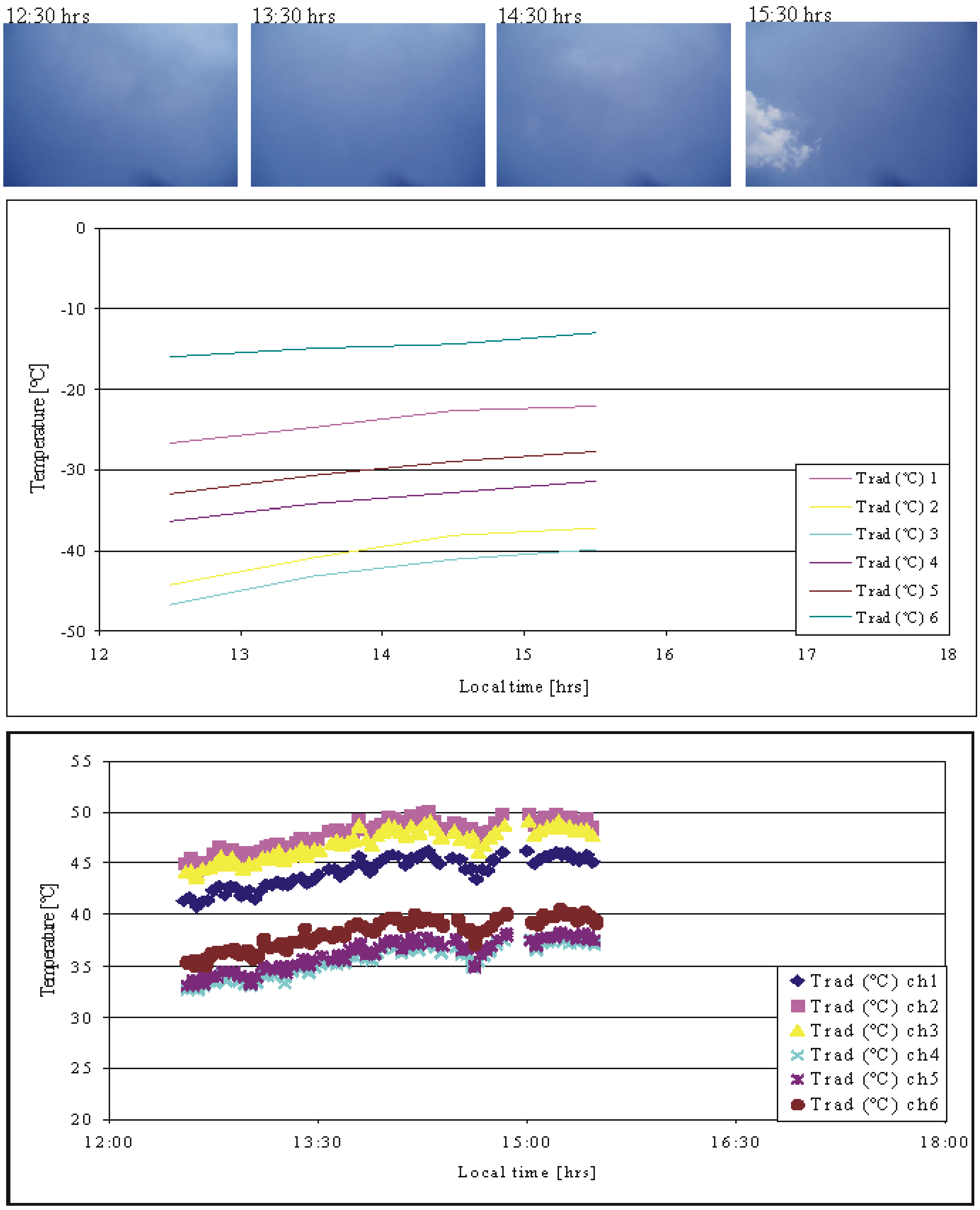

Figure 42. Sky and surface temperature measurements at the Kootwijkerzand using the 6-channel CIMEL CE312-2 radiometer. Also shown are nadir sky photographs taken simultaneously with the radiometer observations.

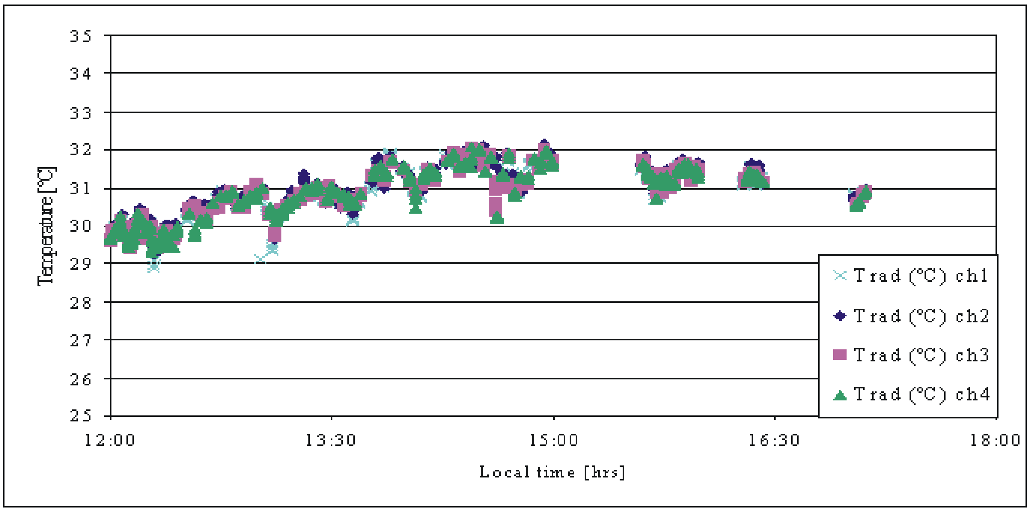

Figure 43. Canopy temperature measurements at the Speulderbos site using the 4-channel CIMEL CE312-1 radiometer.

6.2.7 Data quality

Unknown

6.2.8 Prospects

Future perspectives are:

- Processing of the Field Data, involving analysis of the atmospheric soundings, conversion of radiometric temperatures to LST, emissivity spectrum retrieval and carry out an angular study in the forest.
- Processing of the AHS imagery, involving completing the atmospheric correction, as well as deriving LST, emissivity and evapotranspiration.

Furthermore an analysis of the following satellite data over the test site is foreseen: ASTER, MODIS, AATSR and SEVIRI .

7 Surface energy budget measurements

In order to advance our understanding of land-atmosphere exchanges of water and heat in space and time over heterogeneous land surfaces, in-situ measurements of these exchanges as well as the thermal dynamic states of the atmosphere, soil and vegetation were carried out over several representative land cover units in the area. Since turbulent fluxes occur from scales of an air molecule to regional scale characterized by synoptic circulation and are influenced by both internal biophysical characteristics of the soil and vegetation and external forcing (e.g. solar radiation and wind), the measurements of these fluxes are most challenging over heterogeneous terrain. In addition to cause organized patterns and circulations of turbulent fluxes terrain heterogeneity may also cause local circulation of turbulent fluxes - either due to surface geometrical conditions (roughness) or thermal dynamic conditions (dryness or wetness). A number of ground based instruments was employed for a complete observation and understanding of these turbulent fluxes in space and time.

The two towers at the Speulderbos site were employed for setting up a Large Aperture Scintillometer (LAS) by the WUR Meteorology and Air Quality Group. In addition, on the RIVM tower, the main tower site in the Speulderbos, an eddy correlation system (by ITC) was installed, as well as a standard meteo-station, including a Kipp and Zoonen CNR1 radiometer. A mobile scintillometer, was employed over a grassland cover at the Cabauw site to monitor the sensible heat flux. When these measurements are combined with airborne and satellite data (such as the AHS, CHRIS-PROBA and possibly AATSR), detailed quantification of the characteristics of turbulent fluxes over different surfaces at different scales becomes possible.

Knowledge of the heat transfer is essential in understanding the exchanges of water vapour and energy between a canopy and the surrounding atmosphere. Heat flux estimations over homogeneous areas have been achieved by the use of relatively simple models. The architecture of most vegetation canopies however leads to a complex three-dimensional exchange of heat requiring directional temperature measurements of the different canopy components. Therefore an automated directional acquisition system, a goniometer, was employed for these directional measurements with different sensors, such as thermal cameras and spectrometers. Concurrent to the goniometer measurements the temperatures of different land surface components were monitored. These different components can be divided into 4 pairs (shadowed versus sunlit, leaves versus soil, high versus low leaves, young versus old leaves). This leads to eight canopy component temperatures and two soil component temperatures that were monitored, in order to be implemented into a virtual canopy model for the simulation of directional temperatures.

The meteorological and turbulent flux measurements concentrated on the Speulderbos site because these types of measurements were already standard recorded at the Cabauw site, whereas the directional measurements took place at both sites. However, the goniometer could only be employed at the Cabauw site, due to obvious physical constraints.

7.1 Micro-meteorological measurements

7.1.1 Introduction

This section describes the meteorological measurements carried out at the Speulderbos site. Measurements included standard meteorological measurements at different heights (wind speed and direction, temperature, humidity), sensible heat flux measured with a scintillometer, eddy covariance measurements of heat, water and carbon dioxide transport, contact temperatures of vegetation and soil, soil heat flux, soil moisture content and soil temperature.

Measurements were carried out in and near the 44 m tall tower at the Speulderbos site between 7 and 22 June 2006. In the next sections, the experimental setup and preliminary results of each of the measurements are discussed.

In addition a minor section describes the measurements of the mobile LAS system which was installed at a grassland site next to the Cabauw tower and operated from June 13th I the afternoon till June the 20st of June 2006 in the morning.

7.1.2 Team members

Team leader/contact person: Christiaan van der Tol, email: tol@itc.nl

Team members: Ard Blenke, Oscar Hartogensis, Joris Timmermans, Wim Timmermans

7.1.3 Location

The measurements focused on the Speulderbos site and as such took place at:

- Speulderbos tower (52º15'08.1"N, 5º41'25.8"E)

7.1.4 Timing

The measurements took place from June 7th until the 22nd 2006.

7.1.5 Measurement protocol

Instruments

Table 31 is an overview of the instrumentation at the site. Scintillometer, eddy covariance and radiation measurements were carried out at the top (at 47 m). Other meteorological measurements were carried out just above the canopy crown, around 35 m height. Contact temperatures of different canopy components were measured in the canopy (between 20 and 32 m height), and at ground level. Measurements at ground level were carried out 20 m east of the tower.

Table 31. Meteorological instrumentation Speulderbos. Instruments in italic are owned by Wageningen University, others by ITC.

Datalogger	Sensors	Height (m)
	LAS	47
C23X	CSAT3 sonic anemometer (Campbell Sci. Inc.)	47
	LI7500 gas analyzer (Li-cor Biosciences)	47
CR23X	Combined temperature and humidity sensor (Campbell Sci. Inc.)	43
	Anemometer (Campbell Sci. Inc.)	37
	Wind direction (Campbell Sci. Inc.)	37
	CNR1 radiometer (Kipp and Zonen)	35
	Combined temperature and humidity sensor (Campbell Sci. Inc.)	34
	Combined temperature and humidity sensor (Campbell Sci. Inc.)	27
	9 Contact temperature sensors	17-34
	Barometer (Campbell Sci. Inc.)	1
CR23X	Combined temperature and humidity sensor (MANUF)	1
	3 CS616 for soil moisture (Campbell Sci. Inc.)	-0.05, -0.30 -0.55
	4 soil thermistors for soil temperature	-0.01 -0.03

	-0.08
	-0.90
8 contact temperature sensors	0-1
3 soil heat flux plates HFP01 (Hukseflux)	-0.01

Procedure

All measurements except the scintillometer and eddy covariance were measured and stored at 1-min intervals. The data of the eddy covariance system (20 Hz) were stored on a CR23X (Campbell Sci. Inc.) datalogger of the Wageningen University at 47 m height. Other meteorological measurements in the tower were recorded on a CR23X datalogger at 34 m height, and the measurements on the ground on a CR23X datalogger with an AM16/32 2-wire multiplexer (Campbell Sci. Inc.).

Data level

In the EAGLE2006 data set, the data can be found, as well as the scripts that were used to analyse them and to create the graphs. All analyses were carried out in Matlab. The data are stored in ASCII format.

7.1.6 Data summary

Radiation.

Incoming and outgoing shortwave and long wave radiation was measured with a CNR1 radiometer (Kipp and Zonen, Delft, The Netherlands) at 35 m height. Figure 44 shows incoming (R_{si}) and outgoing (R_{so}) short wave and long wave (R_{Li} and R_{Lo}) radiation as a function of time. The radiation data shown here have been corrected for an overestimate of 10 percent by the sensor. The data will be corrected again after recalibration of the instrument.

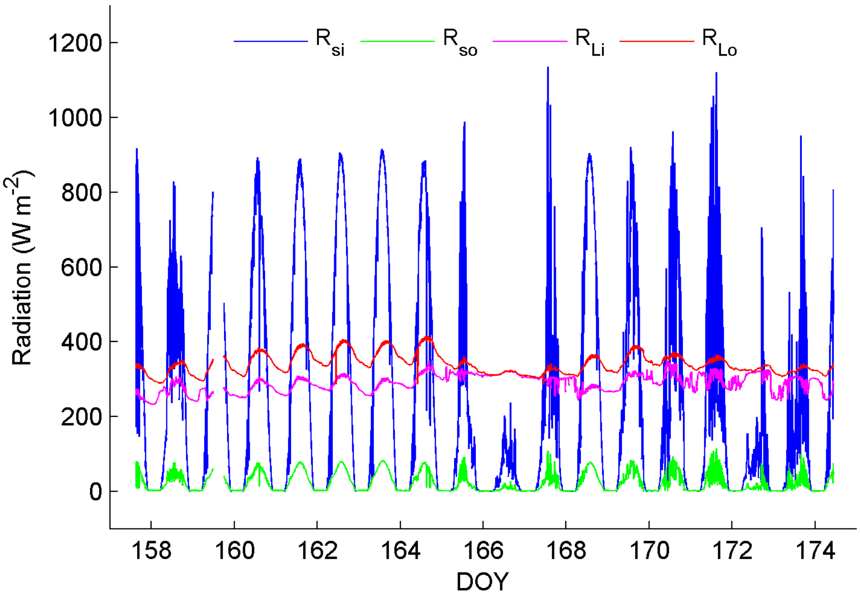

Figure 44. Incoming and outgoing shortwave and longwave ration, measured with a CNR1 radiometer at 35 m height at Speulderbos versus day of the year (DOY).

Temperature and relative humidity

Temperature and relative humidity were measured at 4 heights: 1, 27, 35 and 47 m above the forest floor (Fig. 45). At 1 m height, temperatures are the lowest and relative humidity the highest. In the middle of the canopy, at 27 m, temperatures are the highest and relative humidity the lowest.

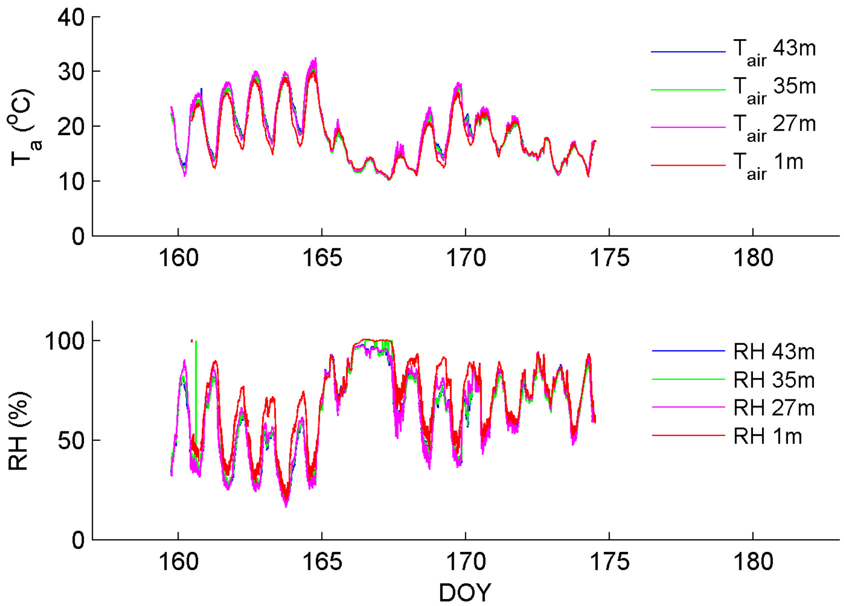

Figure 45. Temperature and relative humidity at different heights in Speulderbos versus day of the year (DOY).

Air pressure

Figure 46 shows air pressure versus day of the year.

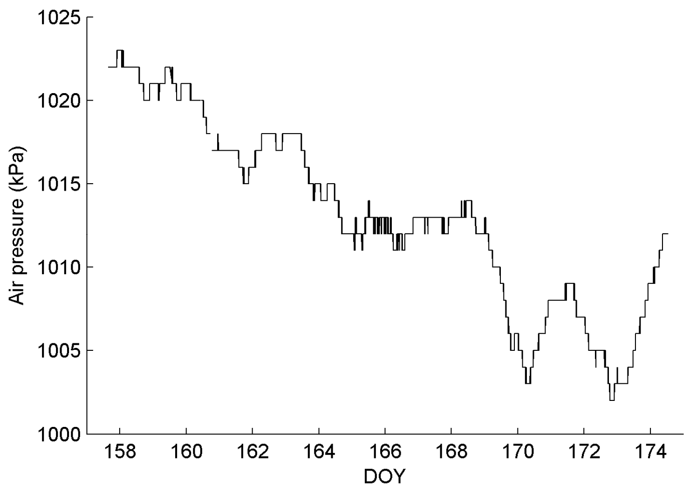

Figure 46. Air pressure measured at 1 m height at Speulderbos, versus day of the year (DOY)

Wind speed and direction

Wind speed and direction were measured just above the crown, at 34 m. Figure 47 shows wind speed and direction during the campaign, and Fig. 48 a wind rose diagram of wind direction distribution. Wind from SSW and from N was dominant.

A comparison is made between wind speed and direction measured at 34 m height, and those derived from the eddy covariance measurements at 47 m height (Fig. 49). A consistent difference in wind direction of about 10 degrees exists, most likely caused by an error in alignment of the instruments. The differences in wind direction on DOY 165 and 166 is still an unresolved issue. Wind speed is consistently higher at 47 m than at 34 m, as can be expected. The comparison is used later to derive roughness parameters.

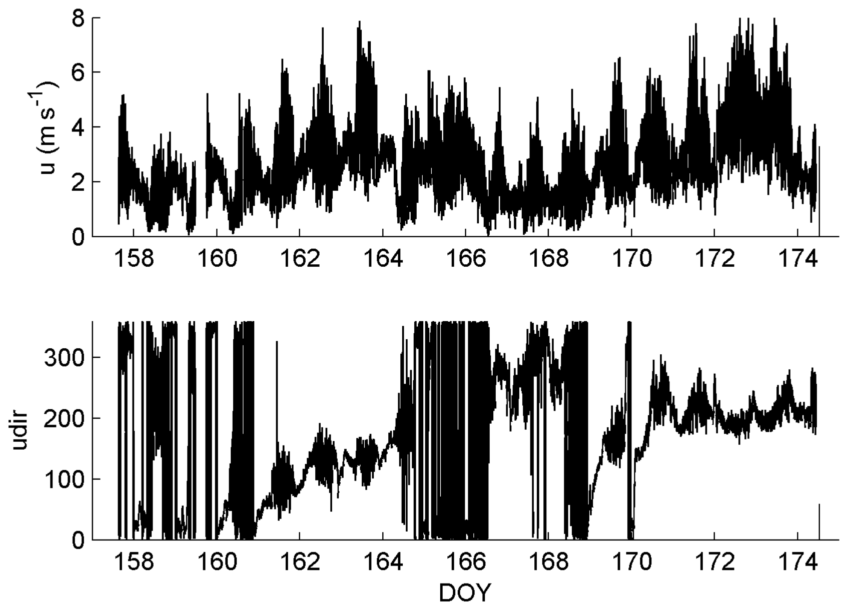

Figure 47. Wind speed and wind direction measured at 34 m height at Speulderbos

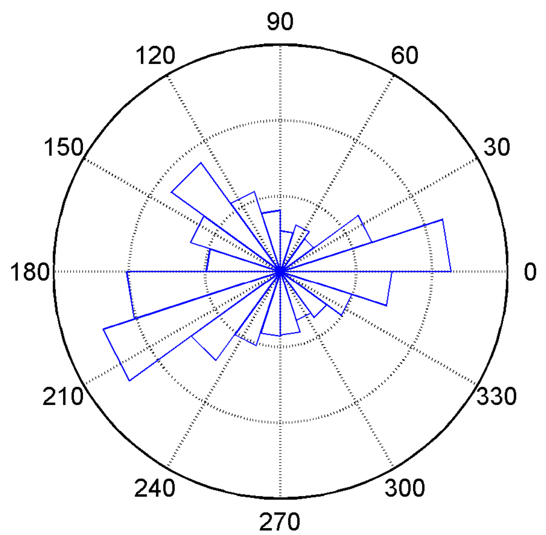

Figure 48. Wind direction distribution between DOY 158 and DOY 174 2006 at 37 m height at Speulderbos

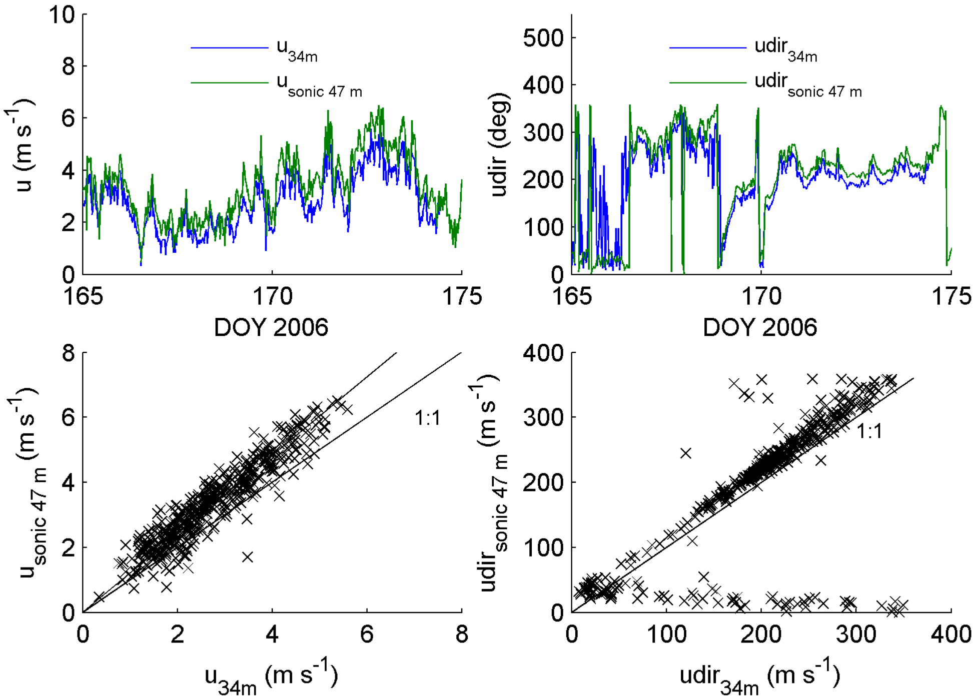

Figure 49. Upper left: wind speed measured with an anemometer at 34 m height and with an EC system. Upper right: wind direction measured with a windvane at 34 m height and with the EC system. Bottom left: wind speed at 47 m height versus wind speed at 34 m height and a linear regression line through the origin, and Bottom right: idem for wind direction.

Soil temperature

Figure 50 shows soil temperature measured at four depths. As expected, there is a phase shift and a decrease in amplitude of the soil temperature signal with depth.

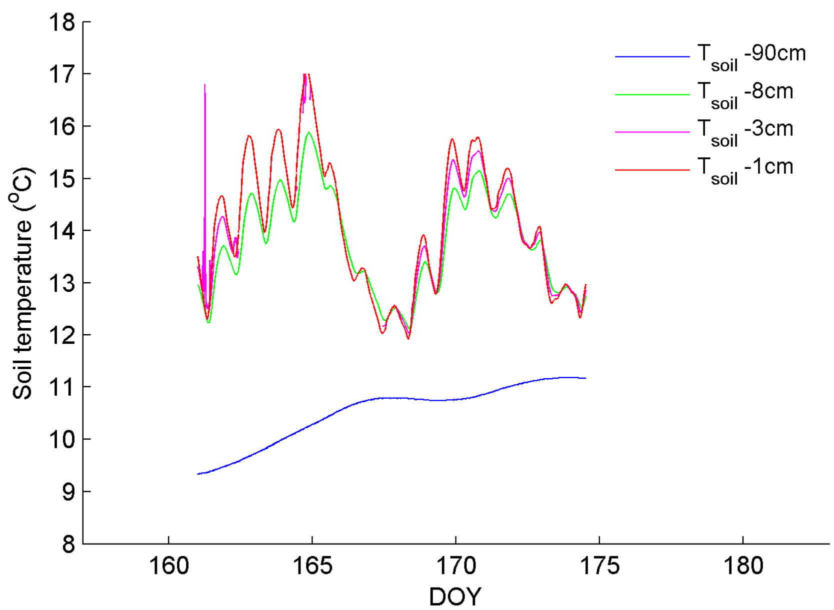

Figure 50. Soil temperatures at 4 depths at Speulderbos

Soil moisture content

Figure 51 shows soil moisture content calculated from measurements with CS616 sensors at three depths. The CS616 uses the dielectric constant of the soil with the frequency domain method as a measure of soil moisture content. The calibration of the sensors is soil specific. Because the sensors were not calibrated for the specific soil, a standard calibration for soils with an electric conductivity less than 0.5 dS/m and a density less than 1.55 g/cm3 and a clay content of less than 30% was used. The values for soil moisture content calculated in this way are unusually lower. For a correct interpretation of the absolute values of volumetric soil moisture content, a calibration against gravimetric measurements is required. The current data can be used to detect changes in soil moisture content with time. The jump the soil moisture content at -5 cm at day 166 is caused by rainfall.

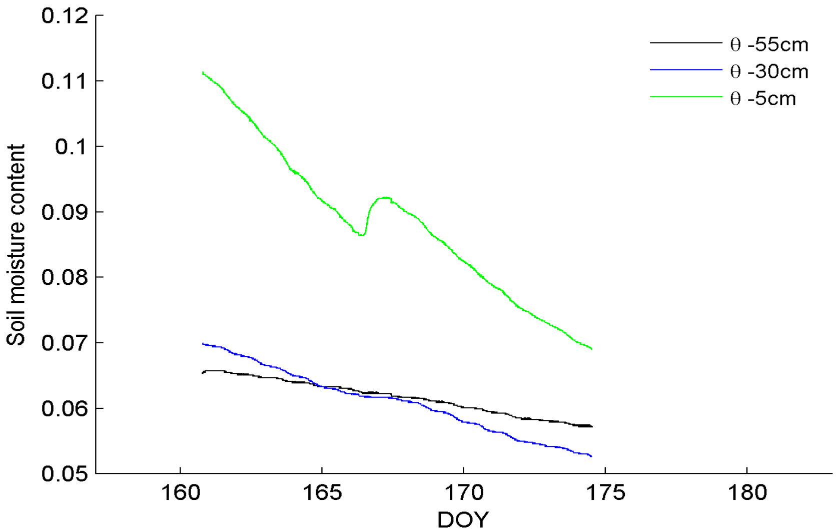

Figure 51. Soil moisture content at 3 depths at Speulderbos versus day of the year (DOY)

Soil heat flux

Figure 52 shows soil heat flux measured with three heat flux plates installed at 1 cm below the surface. Soil heat flux is only 2 percent of net radiation (at the top of the canopy). The soil temperature measurements can be used in a model for soil heat flux to verify whether these values are realistic.

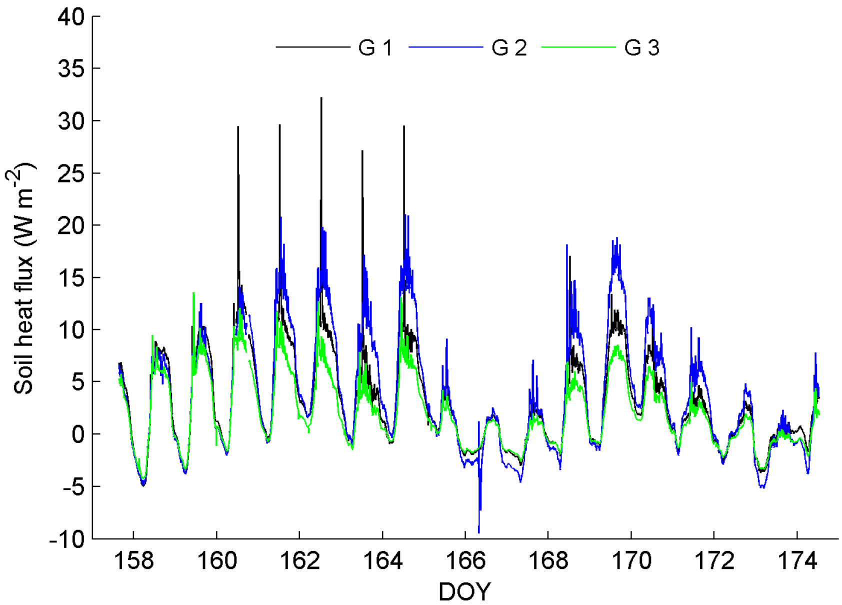

Figure 52. Soil heat flux measured with flux plates at Speulderbos

Surface contact temperatures

Surface contact temperatures were measured with Negative Temperature Coefficient (NTC) sensors on needles, mosses and trunks at ground level, and on needles, branches and trunks in the canopy between 17 and 34 m height (Table 32).

Table 32. Surface contact temperature measurements Speulderbos

Number	**Location**
	0-1 m height
1	Trunk sunlit
2	Trunk Shadow
3	Moss
4	Moss
5	Moss
6	Litter (needles)
7	Litter (needles)
8	Litter (needles)
	17-34 m height
10	Needle on branch pointing north, in shadow below branch
11	Needle on branch pointing north, in shadow
12	Trunk pointing north, in shadow
13	Trunk pointing south, sunlit
14	Needle on south pointing branch, sunlit
15	Needle on south pointing branch, sunlit, below branch
16	Sunlit branch
17	Shadow branch (lower side)
18	Shadow branch at 17 m

Figure 53 shows the surface temperatures for the sensors at ground level (red) and in the canopy (green) as a function of day of the year. Canopy temperatures are higher than soil surface temperatures. The contact temperatures of the canopy on day 165 until 166 fluctuate very rapidly. This is caused by severe rainfall, causing the sensors to malfunction.

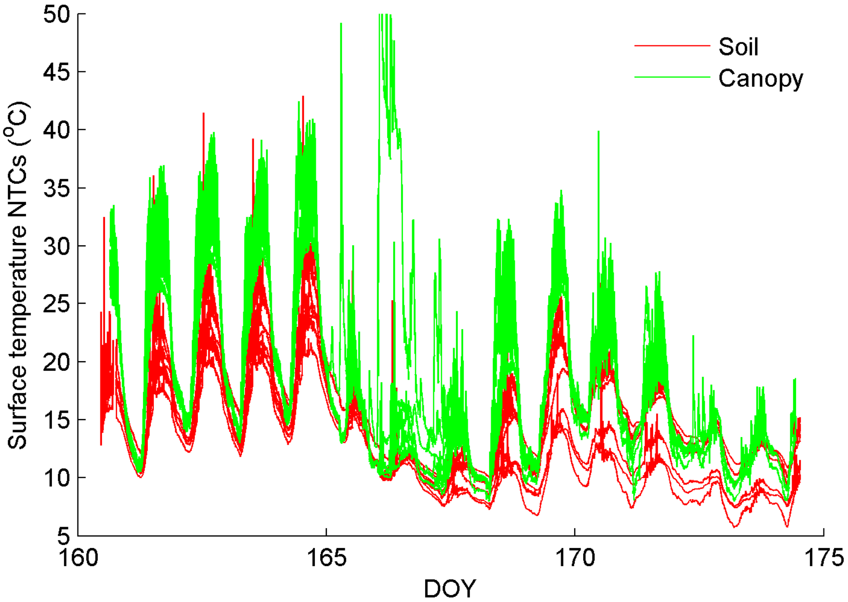

Figure 53. Component surface temperatures of 8 sensors on the litter, moss and trunks at ground level (soil), and 9 sensors on trunks, branches and needles in the canopy (canopy) at Speulderbos in day of the year (DOY)

Mirometeorological measurements

Two measurements systems were used to measure turbulent fluxes. A Large Aperture Scintillometer (LAS) was used to measure sensible heat flux over the trajectory between the Speulderbos tower and the Drie Forestry tower 2 km north (52°15'54.8" N, 5°40'39.4" E). The receiver was installed at the top of the Speulderbos tower. An eddy covariance system (EC) consisted of a sonic anemometer (CSAT3, Campbell Sci. Inc., USA) combined with a gas analyzer (CS7500, Campbell Sci. Inc., USA) used to measure sensible heat flux and the exchange of carbon dioxide and water at the top of the Speulderbos tower.

For the calculation of sensible heat flux from the scintillometer data, surface roughness is required. Surface roughness parameters were derived from the EC measurements, using the method described below. The calculation of sensible heat flux from the scintillometer data was carried out in Matlab, following the manual of the LAS instrument. The scripts are provided with the data (lasspeuld.m and las2.m) for reference.

Figure 54 shows sensible and latent heat flux (upper panel) and the flux of carbon dioxide (lower panel) measured with the EC system, and net radiation and average soil heat flux (upper panel). In general, the Bowen ratio is approximately unity, but on a day with high radiation (day 168, 17 June), sensible heat flux is higher that latent heat flux, and on a clouded day (day 172 or 21 June), latent heat flux is higher than sensible heat flux. Figure 55 shows the energy balance closure: available energy (net radiation less soil heat flux) and the sum of sensible and latent heat flux versus time and as a scatter plot. A 1:1-line and a linear regression line were plotted through the data. The sum of the fluxes is lower than the available radiation: the slope of the regression line is 0.80. This known phenomena can either be attributed to either an overestimate of available energy (an overestimate of net radiation or an underestimate of soil heat flux), or to an underestimate of the latent and sensible heat fluxes.

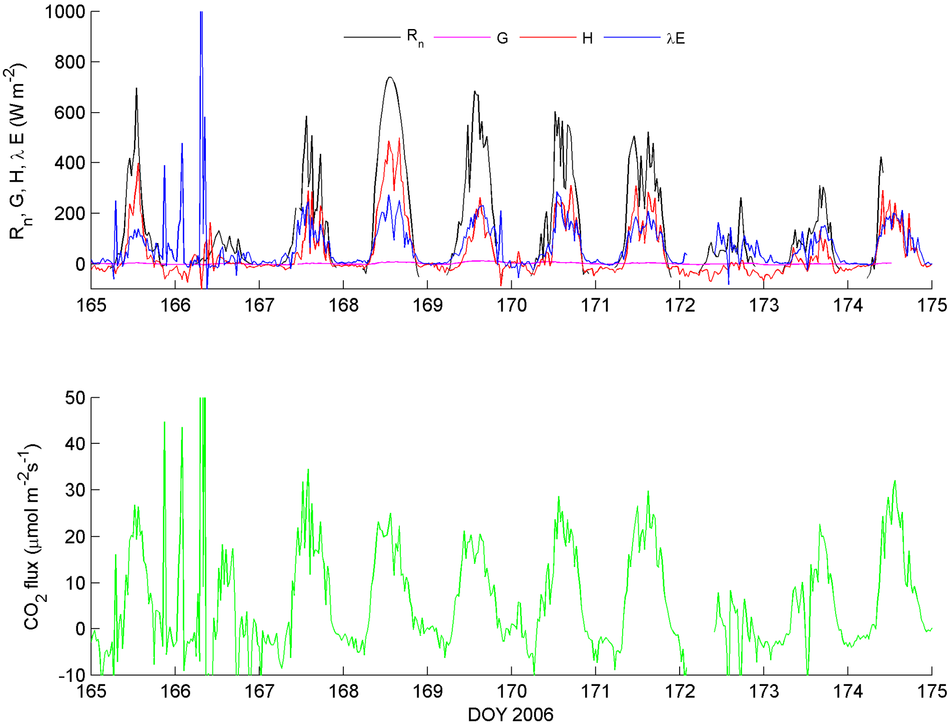

Figure 54. Up: sensible (H) and latent (λE) heat flux measured with the EC system, net radiation (R_n) and average soil heat flux (G). Bottom: downward flux of carbon dioxide

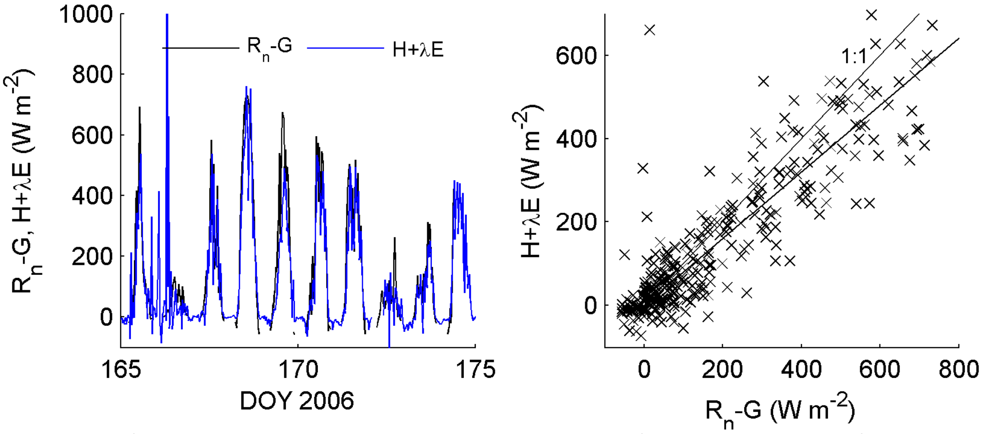

Figure 55. Left: available energy (net radiation R_n less soil heat flux G) and the sum of sensible (H) and latent heat flux (λE) measured with the EC system versus time. Right: Sum of sensible and latent heat flux versus available energy, the 1:1-line and a linear regression line forced through the origin

In Figure 56, the sensible heat fluxes measured with the LAS and with the EC system are compared. In general, the sensible heat flux of the LAS is higher than that of the EC system on clouded days and lower on clear days. The regression line has a slope of 1.2. The systematic difference between the two may be attributed to the sensitivity of H_{LAS} to roughness. To assess the accuracy of H_{LAS}, a sensitivity analysis to the roughness parameters d and z_0 is needed. The difference between the two systems on specific days may be related to a different footprint. A closer look into the effects of wind direction, precipitation and stability is needed to explain those differences.

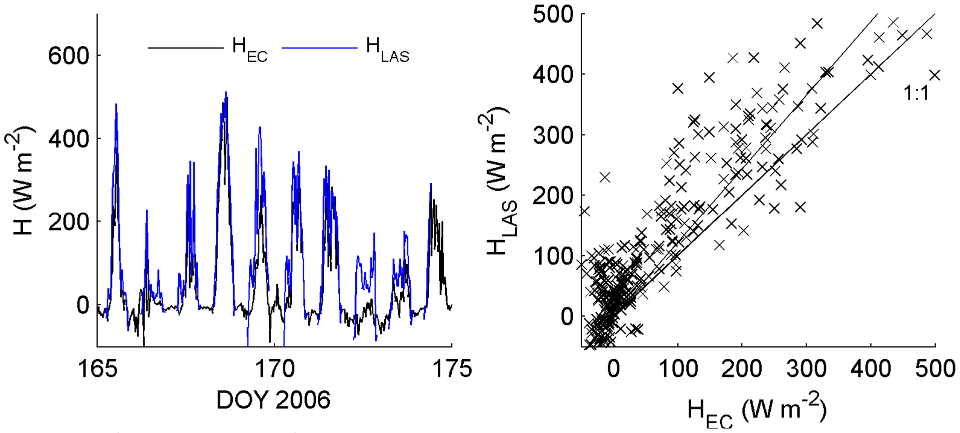

Figure 56. Left: sensible heat flux measured with the EC system (H_{EC}) and with the scintillometer (H_{LAS}) versus time. Right: H_{LAS} versus H_{EC}, the 1:1-line and a linear regression line forced through the origin.

Figure 57 shows friction velocity *u** versus wind speed *u* for stable and unstable conditions. As expected, the friction velocity in unstable conditions is highly correlated with wind speed. The friction velocity measurements under unstable conditions are used to derive roughness parameters d and z0, assuming a logarithmic wind profile.

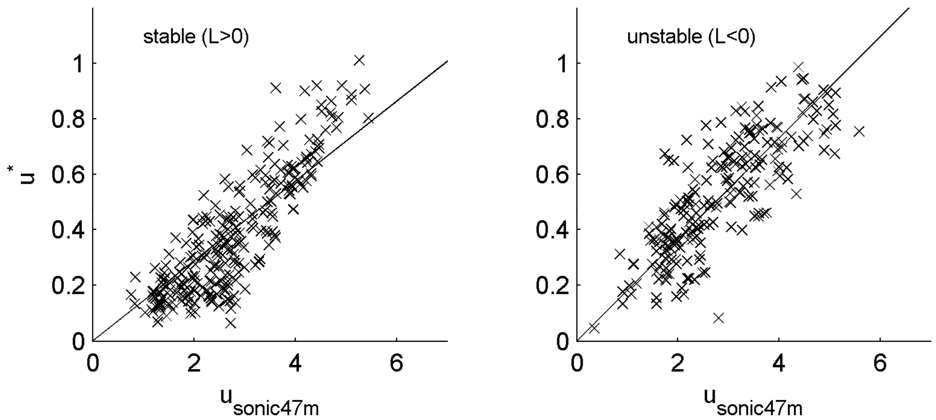

Figure 57. Friction velocity u* versus wind speed u derived from measurements with the EC system for stable (L>1) and unstable (L<0) conditions, with linear regression lines forced through the origin

Derivation of surface roughness parameters

Surface roughness parameters were calculated from the EC and wind data assuming a logarithmic wind profile for non-stable conditions. Wind speed at height *z* is then:

$$u_z = \ln\left(\frac{z-d}{z_{om}}\right)$$

Note that the stability function is neglected (this is the same as assume the neutral condition). This equation holds for neutral conditions and can be used as an approximation for unstable conditions. From the regression between u^* and u_{47} the ratio of the ratio of u^*/u_{47} for unstable conditions is known, and that between u_{47} and u_{34} the ratio u_{47}/u_{34} in Fig. 58. From these two equations, the two unknowns z_{0m} and d are solved.

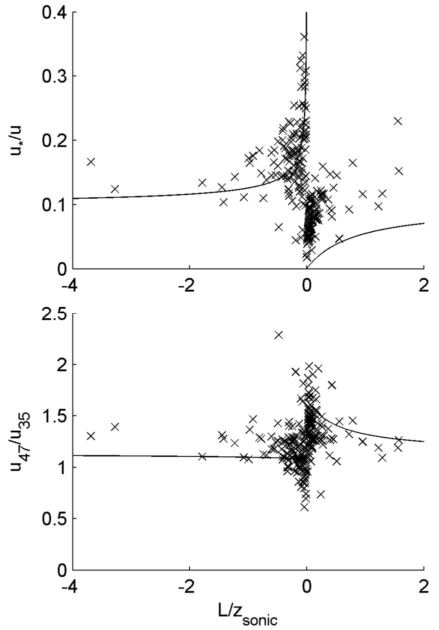

Figure 58. Measured (x) and modeled ratio of friction velocity over horizontal wind speed calculated from sonic anemometer data versus L/z_{sonic} (upper graph), and idem for u_{47}/u_{35} versus L/z_{sonic} (lower figure)

Mobile LAS measurements at the Cabauw grassland site

A mobile measurements system was used to measure turbulent flux at the Cabauw site as well. A Large Aperture Scintillometer (LAS) was used to measure sensible heat flux over a trajectory on a small grassland site 100 meters upwind of the Cabauw tower. Installation height was 2.25 m on average, necessary roughness estimates were taken 8 times as small as the average vegetation height (i.e. 35 cm), resulting in a surface roughness a little higher than 0.04 m. Figure 59 shows the preliminary results.

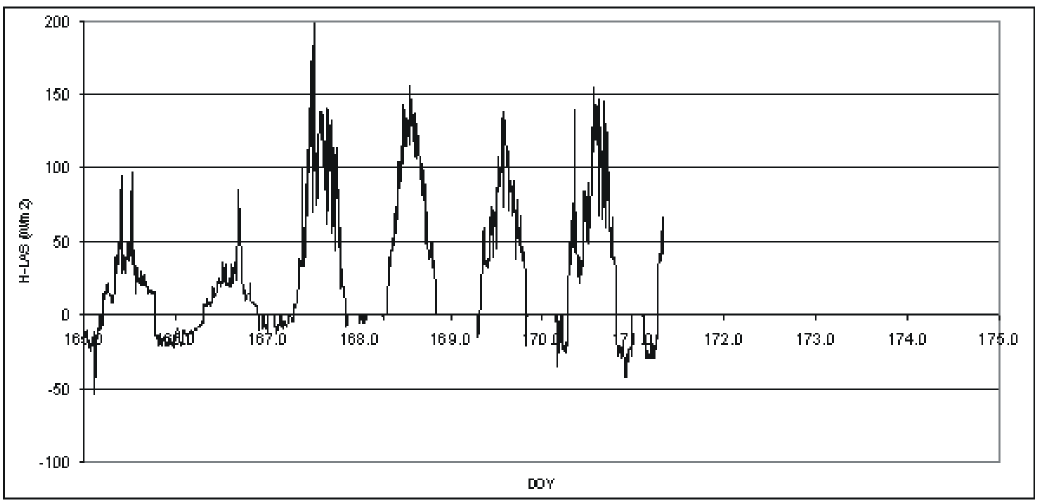

Figure 59. Sensible heat flux measured with the mobile scintillometer (H-LAS) versus time.

7.1.7 Data quality

Generally speaking the data is of excellent quality and a first analysis reveals that most parameters observed show expected behavior. However, the radiation data needs a post-calibration, which is currently being carried out.

In addition, the soil moisture sensors need a soil-specific calibration, which was not carried out prior to the campaign. They should be calibrated versus gravimetric measurements to obtain accurate absolute values.

On a few days the severe rainfall interfered with the canopy contact sensors, causing a malfunction of some of the sensors.

7.1.8 Prospects

A more detailed surface roughness analysis might be carried out, with respect to sensitivity analysis off the scintillometer measurements. This should be done alongside a closer look into the effects of wind direction, precipitation and atmospheric stability.

Soil temperature modeling may be carried out to check soil heat flux measurements.

7.2 Goniometric measurements

7.2.1 Introduction

This section describes the directional and contact measurements carried out at the Cabauw and Speulderbos sites. Measurements included several land cover units using several instruments. Measurements were carried out between 10 and 18 of June 2006. In the next sections, the experimental setup and preliminary results are discussed.

7.2.2 Team members

Team leader/contact person: Joris Timmermans, email: j_timmermans@itc.nl

Team members: Kitsiri Weligepolage, Christiaan van der Tol, Zoltan Vekerdy, Li Jia

7.2.3 Location

The measurements took place over 4 different land covers with their positions given in Table 33.

Table 33. Goniometric measurements overview.

Landcover	Position
Pine Tree	52º09’53.0” N, 05º45’31.9” E
Grass	51º48’18.4” N, 04º55’28.0” E
Maize	51º58’12.5” N, 04º55’29.3” E
Forest	52º15’08.1” N, 05º41’25.8” E

The experiments mainly took place at the Cabauw test site, Figure 60.

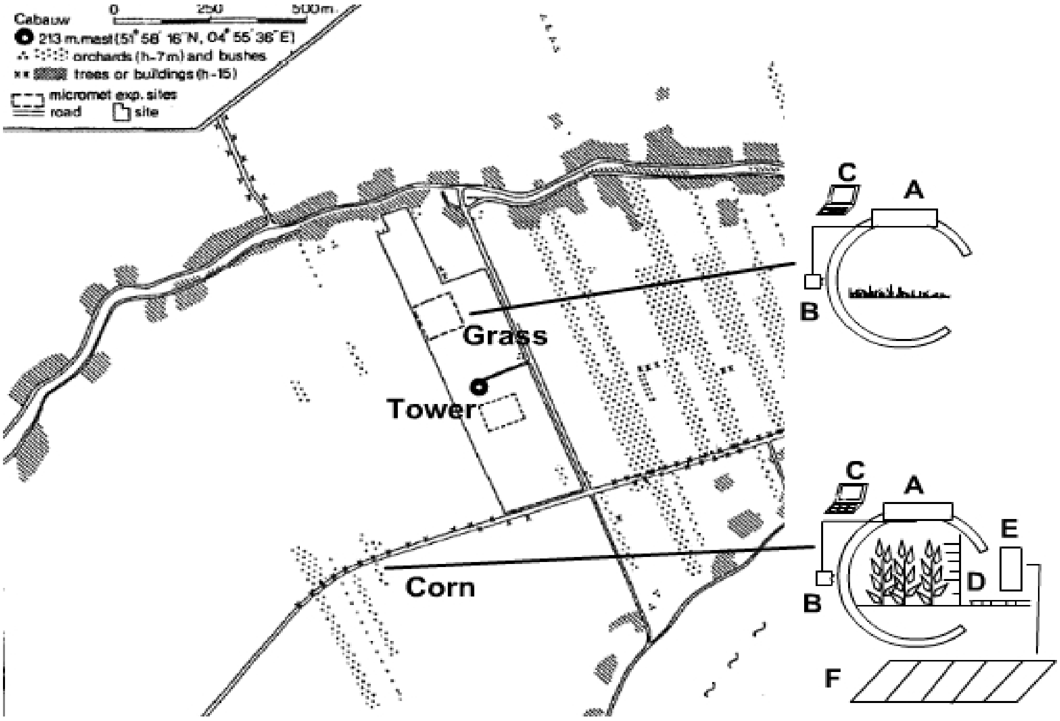

Figure 60. Setup of the instrument in the Cabauw field site, courtesy (Ulden & Wieringa, 1996)

7.2.4 Timing

The measurements took place in the afternoons of 10, 12, 13, 14, 15, 17 and 18 of June 2006.

7.2.5 Measurement protocol

Instruments

The sensors used during the EAGLE2006 field-campaign are:

- Irisys 1011 Thermal camera, with 16x16 resolution and 20^{o} view-angle.
- Everest 3000 Thermal broadband Radiometer, with 15^{o} view-angle.
- GER: spectrometer, with a minimum spectral resolution of 3nm and a view angle of 20º
- CIMEL 312-2 Thermal multi-band Radiometer, with 10^{o} view-angle and 5 thermal bands (corresponding to the ASTER-bands)
- IT-Works Digital camera.

Table 34 shows when the different instruments were used over the different land covers, where a * indicates that successive measurements took place applying a 45 degrees offset to the azimuth angle.

Table 34. Goniometric measurements.

Day	Time	Crop	Instrument
2006-06-10	15:44	Pine-tree	ASD
2006-06-12	11:00	Grass	GER
	12:12	Grass	GER
	15:18	Grass	Everest + Irisys*
	16:52	Grass	Everest + Irisys + IT-Works
	17:28	Grass	Everest + Irisys*
2006-06-13	12:36	Forest	ASD
2006-06-14	11:59	Grass	Everest + Irisys*
2006-06-15	17:10	Maize	Irisys
2006-06-17	14:43	Maize	Irisys*
	15:20	Maize	Everest + Irisys
	18:27	Maize	CIMEL*
2006-06-18	12:16	Forest	ASD
	11:55	Maize	Everest + Irisys*
	12:47	Maize	Everest + Irisys + IT-Works
	13:20	Maize	GER
	15:02	Maize	Everest + Irisys*

Procedure

During the EAGLE2006 field campaign, directional measurements and contact measurements were performed over forest, maize and grass, using various instruments.

The contact measurements were performed continuously for the whole duration of the field-campaign. The directional measurements could not be performed continuously due to the setup, and had to be performed periodically.

For the directional measurements of the grass and maize a goniometer is used, Figure 61. A goniometer is a mechanical system that enables the user to perform hemi-spherical measurements with different sensors.

Figure 61. Goniometer as set up at the Cabauw grassland site.

Depending on the instrument used, the goniometer can be operated in automatic or semi-automatic mode. In automatic mode a single run lasts 3 minutes in which 15 measurements are obtained. The angles corresponding to those measurements are given in Figure 62 and Table 35. After a single run of the goniometer the run is immediately performed again but applying an offset 45 degrees for the azimuth angle.

During the field campaign, the measurements with the ASD and the CIMEL are carried out only once per crop as these instruments take a long time to perform a single run. As BRDF values do not change rapidly, the directional ASD measurements are valid for the whole campaign.

Figure 62. Angular positions of the goniometer setup.

Table 35. Angles of goniometric measurements.

Angle Numbering	Azimuth (º)	Zenith (º)
Angle 01	00	000
Angle 02	00	180
Angle 03	00	090
Angle 04	30	180
Angle 05	30	090
Angle 06	60	180
Angle 07	60	090
Angle 08	90	--
Angle 09	60	000
Angle 10	60	270
Angle 11	30	000
Angle 12	30	270
Angle 13	00	000
Angle 14	00	270
Angle 15	00	000

The reach of the goniometer has a maximum of 2 meters. Therefore to take directional measurements for the forest the goniometer could not be used. Instead the ASD spectrometer was pointed downward on predefined, Table 36.

Table 36. Angles of directional measurements over the forest.

Azimuth	Zenith	Notes
90	N,W	Only on 13-06-2006
80	N,W,S,E	
70	N,W,E	Only on 13-06-2006
60	N,W,S,E	
50	N,W,S,E	
45	N,W,E	Only on 13-06-2006
40	N,W,S,E	
30	N,W,E	Only on 13-06-2006
20	N,W,S,E	
10	N,W,E	Only on 13-06-2006
00	N,W,S	Only on 13-06-2006

Data level

Level 1b; geo-referenced bio-physical parameters.

7.2.6 Data summary

Some examples of the measurements are shown in Figures 63 till 65.

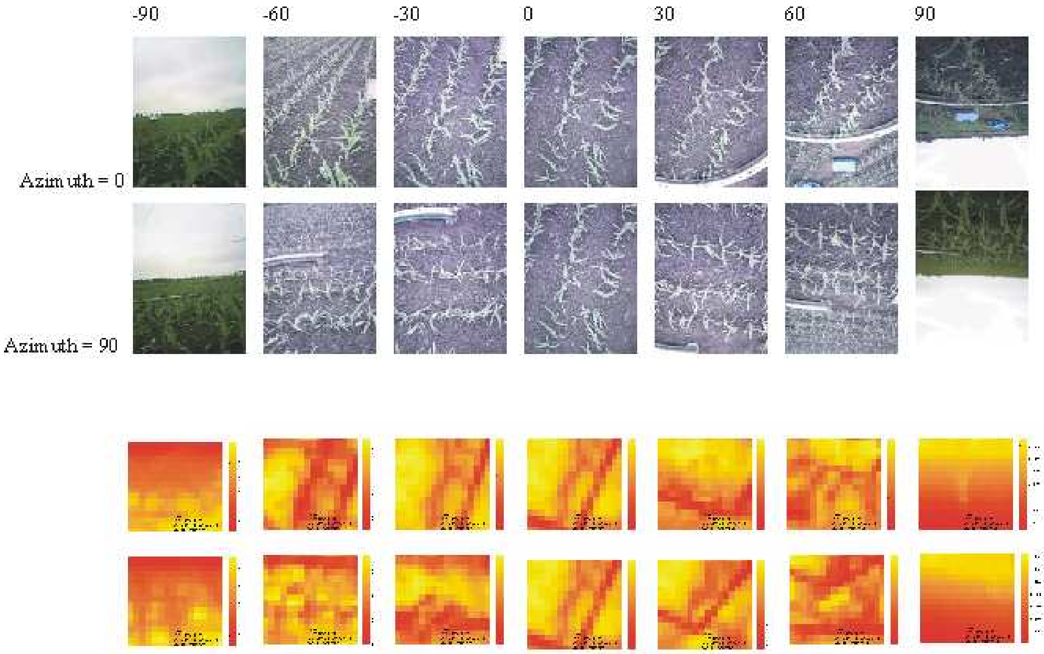

Figure 63. Example output from the goniometer measurements over maize using a digital photocamera (upper panels) and a thermal (lower panels) infrared imager.

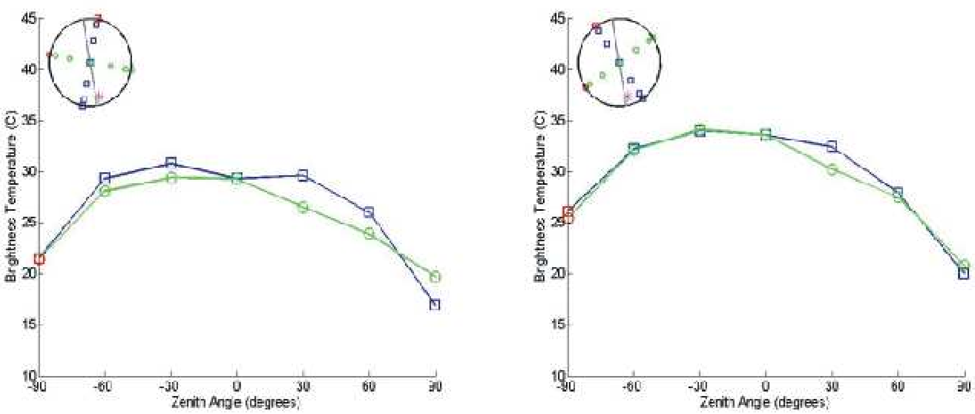

Figure 64. Example output of the angular dependence of thermal infrared radiation over the maize, measured on 18 June 2006, at 11:55 hrs local time.

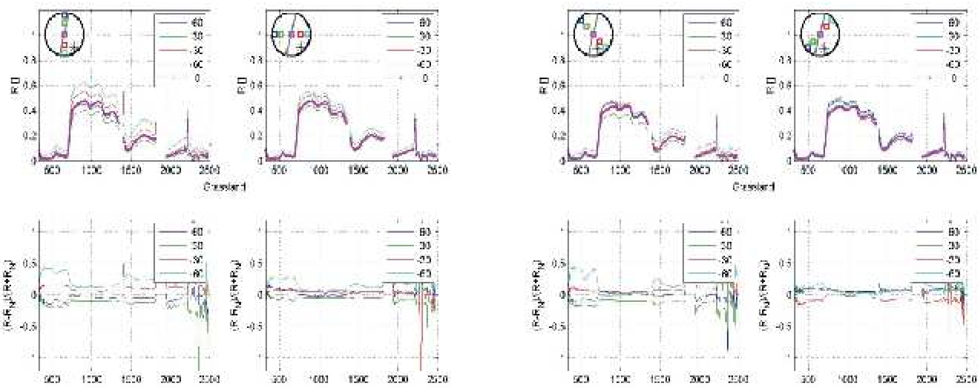

Figure 23. Goniometric ASD measurements over the grassland site on 12 June 2006 at 11:00 hrs local time.

7.2.7 Data quality

Due to the difficulty of 3D radiative transfer of the radiation through the canopy, the data processing of directional data is very slow. The spectral data has been checked for spikes and splices which have been removed. The thermal data has been checked for erroneous values, which also have been removed. Further analysis of the data shows that the data quality is very high.

7.2.8 Prospects

These data will be analyzed further in the NOW-SROn EcoRTM project.

8 Ground biophysical (soil, vegetation and water) measurements

8.1 Bio-physical measurements

8.1.1 Introduction

The bio-physical measurements made during the EAGLE2006 intensive campaign included volume and biomass, as well as radiation penetration and Leaf Area Index measurements.

8.1.2 Team members

Team leader/contact person: Patrick van Laake, email: vanlaake@itc.nl

Team members: Badri Karki, Kwabena Asubonteng

8.1.3 Location

The bio-physical measurements for the forest area were taken at the Speulderbos tower site:

Speulderbos tower (52º15'08.1"N, 5º41'25.8"E)

8.1.4 Timing

The radiation penetration measurements were taken continuously from June 12th until the 20nd 2006.

The volumetric and LAI measurements were taken on 9th and 12th of June 2006.

8.1.5 Measurement protocol

Instruments

PAR sensors were employed for the radiation penetration measurements, whereas the LAI measurements were carried out using a Li-Cor LAI2000 device.

Procedure

Since the measurements were rather different in nature they are described separately hereafter.

Volume and biomass: the biophysical measurements of the forest were taken at the tower in the Speulderbos site. Ten circular plots of 500 m2 each were laid out in a 5 x 2 grid following the general layout of the enclosed area where the tower is located. The ten plots cover approximately 10% of the total enclosed area. All plots consisted of single-species *Picea abies*. On each of the plots the diameter at breast height of all individual trees was measured, with a minimum of 10 cm. The plots had between 20 and 41 specimen. Due to the density of the crown the height could not be measured at the individual plots, but it was determined for the entire site from the tower. Since the canopy has a very uniform height, insofar as could be established from the tower, this should be a good approximation.

Radiation penetration: On four of the ten plots the penetration of the incident photosynthetically active radiation (PAR) was measured. The penetration to ground was determined by comparing PAR measurements at the top of the tower at 46 m above ground level to simultaneous ground level measurements of PAR. Both PAR sensors had previously been cross-calibrated. The measurements at each plot covered between several hours to 2 days. The measurements at the top of the tower were continuous. The sensors were both configured to sample PAR every second and log every minute.

Leaf Area Index: Leaf Area Index was planned to be measured at all 10 locations, using a Li-Cor LAI-2000 device. Unfortunately, the LAI-2000 malfunctioned during the campaign and could not be repaired on time.

Hemispherical photographs have been taken at several sites in the Speulderbos and elsewhere. Their suitability to determine effective LAI (LAIe) is being investigated.

Data level

Data level: Level 1b; Geo-referenced bio-physical data.

8.1.6 Data summary

The average penetration of PAR is about 2.5%, with a weak response to the solar altitude angle, see Figure 66.

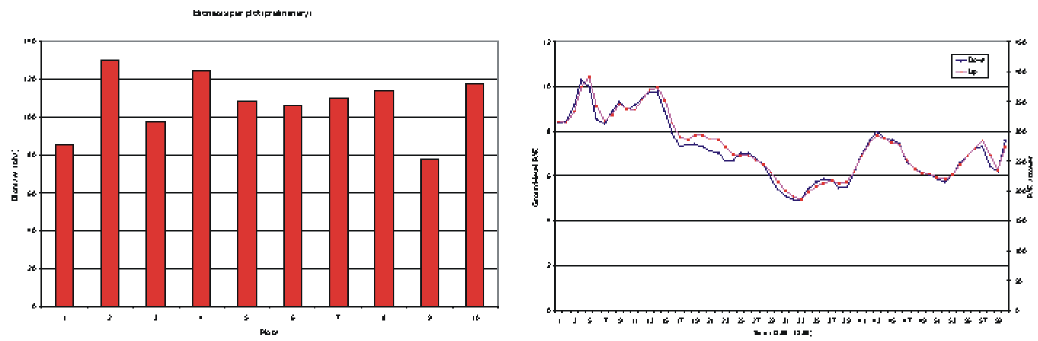

Figure 66. Preliminary bio-physical output; estimates of biomass in the left panel, radiation penetration measured at the Speulderbos tower site in the right panel. Please note the different scales at the two y-axis!

8.1.7 Data quality

The data quality of the measurements was quite variable; the volumetric, biomass and radiation measurements were generally quite good. The LAI measurements on the other hand failed.

8.1.8 Prospects

Concerning the volumetric and biomass data; the measured diameters will be converted to standing volume using default allometric equations developed by Staatsbosbeheer, and then converted to total above-ground biomass using wood density and biomass expansion factor.

8.2 Soil measurements

8.2.1 Introduction

Soil moisture was measured in the field for calibration and validation of soil moisture measurements through remotely sensed data, which have been acquired during the campaign.

8.2.2 Team members

Team leader/contact person: Fouad Khaier, email: khaier@itc.nl

Team members: Ali Abkar, Gabriel Norberto Parodi, George Ndhlovu, Hosea Sanga, Jeniffer Kinoti Mutiga, Madi Sarr, Mary Chiluba, Mayson Saila, Meseret Teka Hunde, Mustafa Gokmen, Rahul Kanwar, Remco Dost

8.2.3 Location

The measurements were carried out on the Cabauw grassland site, where the Cabauw tower has coordinates 51º58'00.0"N, 04º54'00.4"E. An overview of the different fields that were sampled is provided in the following sections.

8.2.4 Timing

The measurements took place during the entire day on 8, 12, 13, 14, and 15th of June 2006.

8.2.5 Measurement protocol

Instruments

Two different measurement techniques were employed.

The Hydra Probe (Stevens Water Monitoring Systems Inc.) performs high frequency electrical measurements which are directly related to simultaneous measurement of soil moisture. Hydra Probe provides output of data in water fraction by volume. More information on this device is available on: http://www.stevenswater.com/catalog/

In addition gravimetric measurements were done by taking soil samples by augering in soil rings. Then, the samples were taken to the laboratory to carry out the measurements. In the laboratory, soil moisture was first measured gravimetrically by weighing the wet volume of soil, oven drying at 105 ºC, and then re-weighing. The difference in mass corresponds to the mass of water then gravimetric water content of the soil can be determined. Using known soil density, volumetric water can also be determined.

Procedure

The points of measurements were distributed in the four fields, see Figure 67, and marked with numbered sticks to repeat the measurements in the same position every time. The exact locations of the points were taken via the GPS station so can be referenced to the satellite images and airborne data.

Sampling took place once a day, where the approximate distance between the points was 20-30 meters. The sampling was carried out at two depths; one at 5 cm and another one at 10 cm depth. There is no need for processing the soil moisture measurements from the hydra probe, since they are straight forward and ready to use. The gravimetric method needs some laboratory work which already has been done and the results are ready to use for calibrating the image data.

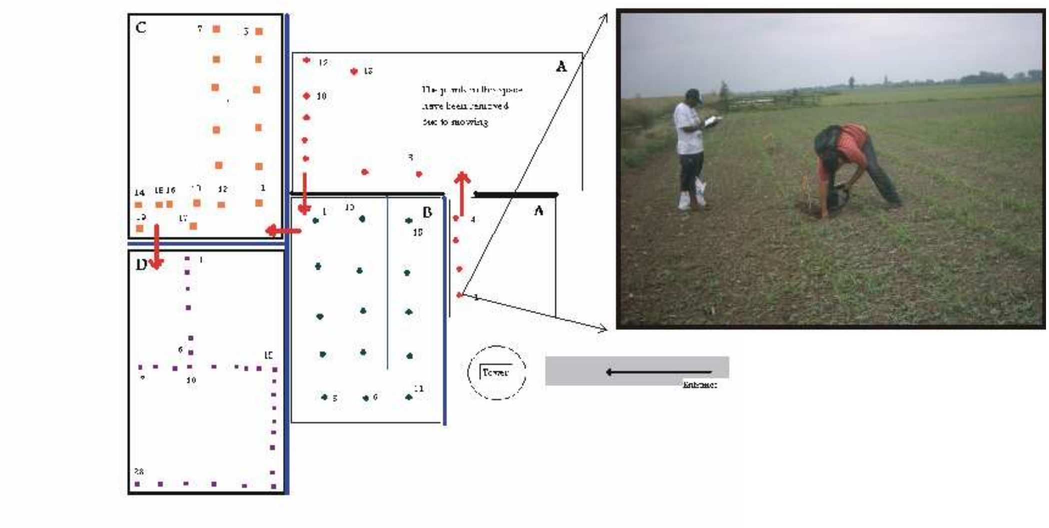

Figure 67. Sampling strategy of the oil moisture measurements at the Cabauw site. A, B, and C are grassland sites, D represents a maize field. The right panel shows part of the team at work.

Data level

Level 1b: Geo-referenced bio-physical data.

8.2.6 Data summary

The data is available from the EAGLE2006 database in an excel spreadsheet. An example output of the interpreted measurements at two depths is provided in Fig. 66.

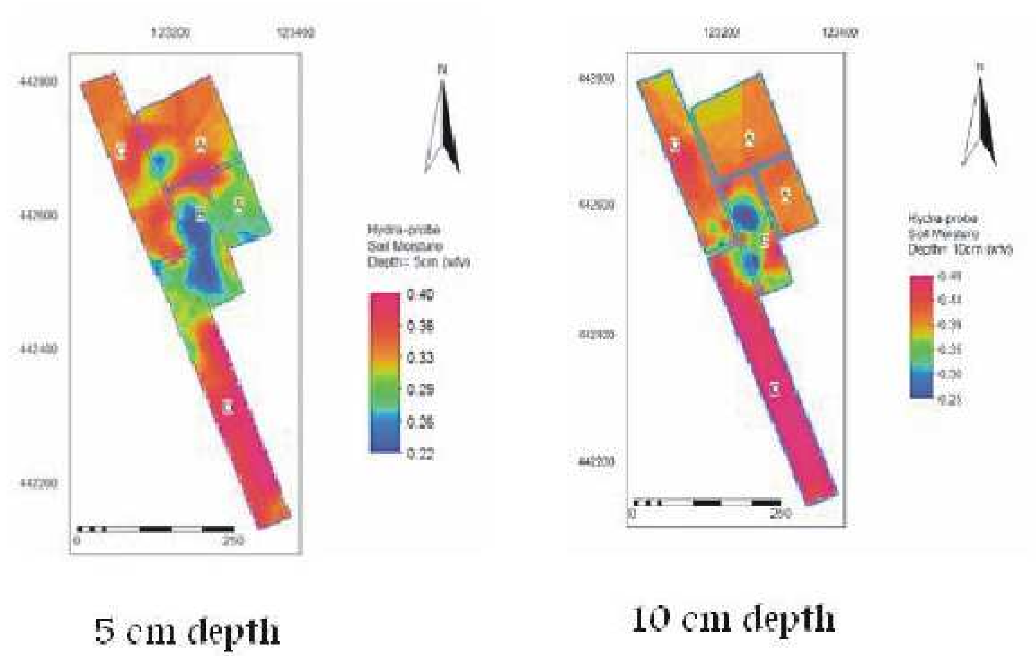

Figure 68. Spatial distribution of soil moisture in the Cabauw test site at 5 and at 10 cm depth, obtained through Kriging interpolation.

8.2.7 Data quality

Generally the data quality is good.

8.2.8 Prospects

No further processing is required.

8.3 Water measurements

8.3.1 Introduction

The main objective for doing these measurements is to obtain information on the water quality parameters - Secchi depth, turbidity and Chl-a. Since there was no sufficiently large representative waterbody in the direct vicinity of the tower sites the measurements were carried out outside the direct EAGLE2006 campaign domain, i.e. outside the direct campaign. Unfortunately, it was not possible to take spectra for water quality measurements during the AHS overflight. Due to weather conditions, the first suitable day was 4 July. Measurements were carried out at the open water of the “Wolderwijd” (which was covered by AHS airborne imagery for this purpose but at an earlier date) near the city of Harderwijk.

8.3.2 Team members

Team leader/contact person: Zoltan Vekerdy, email: vekerdy@itc.nl

Team members: Chris Mannaerts, Patrick van Laake

8.3.3 Location

The measurements took place over open water in the "Wolderwijd" near Harderwijk on July 4th 2006 and in the Lek near Cabauw on 13th of June 2006 (Fig. 69). Exact coordinates of the measurements are:

Wolderwijd: 52º19'12.0"N, 05º36'12.0"E.

Lek: 51º57'38.6"N, 04º57'59.9"E.

8.3.4 Timing

The measurements took place on the 13th of June and on the 4th of July 2006.

8.3.5 Measurement protocol

Instruments

In addition to the ASD spectra, in situ measurements were taken for the water quality parameters shown below in Table 37.

Table 37. Water quality sampling overview.

Parameter	Instrument	# of measurements
Transparency	Secchi disk	10
Turbidity	Aquafluor & 2100 P Turbidity meter	9
Chlorophyl-a	Aquafluor	10

Procedure

Figure 69. Preparing for sampling in the Wolderwijd (left panel) and spectra taken in the Lek (middle and right panels).

Water samples were taken at each observation point for total suspended solids and Chlorophyll-a analysis in laboratory. The samples were cooled and delivered to the laboratory within 20 hours after taking the first sample.

Data level

Level 0; Unprocessed raw data.

8.3.6 Data summary

Water samples as well as raw (but processing work is on-going) spectra data is available, of which an example is provided in Figure 70.

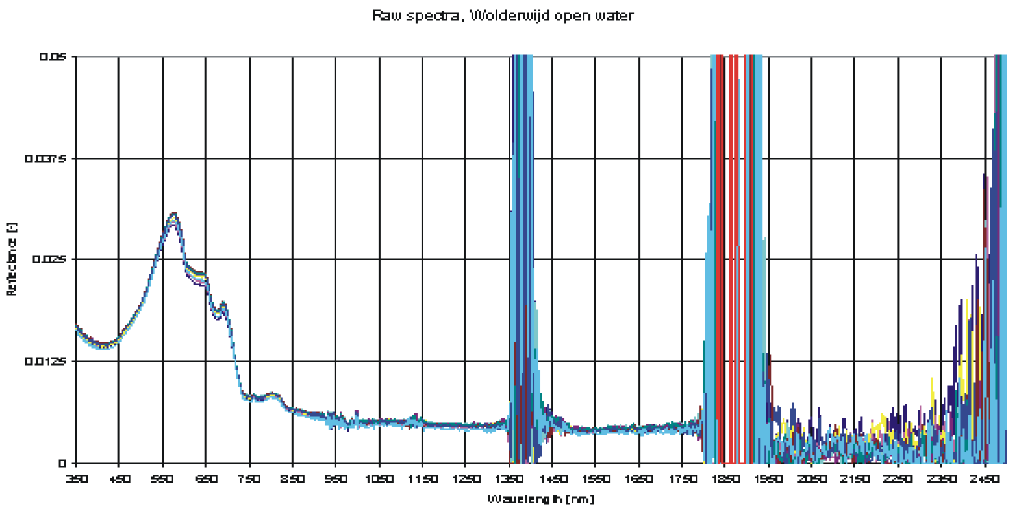

Figure 24. Wolderwijd (open water) spectrum as measured on 4th of July 2006.

8.3.7 Data quality

Generally the data quality is rather good, due to good weather conditions.

8.3.8 Prospects

Further analysis is on-going for achieving the research objectives.

8.4 LAI measurements

8.4.1 Introduction

Although these type of measurements were also scheduled to be taken using the LI-Cor LAI-2000, another approach was followed here to arrive at the same parameter, namely Leaf Area Index.

8.4.2 Team members

Team leader/contact person: Hans van der Kwast, email: J.vanderKwast@geo.uu.nl

Team members: Remco Dost, Rahul Kanwar

8.4.3 Location

The method was applied on both the Cabauw grassland as well as the Speulderbos tower site. Hence the coordinates are:

Cabauw tower: 51º58'00.0"N, 04º54'00.4"E.

Speulderbos tower: 52º15'08.1"N, 5º41'25.8"E

8.4.4 Timing

The Cabauw measurements took place at 10th of June 2006, whereas the next day, 11th of June 2006, the Speulderbos measurements were taken.

8.4.5 Measurement protocol

Instruments

The instrument used here is a camera with a fish-eye lens.

Procedure

The procedure consists of taking a hemispherical photo, with geo-location, which is then analyzed following the method as described by Anderson (1964, 1981) and Bonhomme & Chartier (1972). The software (to be) used is Winphot, by Nationaal Herbarium Nederland (1996). For a sequence of events, see Figure 71.

Figure 25. Leveling of the camera, photograph taken and Winphot processed result.

Data level

Data level is kind of 1b. The data is processed to a certain level, but not yet into LAI. It does contain coordinates though.

8.4.6 Data summary

The data is not yet fully processed and at an intermediate level, see: *Procedure*.

8.4.7 Data quality

Generally the data is rather poor. Over grassland the method is quite difficult to apply, since the camera cannot be lowered sufficiently. For the forest site the products contain some direct sunlight; this should be corrected for manually.

8.4.8 Prospects

Some additional manual processing is needed to obtain suitable end-products.

8.5 Surface roughness measurements

8.5.1 Introduction

The objective of the current measurements was to obtain surface roughness for the Cabauw grassland site.

8.5.2 Team members

Team leader/contact person: Hans van der Kwast, email: J.vanderKwast@geo.uu.nl

Team members: Remco Dost, Rahul Kanwar

8.5.3 Location

The method was applied on the Cabauw grassland and maize sites. Hence the (general) coordinates are:

Cabauw tower: 51º58'00.0"N, 04º54'00.4"E.

8.5.4 Timing

The measurements took place on 9, 10 and 13th of June 2006.

8.5.5 Measurement protocol

Instruments (Fig. 72)

Figure 26. The instruments used consisted of a fishing rod with camera and a DGPS.

Procedure

The procedure consists of stereo photogrammetry using NEar Sensing Camera Field Equipment (NESCAFE). NESCAFE has a close range remote sensing technique for measurement of surface geometric roughness, i.e. DEM's of an area of circa 10x10 m, with resolution of about 2cm using a DGPS. Roughness measurements were made over grassland and young maize crops (Fig. 73).

ID	X	Y	Z
CORNER1	123261.2	442485.9	-0.422
CORNER2	123269.3	442489.2	-0.602
CORNER3	123265.7	442498	-0.653
CORNER4	123257.8	442494.7	-0.474
GCP1	123261.1	442494.7	-0.429
GCP2	123264.8	442493.6	-0.472
GCP3	123263.3	442491.9	-0.376
GCP4	123260.9	442491	-0.397
GCP5	123263.9	442489.5	-0.37
GCP6	123266.9	442490	-0.476

Figure 27. Example of roughness measurement using NESCAFE.

Data level

Data level is 1b. The data is processed into a DEM containing coordinates.

8.5.6 Data summary

The following measurements were carried out at Cabauw (Table 38).

Table 38. Roughness measurements.

Site	Landcover	# of observations	Date
1	Grassland	8	09/06/2006
2	Grassland	8	09/06/2006
3	Grassland	5	10/06/2006
4	Grassland	6	10/06/2006

5	Maize	7	10/06/2006
6	Grassland	3	13/06/2006

8.5.7 Data quality

The data quality is generally quite good.

8.5.8 Prospects

Unknown.

8.6 Surface emissivity measurements

8.6.1 Introduction

The measurements were carried out to estimate the thermal-infrared emissivity of grassland surfaces, required to derive temperatures from radiometric measurements.

8.6.2 Team members

Team leader/contact person: Hans van der Kwast, email: J.vanderKwast@geo.uu.nl

Team members: Remco Dost, Rahul Kanwar

8.6.3 Location

The method was applied on both the Cabauw grassland as well as the Speulderbos tower site. Hence the coordinates are:

Cabauw tower: 51º58'00.0"N, 04º54'00.4"E.

Speulderbos tower: 52º15'08.1"N, 5º41'25.8"E

8.6.4 Timing

The measurements took place on 9, 10 and 11th of June 2006.

8.6.5 Measurement protocol

Instruments

Two-Lid emissivity box method developed by Sobrino and Caselles (1993) and described further by Rubio et.al. (2003). It generally consists of an aluminum box with a dimension of 30 x 30 cm which is 80 cm high. An EVEREST 210 infrared radiometer (8 – 14 µm, Field Of View 2°, sensitivity 0.1°C) and a DGPS were used.

Procedure

In short the method consists of measuring surface temperatures when cold-lit and hot-lid were covered, Figure 74.

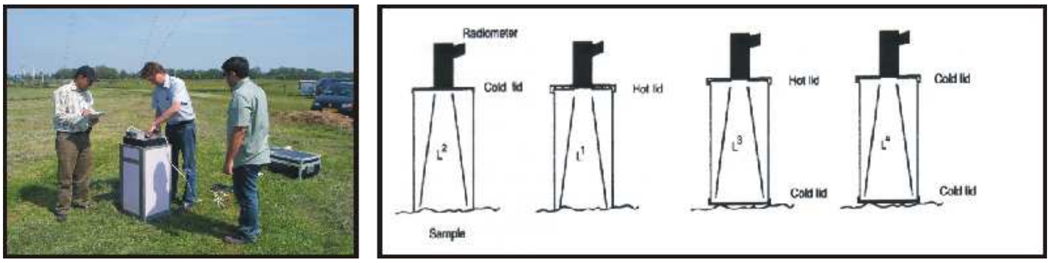

Figure 28. Emissivity measurements using the "box-method". Details in Rubio et.al. (2003).

Data level

The data is available in an Excel spreadsheet. Data level is 1b; Geo-referenced bio-physical parameters.

8.6.6 Data summary

The following measurements (Table 39) were carried out.

Table 39. Emissivity measurements overview.

Site	Landcover	# of observations	Date
1	Grassland	4	09/06/2006
2	Grassland	29	10/06/2006
3	Grassland	30	10/06/2006
4	Grassland	30	10/06/2006
5	Forest (floor)	30	11/06/2006

8.6.7 Data quality

Generally the data quality is good.

8.6.8 Prospects

No further processing is required.

8.7 Laser scan measurements

8.7.1 Introduction

To obtain a high accuracy, detailed 3-D representation of the Speulderbos forest site, necessary for a.o. within-canopy radiation transfer modeling and surface roughness estimates a laser scanning was carried out around the Speulderbos tower site.

8.7.2 Team members

Team leader/contact person: Erik Claassen, email: e.claassen@fugro-inpark.nl

Team members: Patrick van Laake, Zoltan Vekerdy, Ron Rozema, Remco Dost

8.7.3 Location

The method was applied around the Speulderbos tower site. Hence the coordinates are:

Speulderbos tower: 52º15'08.1"N, 5º41'25.8"E

8.7.4 Timing

The measurements took place on 20st of June 2006.

8.7.5 Measurement protocol

Instruments

The HDS2500 is Leica’s patented, second generation laser scanner and consists of a state-of-the-art, fully addressable, pulsed laser scanner. With a single-point range accuracy of +/- 4mm, angular accuracies of +/- 60 micro-radians, and a beam spot size of only 6mm from 0-50m range, including point-to-point spacing as fine as 1.2mm @50m, the HDS2500 can capture fine details and determine edge locations.

Procedure

The procedure consists of a fully automated scan, where the scanner was mounted on the Speulderbos Tower site elevator to carry out a scan at different heights, see also Figures 75-76.

Figure 29. The Leica HDS2500 3D Laser Scanner by FUGRO-INPARK, left panel complete instrument set-up, middle and right panel shows the scanner at work on the Speulderbos tower.

Data level

Level 1B; Geo-referenced.

8.7.6 Data summary

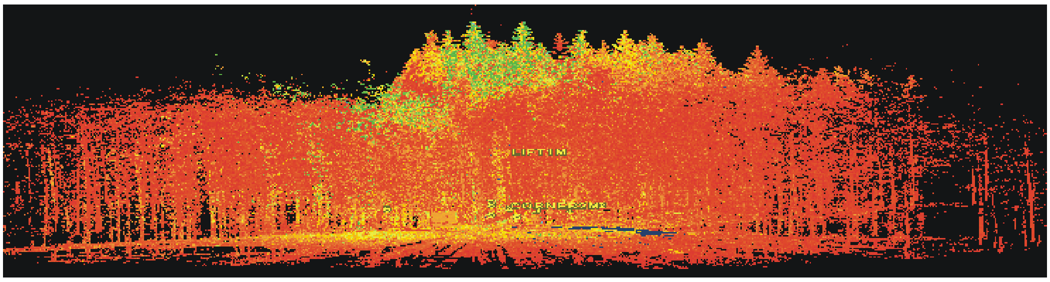

Figure 30. Example output from the Speulderbos site laser-scanning recorded on 20/06/2006.

8.7.7 Data quality

Generally the data quality is very good.

8.7.8 Prospects

Unknown.

8.8 GPS measurements

8.8.1 Introduction

To be able to process measured and obtained ground data to level 1b, the geo-location of a number of different observations have been measured using a Leica 1200 RTK-DGPS.

8.8.2 Team members

Team leader/contact person: Remco Dost, email: remcodost@itc.nl

Team members: Rahul Kanwar

8.8.3 Location

Due to the nature of these measurements the location is the measurement itself, see also Table 40. The data is available from the EAGLE2006 database.

8.8.4 Timing

Due to the nature of these measurements the timing is also part of the measurement itself, see also Table 40. As such, the data is available from the EAGLE2006 database.

8.8.5 Measurement protocol

A minimum of 6 measurements is automatically averaged to obtain a geo-location at an observation site. The observation sites are indicated by EAGLE2006 participants requesting a high accuracy geo-location measurement. The location has been measured in the Dutch Rijks Driehoekstelsel Coordinate system with elevation measured with respect to N.A.P. ("Normaal Amsterdams Peil").

8.8.6 Data summary

Table 40. Listing of datasets sampled with the Leica RTK-DGPS.

Observation	Site	# of measurements	Date	Max. Error (m)
Emissivity	Cabauw	4	09&10/06/06	0.05
Emissivity	Speulderbos	1	11/06/06	3.08 (large GDOP)
ESAR reflectors	Cabauw	3	14/06/06	0.03
ESAR reflectors	Speulderbos	3	14/06/06	0.04
Goniometer	Cabauw	1	10/06/06	0.06
LAI	Cabauw	1	10/06/06	0.04
LAI	Speulderbos	1	11/06/06	Faulty (large GDOP)
LAS	Cabauw	8	14/06/06	0.04
Laserscan	Speulderbos	13	20/06/06	8.91 (Large GDOP)
Roughness	Cabauw	60	09, 10 & 15/06/06	0.05
Soil moisture	Cabauw	175	12& 21/06/06	0.31

8.8.7 Data quality

The receiver is capable of measuring with an accuracy of 1cm + 1 ppm with differential GPS (DGPS) that was achieved by using the LNR GlobalNET Reference network. Because the receiver is a RTK receiver, no further post-processing is required. The maximum error obtained per dataset is listed in Table 40, where the large errors measured in the Speulderbos site are caused by a large GDOP and lack of satellite reception, due to interference with the GPS signal caused by the trees.

8.8.8 Prospects

No further processing is required, unless the coordinates are required in another projection; then any GIS software can be used to perform this transformation.

9 Reference meteorological measurements

9.1 Grassland, Cabauw - KNMI

The Cabauw observational program on land surface-atmosphere interaction aims at monitoring quantities relevant for evaluating land surface schemes in atmospheric models and satellite retrieval schemes. Part of the program has an operational status, these measurements are used also by the weather service. Observed are the profiles of wind speed and wind direction, temperature and humidity along the 200 m Cabauw meteorological mast, the surface flux of precipitation, the surface radiation budget in its four components short wave up- and downward radiation and long wave up- and downward radiation, the components of the surface energy budget, sensible heat flux, latent heat flux, soil heat flux, and the momentum flux.

The Cabauw site is situated in the centre of the Netherlands at 51º 57' 00”” Northern latitude and 04º 54' 00” Eastern longitude.

The data available to the EAGLE2006 Campaign participants concerns the entire month of June 2006.

9.1.1 Setting

The vegetation cover at Cabauw is close to 100 % all year round. Even in winter, after mowing or after a dry spell it is unusual to see any bare soil. The leaf area index has never been measured, but it is considerably larger then one (for a leaf area index near one, the bare soil would be visible). Saugier and Ripley (1978) give typical values for natural grassland (not at Cabauw). They specify a leaf area index of 0.35 to 1.5 for the green leaves, dependent on season, and an index of 3 to 4.2 for the dead leaves. Subjective estimates of the dominant grass species at the measuring field are *Lolium perenne* (55%), *Festuca pratense* (15%), and *Phleüm pratense* (15%). The surrounding area is dominated by *Lolium perenne* (40 %), *Poa trivialis* (20%) and *Alopecurus genculatus* (10%). The mixture of grass species in this area has been selected for high yield under the given climatological conditions and for the given soil type.
A characterization of the soils is given in Beljaars and Bosveld (1997). This characterization is based on an in situ survey described in Jager et al. (1976) and on the soil classification described by Wösten et al. (1994).
Drainage of the terrain is through narrow parallel ditches, which are on average 40 m apart. The water level in the ditches is artificially maintained at about 40 cm below the surface. This keeps the peat layer and bottom part of the clay always saturated. The height of the water table in the soil depends on the distance from the nearest ditch. It can be very close to the surface after abundant rain and can go down to the top of the peat layer after dry spell.

9.1.2 Measurements

The first measurements in this new observational program became available in May 2000. In the course of time more instruments became operational. Here is the list with start dates of the observations:

Table 41. Cabauw observations.

Instrument	Start date of observation series
Surface pressure	June 2000
Rain	June 2000
Wind profile	June 2000
Temperature profile	June 2000
Humidity profile	June 2000
Radiation	June 2000
Net radiation	Nov2002
Turbulent surface fluxes	Sep 2000
Soil heat flux	Aug 2001
Soil water content	Jan 2003
Ground water level	Jun 2000
Soil temperature	Mar 2003

Surface pressure is measured at the automatic weather station site, 200 m South-West of the main tower. The instrument is a Paroscientific 1016B-01. Provisions are made against dynamic pressure effects. Calibration is done at KNMI. Instruments are replaced after 26 month. Accuracy is 0.1 hPa. Resolution is 0.1 hPa. Datalogging is with the KNMI XP1-SIAM Pressure.

Rain amount and duration is measured at the radiation field South to the main tower. To reduce flow obstruction the rain gauge is positioned in a circular pit of 3 m diameter, which is surrounded by a circular slope. Rain duration is derived from the rain gauge observations. Rain is measured with the KNMI rain gauge. Calibration is done at KNMI. Instruments are replaced after 14 month. Accuracy is 0.2 mm. Resolution is 0.1 mm. Datalogging is with the KNMI XR2-SIAM Neerslag.

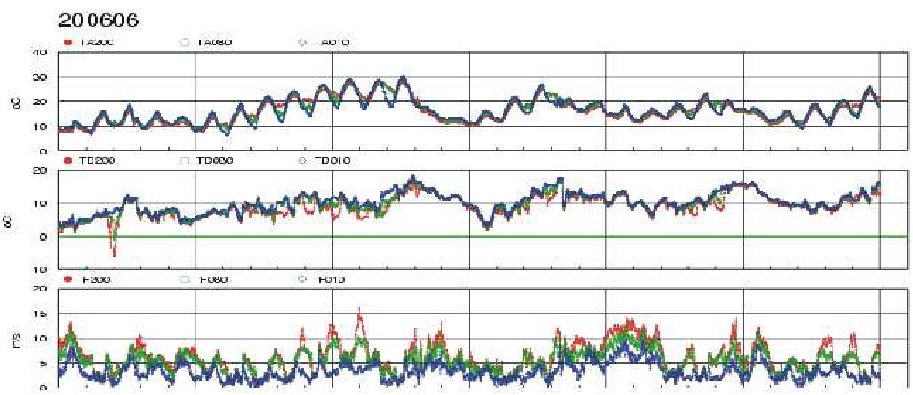

Figure 31. Profiles of air- and dewpoint -temperature and windspeed. Measured at 10, 80 and 200 meters above the surface during June 2006.

Wind speed and wind direction is measured at six levels, 200, 140, 80, 40, 20 and 10 m. To avoid too large flow obstruction from the mast and the main building measurements are taken on booms in three different directions. At the levels 200, 140, 80 and 40 m the wind direction is measured at all three booms and wind speed is measured at two booms (South-West and North). At the levels 20 and 10 m the wind

direction and wind speed are measured at two separate masts South (B-mast) and North (C-mast) of the main building. For each 10 minute interval instruments are selected that are best exposed to the undisturbed wind. Still some flow obstruction remains due to the presence of the tower and the supporting booms. Corrections in the wind speed are maximal 3% and corrections in wind direction are maximal 3 degrees.
Wind speed is measured with the KNMI cup-anemometer. Cup diameter is 105 mm and the distance between the centre of the cups to the rotation axis is 100 mm. Wind direction is measured with the KNMI wind vane. Distance between axis and the outer side of the vane is 535 mm. The azimuth of the wind vane plugs, at the tip of the booms are determined with a camera relative to distant objects at close to the horizon. The instruments are logged with the KNMI wind SIAM. Wind gusts are determined from a running 3 sec mean value. Calibration of the cup anemometers is done in the wind tunnel of KNMI. Wind vanes are balanced and the direction of the vane is tested. Sensors are replaced after 26 month. The cup anemometer contains a photo-chopper with 32 slits. The accuracy is 0.5 m/s. The threshold velocity is 0.5 m/s. The resolution is 0.1 m/s. The response length is 2.5 m. The wind vane contains a code disk. Accuracy is 3º. Resolution is 1º.

Air- and dewpoint temperature are measured at seven levels, 200, 140, 80, 40, 20, 10 and 1.5 m. The highest 4 levels are measured at the South-East booms of the main tower. The lowest three levels are measured at the B-mast, south of the main building. Air temperature is measured with a KNMI Pt500-element in an unventilated KNMI temperature hut. Dew point temperature is measured with a Vaisala HMP243 heated relative humidity sensor with a metal filter in a separate Vaisala unventilated hut. This hut is open in construction. The humidity data often overestimates during drying episodes after dew, fog or rain, because of a wet shielding or sensor. This may result in observed dew-point temperatures higher than the air temperature. Heating of the sensor, the change to metal filter and the open hut improves the functioning during high humidity conditions.
Calibration is done at KNMI. Temperature sensors are replaced each 38 month. Accuracy is 0.1 ºC. Resolution is 0.1 ºC. Dew point sensors are subject to contamination and drift of calibration this makes it necessary to replace them each 8 month. Accuracy is 3.5% RH. Resolution is 0.1 ºC. Data logging is done with the KNMI XU2-SIAM Temperatuur/Vocht HMP243.

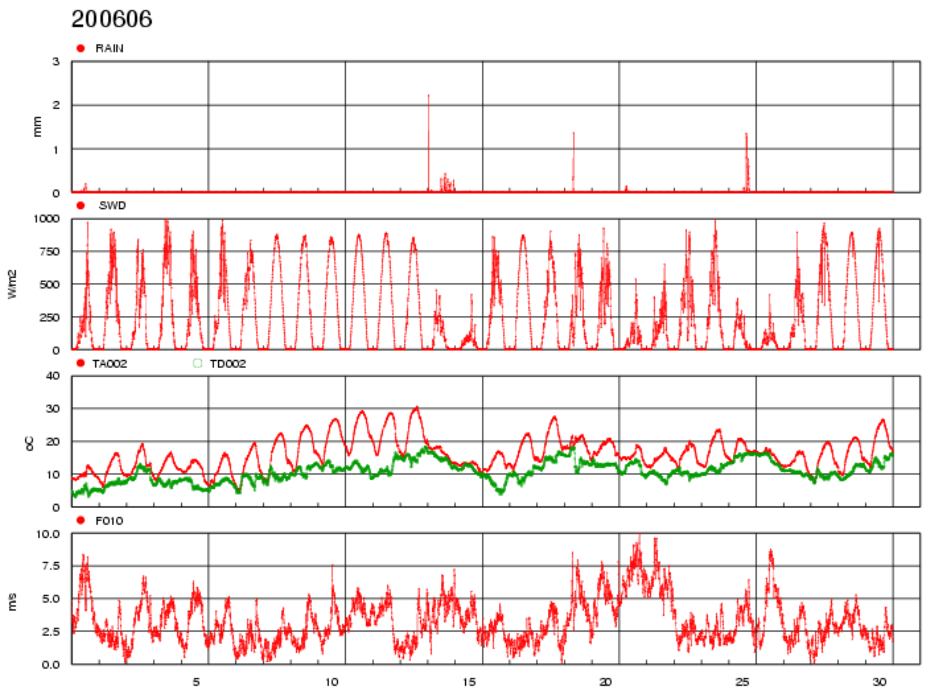

Figure 78. Rainfall, downward shortwave radiation, air- and dewpoint-temperature at 2 meters height and wind speed at 10 meters height, measured during June 2006.

Short wave upward and downward radiation is measured at the radiation field South of the tower at 1.5 m height. The downward looking sensor (albedo) is on a boom. The porting structure is painted black to get a well defined radiation condition. Since December 2002 the instruments are ventilated and heated to avoid formation of dew, snow and rime. The instruments are Kipp&Zn CM11 pyranometers. Data logging is done with the KNMI XQ1/XD0/XF0-SIAM Radiation. Calibration is done at KNMI against a reference instrument which itself is calibrated at Davos (Switserland).
At the 16th of January 2003 the albedo instrument was moved some 10 m to the West. The reason is the presence of a small ditch in the field of view of the instrument, which could reflect direct sunlight into the instrument. This became particularly obvious during a cold spell period with ice forming in the ditch. At this new location a small depression in the field close to the albedo instrument was present in which surface water could form during very wet episodes. At the 10th of February 2003 the grass around the new location was removed, soil was applied and the grass was replaced again. At the start of the growing season the surface at the albedo location rapidly became the same as its surroundings.
The instrument for short wave downward radiation has small offsets (a few W/m2) due to long wave cooling. This results in negative values during night time. These values are set to zero.
Long wave upward and downward radiation is measured at the radiation field South of the tower at 1.5 m height with sensors mounted on a boom. The instruments are mounted in one housing to get equal house temperatures. They are ventilated to avoid formation of dew, snow and rime and to minimise heating of the domes through irradiation. The domes are equipped with small thermistors. Corrections are applied for heating of the domes. The instruments are Eppley pyrgeometers (PIR). Data logging is done with the KNMI XL0-SIAM Eppley Radiation. Calibration is done in Davos (Switserland).

Net radiation is measured at the radiation site south of the main tower at 1.5 m height. The sensor is at a boom of 0.8 m. The instrument is a Schulze net radiometer type LXG055 (Schulze-Daeke type). The instrument measures the total downward radiation and the total upward radiation separately. The instrument is ventilated and heated to prevent dew formation and to keep temperature differences small. Calibration is done at KNMI (only short wave calibration). Datalogging is done with KNMI SIAM net radiation.

Turbulent surface fluxes are measured at 5 m height approximately 200 m south of the main tower. A sonic anemometer/thermometer is used to measure turbulent fluctuations of the three wind components and (sonical) temperature. The sonical temperature is measured along the vertical transducer pair. An open path infrared fluctuation meter is used to measure turbulent fluctuations of humidity and carbon-dioxide. The sonic anemometer has an azimuthal opening angle of 120º for horizontal wind measurements. The open path sensor is positioned vertically just behind the sonic probe at a distance of 0.3 m from the vertical sonical path. The instruments are mounted on a 1 m thin vertical cylinder to avoid a too strong flow obstruction due to the supporting mast. The vertical cylinder is supported by a rotator which is controlled by a wind direction tracking system and automatically turned into the mean wind direction each 2 hours. An inclinometer is positioned between the rotator and the supporting cylinder.

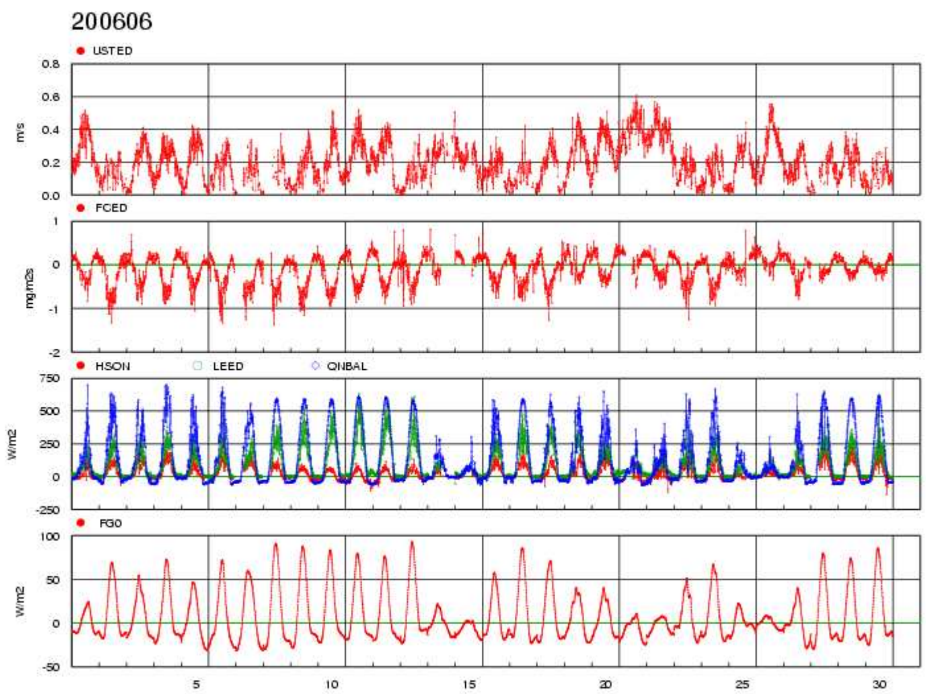

Figure 79. Turbulence observations (friction velocity, upper panel), surface fluxes (carbon, second panel, sensible and latent heat plus net radiation, third panel from top) and soil heat fluxes (lower panel) measured during June 2006.

The sonic anemometer is a Kaijo-Denki, probe type TR60-A, electronic unit DAT-300 or DAT-600. The sonic path is 0.2 m. Resolution is 0.1 K. The H2O/CO2-sensor

is a KNMI Infrared Fluctuation meter. Path length is 0.3 m. Resolution is 0.003 g/m3 H_2O and 0.15 ppm CO_2.
Data are logged at a rate of 10 Hz through a PC-Microstar A/D combination. Fluxes are calculated on a 10 minute time basis. Corrections on the sonical temperature are applied for moisture and lateral wind. Humidity and CO_2 fluctuations are corrected for density fluctuation induced by temperature and humidity fluctuations (Webb-correction).

Soil heat flux is measured at the soil-terrain, 100 m south of the main tower, with soil heat flux plates. The six plates are buried at the three vertices of an equilateral triangle with sides of 2 m at depths of 0.05 and 0.10 m. The measurements are averaged over the three plates at each depth. To obtain the surface soil heat flux a Fourier de-composition method is used.

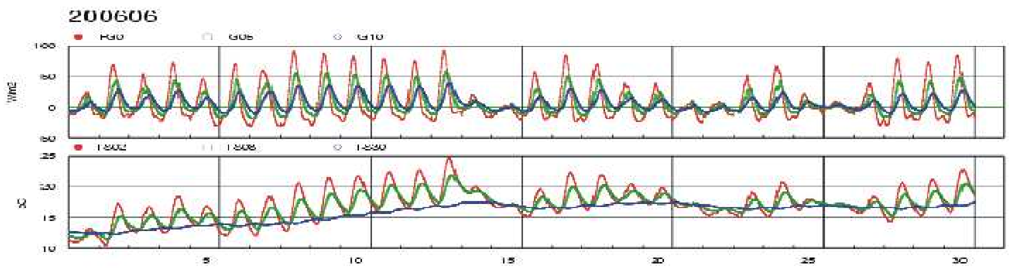

Figure 80. Soil heat flux and soil temperatures as measured during June 2006.

The instruments are manufactured by TNO-Delft. Type: WS31S, principle: thermo-pile, diameter 0.11 m, thickness 5 mm, sensitive surface: central square of 25*25 mm^2. Calibration is done by TNO-Delft. Data logging is with a Campbell Scientific CR21X data-logger. Measurements are taken 5 times in a 10 minute interval. Averages over 10 minutes are saved. At high rain intensities soil heat flux sensors, especially at the 0.05 m depths may give peak values which are probably not realistic estimates of the actual soil heat flux.

Soil water content is measured at the soil-terrain, 100 m south of the main tower, with TDR-sensors. Three sensors are buried horizontally at depths of 0.04, 0.08 and 0.20 m. The instruments are manufactured by Campbell Scientific. TypeCS615, principle: Time domain reflectometry, rod length = 30 cm, width between the two rods: 32 mm. Calibration is done by Campbell Scientific. Data logging is with a Campbell Scientific CR21X datalogger. Measurements are taken 5 times in a 10 minute interval. Averages over 10 minutes are saved. Soil water content is only available on a continuous basis after the 6th of January 2003.

Ground water level at Cabauw is managed. This means that water level in the ditches is regulated to get water out of the polder during wet episodes and into the polder during dry spells, the latter being the exception the first being the rule. Ground water level is measured at 5 positions along an East-West line 100 m south of the main tower. The line crosses a ditch. One of the positions is in the ditch. Pressure sensors (Keller, 26W/8369, 0-250mbar) are used to measure the ground water table. Ground water table is measured at 5 locations. A hole of 1.5 m depth and 15 cm diameter is drilled into the ground. A tube with a diameter 48.2 mm is led into the hole and the region between the tube and the hole is filled with small stones. The upper part is

filled with the local soil. The tube has holes in the lower part to give access to the ground water. The holes are covered with a fine metal grid to avoid particles entering the measuring region. The sensor is led down into the tube to a well defined depth. This is defined by the length of a PVC pipe through which the sensor cable is led, with the sensor tight to the lower end of the pipe and the top of the pipe positioned at the cover which is connected to the upper side of the tube.
For the sensor in the ditch levels vary with a few cm on short time scales (within 10 minutes) due to wind effects. The instruments are Keller, type 26W/8369, 0-250mbar. Datalogging is on a PC-MicrostarA/D combination.

Soil temperatures are measured at the soil-terrain 100 m South of the main tower. The temperature needles are buried horizontally at depths of 0.004, 0.02, 0.04, 0.06, 0.08, 0.12, 0.20, 0.30 and 0.50 m. Instruments are manufactured at KNMI. They are Nickle wired needles with an electric resistance of 500 Ohm and a sensitive length of 0.35 m. Calibration is done at KNMI. Data-logging is at a Campbell Scientific CR21X.

9.1.3 Data processing

After the data has been stored in the database, corrections and derived quantities are calculated and stored. Recalibration is the main reason for correcting the basic data. Derived quantities include calculated fluxes from turbulence covariances. This includes corrections for density effects and flow obstruction.

9.1.4 Data quality control

The measurements that are logged with SIAM's have an automatic quality control, which consists of tests of the electronics and of the exceedance of physical limits for the parameter at hand. The other instruments have no automatic quality control.
After the data are stored in the database a manual (on-eye) check is performed and together with information from the logbook data are rejected if appropriate. Rejection means for the SIAM logged data that the corresponding quality number is changed. For the other data a copy of the database is made in which the data-value is set to a missing value code.

Parts of this text have been taken from http://www.knmi.nl/~bosveld/

9.2 Forest-site, Loobos - ALTERRA

9.2.1 Setting

The observations that are available in the current campaign are obtained at the Loobos site, established in the year 1995, which is part of the CARBOEUROPE network of flux sites. The site is located near the town of Kootwijk in The Netherlands, at 52° 10’ 03’’ N, 5° 44’ 38’’ E. The area is quite flat, with an average elevation of 25 m above the mean sea level. Loobos is a forest site on sandy soil. The dominant tree species is Pinus Sylvestris and the average canopy height is 15.5 m. The Leaf Area Index (LAI) of the trees is about 2, and varies roughly between 0 and 1 for the undergrowth.

The data available to the EAGLE2006 Campaign participants concerns the entire month of June 2006.

9.2.2 Measurements

Turbulent fluxes are obtained using the eddy-correlation (EC) technique. The EC system consists of a 3D ultrasonic anemometer (Solent, Gill) in combination with a fast infrared gas analyzer (Li-Cor 6262) placed on the top of a 26 m tower, with a fetch of 2-3 km, see Figure 81.

Figure 81. Eddy correlation devices at the Loobos site. Left: Ultrasonic Anemometer and air inlet for CO2 and H2O measurements. Middle: gas analyzer. Right: Sketch of general Loobos set-up; Nomenclature of the symbols and heights are provided in Table 42.

A full description of the system may be found in Moncrieff et al. (1997). Additionally, CO2 and H2O concentrations are measured at five levels, (CIRAS-SC, PP systems), along with wind speed and temperature. The four components of the net radiation balance are observed separately: incoming and reflected short wave radiation are determined using two pyranometers (CM21, Kipp). The long wave components are measured by pyrgeometers (CG1, Kipp), with the sensor for the incoming long wave radiation being ventilated. At the scaffolding tower meteorological measurements of precipitation, horizontal wind speed, wind direction, relative humidity and air temperature are performed as well. Soil heat flux is measured using four heat flux sensors (TPD-TNO), under the litter layer at a small depth in the mineral soil. Soil moisture and temperature are also measured at five depths.

Table 42. Details of the parameters and sensors operational at the Loobos tower site.

	Parameter	*#*	*Height meter a.g.l*	*Instrument*
B	Turbulence components	1	26.0	Windmaster
A	Virtual temperature	1	26.0	Windmaster
B	CO2/Specific humidity fluctuations	1	26.0	LI-7500
H	Incoming/outgoing short wave radiation	1	21.9	CM21
I	Incoming/outgoing long wave radiation	1	21.9	CG1
I	Temperature long wave radiation sensors	1	21.9	PT100
G	Photosynthetically active radiation	1	24.5	LI-190SZ
E	Air temperature	3	23.5, 7.5, 5.0	HMP35A

J	Air pressure	1	15.0	PTB101C
E	Relative humidity	3	23.5, 7.5, 5.0	HMP35A
C	Wind speed	3	24.4, 7.5, 5.0	A101ML
D	Wind direction	1	24.0	W200P
A	CO2/H2O-concentration	5	24.4, 7.5, 5.0, 2.5, 0.4	CIRAS-SC
F	Precipitation	2	23.8 (tower), 0.4 (open field)	ARG100
F	Throughfall	1	1.0	IMAG
K	Soil heat flux	1	-0.1	PU43T
L	Soil moisture/ temperature	5	-0.03, -0.10, -0.25, -0.75, -2.00	Mux
-	Groundwater level (filter depth)	2	-6.5, -4.8	-

9.2.3 Data processing

The averaging period of the observations is 30 minutes and automatically stored.

9.2.4 Data quality control

The data in the EAGLE2006 database is level 2 data. In this case that means it contains the original data without any centralized quality check, gap-filling and partitioning.

10 EAGLE2006 Data Analysis and Results

As a result of the EAGLE2006 field data campaign, the dataset acquired within the days of the Field Experiment have been analyzed by the different teams involved. In this chapter a description is provided of the results from analysis after data processing.

At first a detailed description of the Sentinel-1 and Sentinel-2 simulations, as part of the objectives of EAGLE2006, is provided. Furthermore, results from characterizing the biophysical parameters measured during the EAGLE2006 campaign are included in the second part. A third and last part presents the results obtained from obtaining more advanced products, focusing on advancing our understanding of land-atmosphere interaction processes.

10.1 Simulation products

10.1.1 Sentinel-1 simulation

Team responsible: Scheiber, R, DLR-HR

Team members: Scheiber, R.; Keller, M.

Overview

For the assessment of specific programmatic needs of the Sentinel program and for the understanding and quantification of bio-geophysical parameters of different vegetated surfaces ESA has initiated and partially funded this airborne campaign in 2006. In the campaign the airborne SAR system of DLR, E-SAR was employed to acquire multi-frequency and multi-polarisation data over the different test sites.

For the EAGLE project two test-sites have been flown, Cabauw for specific investigations on agricultural areas and Speulderbos for forest parameter assessment.

This paragraph deals with the adopted methodology for processing the acquired E-SAR data, where the standard processing approach which leads to RGI (radar geometry images) and GTC (geocoded terrain corrected) products is described. Furthermore is included the generation of synthetic QUAD-POL products in C-band performed for the EAGLE project.

A section is devoted to the generation of Sentinel-1 like data quality products from high resolution C-band data as is requested by the specific programmatic needs of ESA.

Input data used

E-SAR C-band data of Cabauw test site

Processing and/or analysis done

Degradation of spatial resolution in slant-range and azimuth

- for stripmap mode (single-look): 5m in azimuth and 5m in ground range @ 20 deg incidence angle)
- for IWS (interferometric wideswath mode) (single-look): 20m in azimuth and 5m in ground range @ 25 deg incidence angle)

- decrease of PSLR (peak-sidelobe-ratio) (-25 dB)
- increase of noise level (NESZ = -22 dB)
- decrease of DTAR (point target ambiguity ratio) (-22dB)

Results/Output description

An example of the Sentinel-1 stripmap simulation (Fig. 82) compared to the full resolution high quality E-SAR data (Fig. 83) is shown in the attached multilook images (3 effective azimuth looks were used in both cases). Range resolution is almost identical, whereas azimuth resolution is 3m in the E-SAR case and only 12.5 m for the simulated Sentinel-1 product. The synthetic Quad-Pol products are displayed (RGB=HH-HV-VV).

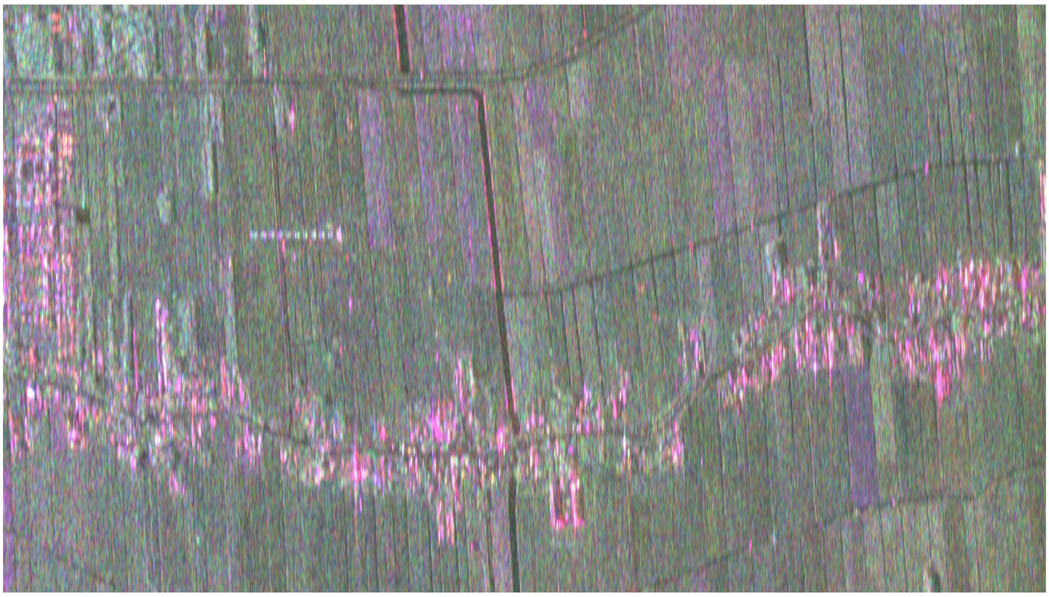
Figure 82. Stripmap simulation

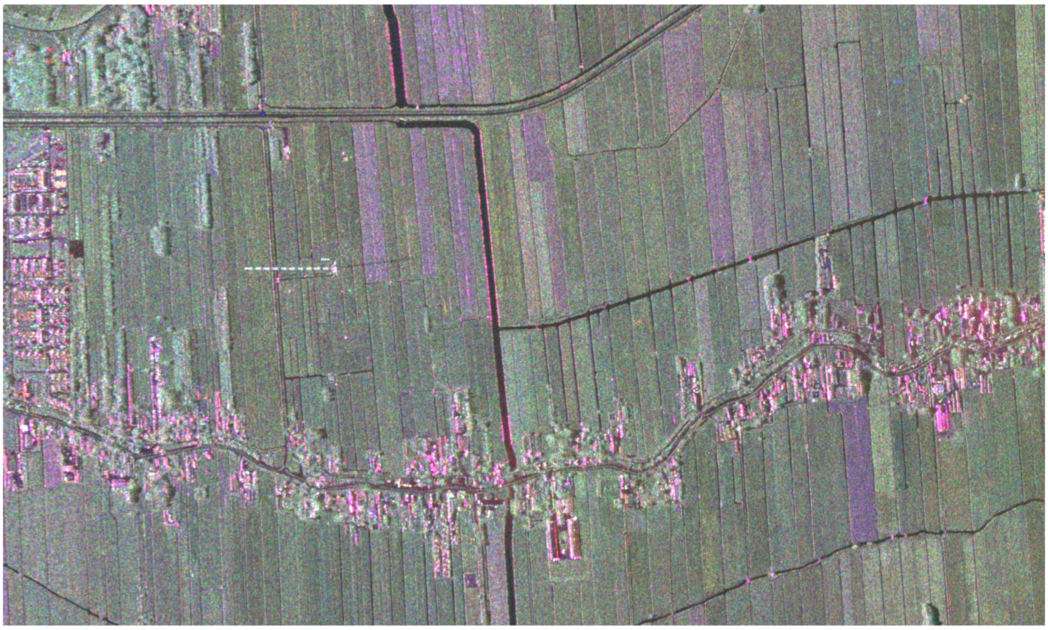
Figure 83. Full resolution

Conclusion and/or recommendation

Sentinel-1 stripmap simulation shows similar level of detail compared the original E-SAR images, especially in the single-look case.

However, in the Cabauw scene under consideration the discrimination of the small scale field structure poses problems in the IWS mode simulation (anticipated; not yet processed).

10.1.2 Sentinel-2 data simulation using AHS Hyperspectral imagery.

These simulations were carried out by both the Spanish INTA team as well as by the ITC-WRS team. Both approaches are described below.

INTA-approach

Team responsible: José Antonio Gómez

Team members: Alix Fernandez-Renau; Óscar Gutiérrez-de-la-Cámara; Eduardo de Miguel; Elena Prado; Ricardo Puente Robles

Overview

In the frame of the Global Monitoring for Environment and Security programme (GMES), ESA is undertaking the development of the Sentinel-2 optical mission providing enhanced continuity to Landsat/SPOT type measurements. ESA is using airborne campaigns carried out in the framework of Earth Observation Programmes to simulate the data and products of Sentinel-2. Imaging spectrometers become one of the best procedures to simulate future satellite performance. Within the context of the EAGLE2006 project the available AHS airborne hyperspectral imagery has allowed the simulation of sentinel-2 expected data. The AHS is an 80-band airborne line-scanner radiometer which spectral bands are laid out along the optical spectrum from the visible to the thermal infrared regions. It has been installed in a CASA C-212 aircraft and is complemented with an INS/GPS module to gather accurate positioning and attitude measurements. The AHS imagery was collected during the summer of 2006 with ground sample distance (GSD) of 2.4 and 6.9 meters, setting the flight parameters of acquisition time and directions according to project requirement but no for Sentinel-2 configuration. In EAGLE2006 the airborne campaign was carried out on June 13th over Cabauw, Loobos and Speulderbos test sites (The Netherlands). The AHS data were processed at INTA premises in Madrid, through an ad-hoc processing chain generating L1a, L1b and L2b products and delivered to the project partners. The geometric processing was applied with PARGE (ReSe Applications Schälpfer & RSL, University of Zurich)) using INS/GPS of the Applanix 440. The atmospheric correction was applied with ATCOR-4 (Dr. R. Richter, DLR & ReSe Applications Schälpfer) validated with ground field spectroscopy. An AHS imagery set was selected for the Sentinel-2 data simulation, giving priority in the selection for a flight direction close to the satellite future orbit, and images which include as much as possible urban, agricultural and natural areas. Two kinds of processes were applied depending on the simulation aim. • Process 1: with the aim to serve as input for the Image Performance Simulation (ASTRIUM) a set of L2c level AHS imagery were delivered to ESA Sentinel-2 group with the spectral and spatial resolution of the original AHS settings. • Process 2: with the aim to simulate directly the sentinel-2 images, AHS data were spectral and spatial resampled to Sentinel-2 configuration.

Input data used

Figure 84 (left part) shows the several spectral widths and spatial resolutions of the 13 bands designed for Sentinel-2. To address the specific needs on radiometric and geometric performance of Sentinel-2 mission the ESA defines some requirements for airborne hyperspectral data acquisition, those requirements determine the airborne campaigns definitions and are summarized in fig. 84 (right part).

Within the context of ESA ground-based and airborne campaigns AGRISAR and EAGLE2006, carried out during summer 2006, airborne hyperspectral imagery was collected with the INTA-AHS system. Although those campaigns are not specific designed for Sentinel-2 simulation, the hyperspectral data are good enough to test some aspects of the Sentinel-2 future performance. INTA Remote Sensing Laboratory processed AHS imagery available with the aim to provide spectrally, radiometrically and geometrically representative Sentinel-2 data.

Band #	Centre λcenter (nm)	Spectral width $\Delta\lambda$ (nm)	SNR @L_{ref}	SSD
1	443	20	129	60
2	490	65	154	10
3	560	35	168.4	10
4	665	30	142.1	10
5	705	15	117	20
6	740	15	89	20
7	775	20	105	20
8	842	115	174.6	10
8a	865	20	72	20
9	940	20	114	60
10	1375	20	50	60
11	1610	90	100	20
12	2190	180	100	20

Requirement	Description
Test site	Images over an urban, agricultural, and forest area
Time acquisitions	Local solar time close 11:00 (mid-latitude)
Flight track	Sun-synchronous orbit
View geometry	< 20º (zenith angle)
SSD (Spatial Sampling Distance)	3 times better than the lowest S-2 SSD (10m)
Spectral Domain	Requirement to cover the spectral regions necessary to simulate S-2 bands. Band 10 is not consider mandatory as it is only used for cirrus
Digitazion levels	At least 12 bits

Figure 84. Left part: Sentinel-2 spectral and spatial characteristics. Right part: airborne data acquisitions requirements for Sentinel-2 data simulation (extracted from Statement of work AIR-S2)

Processing and/or analysis done

AHS IMAGERY

AGRISAR/EAGLE2006 AHS imagery was collected during the summer of 2006. The flight tracks and AHS acquisition parameters were designed according to project requirements but not specifically for Sentinel-2 configuration.

For EAGLE2006 project the airborne campaign was carried out on June 13th over Cabauw, Loobos and Speulderbos test site (The Netherlands). Nominal low and high flight altitudes parameters setting were acquired, programming in this case several flight tracks to gather imagery in all of the test sites. Time acquisition was from 9:57 to 12:41 UTC.

SENTINEL-2 BOA REFLECTANCE SIMULATION METHODOLOGY

AHS imagery set was selected for the Sentinel-2 data simulation, priority selection was given to flight track close to the satellite future orbit, and images which include as much as possible urban, agricultural and forest areas. 2.4m and 6.9m spatial resolution AHS imagery came into the process. Depending on the simulation aim and user two kinds of processes were applied:

- Process type 1 (For ESA Sentinel-2 team): with the aim to serve as input for the Sentinel-2 Image Performance Simulator orthorectified BOA reflectance imagery was delivered with spectral and spatial resolution of the original AHS setting.
- Process type 2 (For AGRISAR/EAGLE2006 partners): with the aim to simulate directly the Sentinel-2 BOA reflectance, AHS data was spectrally and spatially resampled to Sentinel-2 configuration.

Both type processes overcame BOA reflectance data and for that reason the start point of each process was from nominal L2b INTA-AHS data product.

1) Nominal INTA-AHS data process

The INTA-AHS data distribution protocol delivers ungeocoded raw data (L1a) and georeferenceable at-sensor radiance (L1b) and ground reflectance and temperature (L2b) products, which are attached with geographic look-up table (*igm ENVI file) for the georeferenced process.

L1a (raw data, *L0R000* in INTA code): no processing, raw data imported to BIL format + ENVI header, 753 values per line (includes maker bit, BB1 and BB2), image and navigation stats computed for quality check,
L1b (at-sensor radiance, *L10020 / L00120*): The VIS/NIR/SWIR bands were converted to at-sensor radiance applying the absolute calibration coefficients obtained in the laboratory using the integrating sphere. The MIR/TIR bands were converted to at-sensor radiance using the information from the onboard blackbodies and the spectral response curves obtained by the AHS spectral calibration. The resulting files were converted to BSQ format + ENVI header and scaled to fit an unsigned integer datatype. The specifications are: NedL VIS-NIR : <0.2 w/(m^2srum), NedL SWIR: <0.3 w/(m^2srum) NedT TIR: <0.33 ºC,
L2b (Ground reflectance and temperature *L20020 / L00220*): ATCOR4 [6] code is used for the atmospheric correction of AHS imagery. ATCOR4 is based on MODTRAN-4 and performs a scan angle atmospheric correction taking into account flight altitude and illumination conditions. Water vapour is estimated directly from the image using the 940nm absorption band and aerosol type and visibility estimated by field spectroscopy and meteorological auxiliary data acquired by AGRISAR/EAGLE2006 ground teams.

Georeferenced process is made using the parametric code PARGE [7]. As input for the model a digital elevation model must be spatial resampled, for the AHS pixel sized. For AGRISAR the digital elevation model was delivered by the DLR with 2 meters of spatial sampling for the centre part of test site, the rest area covered and also for EAGLE2006 the DEM was extracted from the SRTM [http://www2.jpl.nasa.gov/srtm/index.html]. Also PARGE integrates the attitude info: Applanix POSAV-POSEO roll-pitch-heading and position info.

2) BOA reflectance Sentinel-2 simulation: process type 1

With the aim to serve as input for the Sentinel-2 Image Performance Simulator allowing the ESA Sentinel-2 team simulate Sentinel-2 at-sensor radiance, a set of AGRISAR AHS imagery was processed to orthorectified BOA reflectance and delivered with the spectral and spatial resolution of the original AHS settings.

AGRISAR AHS flight lines with headings of 202º-022º which are closer to future Sentinel-2 orbit were taken into account. To have examples from both AGRISAR missions, flight lines of June 6th and July 5th were selected. Images with pixel size of 2.4m suitable for Sentinel-2 10m band simulation, and 6.9m suitable for 20m and 60m bands were processed.

L2b INTA-AHS product is georeferenceable BOA reflectance. For the selected imagery geocoded process was applied using PARGE and keeping the spatial and spectral configuration of AHS. PARGE needs that the spatial resolution of the input DEM be slightly higher than the nominal resolution of the original image, so the final spatial resolution was 2m for low flight lines and 6m for the high flight lines. Spatial resampling applied to the output images was nearest neighbour in order to avoid spatial interpolation.

To facilitate the Sentinel-2 at-sensor radiance simulation by ESA Sentinel-2 team, the DEM used for the orthorectification process and the information of the meteorological and illuminating conditions of each image was provided.

3) BOA reflectance Sentinel-2 simulation: process type 2

With the aim to simulate directly the Sentinel-2 reflectance data, allowing AGRISAR and EAGLE2006 partners to simulate Sentinel-2 data products, AHS imagery was processed to orthorectified BOA reflectance and spectrally and spatially resampled to Sentinel-2 configuration (see Figs. 84-85) .

Same imagery set as AGRISAR for process type 1 plus June 13th EAGLE2006 flight lines with headings of 161º and 158º were selected for this process.

Original spectral configuration of AHS was spectrally resampled to Sentinel-2 using ENVI spectral resampling tool [http://www.ittvis.com/envi/index.asp], assuming gaussian spectral response of each band (Figure 3). Sentinel-2 B1 centred at 443 nm and with spectral width of 20 nm was simulated with the AHS-1 centred 455 nm and with a Full Width at Half Maximum (FWHM) of 30 nm. Sentinel-2 B-10 was not covered by AHS.

In order to keep as much as possible the spatial conditions of Sentinel-2, only pixels observed with a zenith angle lower than 20º were taken into account, for each image processed pixels out of that limits were discarded. That observation limits represents imagery of lines with 336 pixels instead of the original 750. PARGE was configured to orthorectify the subset AHS imagery with the 20º limit observation, the output spatial resolution was, like in process type 1, 2m for low flight lines and 6m for the high flight lines. Entire Sentinel-2 spectral configuration was orthorectified.

To achieve the different Sentinel-2 pixel sizes (10m, 20m and 60m) AHS imagery geocoded outcome were spatially degraded using ENVI pixel aggregated method. This method convolve the original pixels that going to be part of the desired spatial resolution averaging the corresponding square kernel, in the case of 2m pixel imagery those 336 pixels represents just 12 pixels in 60m Sentinel-2 bands so only 6m imagery was finally delivered. For each image processed the completely Sentinel-2 spectral configuration was generated in the three different spatial resolutions.

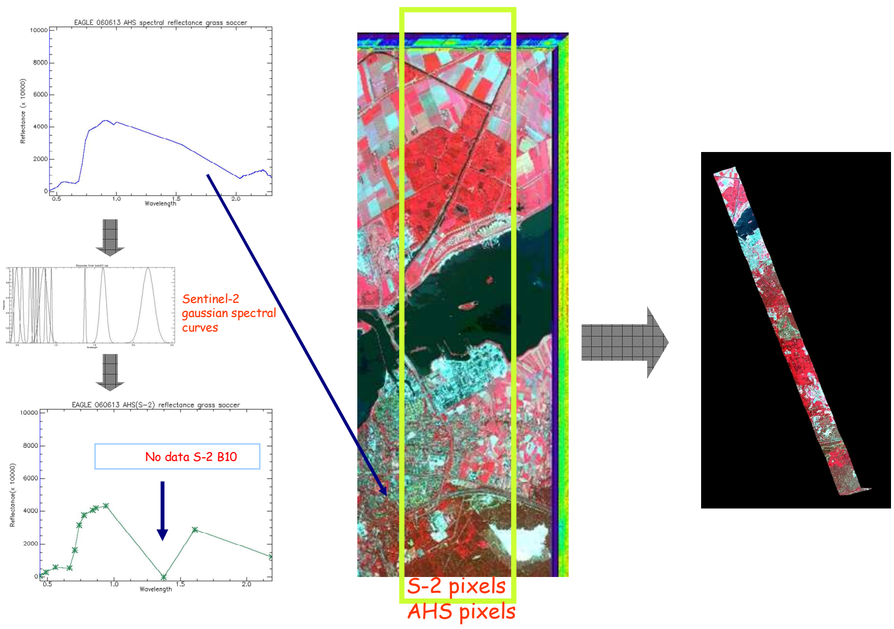

Figure 85: Spectral resampling and geocoded process of AHS imagery to Sentinel-2

Results/Output description

For both type of processes complete ENVI compatibility imagery was delivered with orthorectified BOA reflectance binary data and header ENVI files.

1) Reflectance Sentinel-2 AHS process type 1

Orthorectified BOA reflectance imagery, as it can be seen in the Fig. 86, was obtained with the original AHS spectral and spatial configuration. Also the output image maintain the fully spatial cover of the original AHS image, georeferenced system was UTM WGS 84 zone 33 and the geometric accuracy was below 2 pixels.

The outcome imagery is going to serve as map reflectance so no image noise was added. In order to avoid spatial interpolation the resampling method applied in the geocoded process was the nearest neighbour.

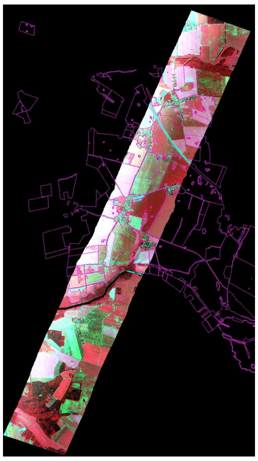

Figure 86: Orthorectified BOA reflectance AGRISAR AHS imagery for Sentinel-2 simulation process type 1.

2) Reflectance Sentinel-2 AHS process type 2

The outcome image for process type 2 is also orthorectified BOA reflectance but with Sentinel-2 spatial and spectral configuration (see Fig. 87), this means an output image with 13 bands (but with no dada for S-2 B-10) in the three different spatial resolutions but only with the central part of the AHS image.

Figure 87 shows a image subset, as an agricultural area example, in the different Sentinel-2 spatial resolution defined (10m, 20m and 60m), suitable obtained by spatially degrading the 6m pixel size of the AHS due to the relative low spatial frequency. ENVI pixel aggregated method applied was no taken into account the influence of the neighbour pixels.

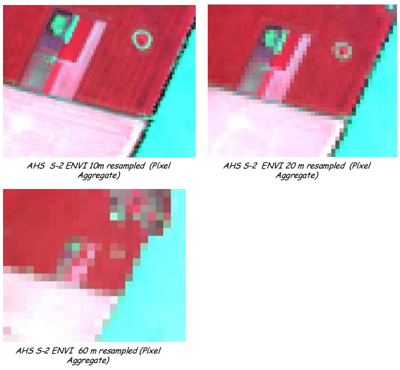

Figure 87: Sentinel-2 spatial resolutions simulated with AHS 6m imagery

The Sentinel-2 spectral band synthesis combining AHS spectral bands have a few inconveniences. Sentinel-2 B1 centred at 443 nm and with spectral width of 20 nm was simulated with the AHS-1 centred 455 nm and with FWHM of 30 nm. Sentinel-2 B-10 was not covered by AHS, but is not consider by ESA mandatory band for simulation. Sentinel-2 bands 5,6,7 8a, 9 and 11 have minor spectral width than the AHS has in their corresponding bands.

Conclusion and/or recommendation

Process type 1 was delivered to Sentinel-2 team on February 2007, and process type 2 was delivered to AGRISAR / EAGLE2006 partners on April 2007

Sentinel-2 BOA reflectance data simulated by AHS data provides ability to simulate Sentinel-2 at-sensor radiance data and also define different products. Through simulation, data requirements can be assessed against application and research needs.

Although AGRISAR and EAGLE2006 campaigns are not specific designed for Sentinel-2 simulation, the airborne hyperspectral data gathered was good enough to test some aspects of the Sentinel-2 future performance. INTA Remote Sensing Laboratory processed AHS imagery available with the aim to provide spectrally, radiometrically and geometrically representative Sentinel-2 data.

ITC-WRS approach

Team responsible: Joris Timmermans

Team members: Joris Timmermans and Wout Verhoef.

Overview

The need for multi-spectral high-resolution optical images is high. Such images are used in remote sensing for services like “Inland Water quality”, “Crop Yield assessment” and “Flood Risk Analysis”. The GMES program ensures continuity of these services by planning future earth observation platforms like Sentinel 2. In the framework of the Sentinel 2 mission a database has to be constructed for the investigation and validation of the retrieval algorithms for bio-geophysical parameters. The objective of this research is to simulate Sentinel 2 images that have the same spectral characteristics as the future satellite. The images can then be used to investigate retrieval algorithms. Three parameters have to be taken into account when simulating the satellite imagery: reflected radiation, atmospheric conditions and sensor characteristics. The radiation reflected by the surface is measured by a hyperspectral instrument. The dark-pixel approach was used to estimate atmosphere conditions. The surface reflectance was derived by an atmospheric correction algorithm, taking into account adjacency effects. The top-of-atmosphere radiation was generated using forward modelling of the atmospheric effects. Sentinel 2 images were created by applying the associate sensor response functions. The Sentinel 2 simulated image is based on the hyperspectral high-resolution images acquired by INTA. These images were acquired with the AHS instrument on 13-06-2006 during the EAGLE2006 field campaign in the Netherlands. MODTRAN was used for the dark-pixel approach. This contribution describes the methodology, the measurements by AHS instrument, the image simulations, and discusses the final results obtained.

Input data used

INTA AHS airplane images

PO1A, 11:34 UTC, airplane height: (2789m), ground resolution 6.9m

PO2B, 11:50 UTC, airplane height: (2789m), ground resolution 6.9m

ASD/GER hyper spectral derived reflectances

Forest, Grass, Young corn, Heath

Processing and/or analysis done

The overall data flow is given in Fig. 88. The processing procedure is as follows:

- Using the water bodies in the PO2B image, the atmospheric profile during the time over overpass is established.
- This Atmospheric profile is used atmospherically correct the radiances. The adjacency effect was corrected using a spatial filter.
- TOC reflectances are created from the radiances.
- The TOC reflectances obtained here are compared to the ground measured TOC reflectances of the hyperspectral sensors. The comparison resulted in quality indicators of the atmosphere and AHS acquisition.
- Using forward modelling in combination with the retrieved atmospheric profile, TOA radiances were obtained.
- The Sentinel-2 spectral and spatial sensor characteristics were implemented on the TOA radiances.
- Sensor noise was added.

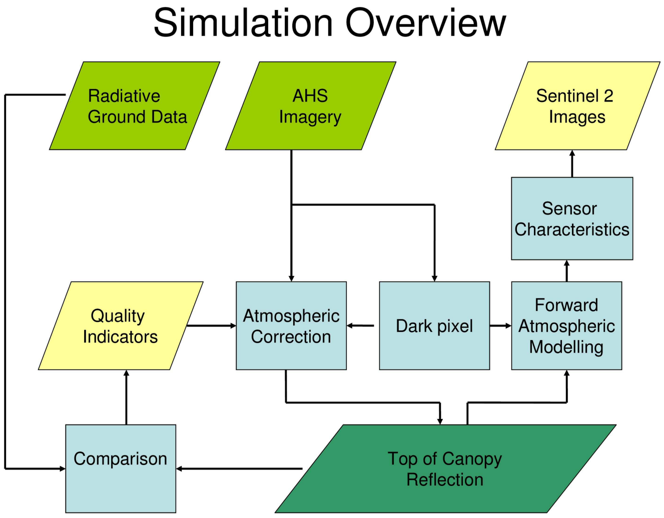

Figure 88. Overall data flow

Results/Output description

The final output of the simulations is the Sentinel-2 simulated image, the quicklooks are shown in Fig. 89-91. Band 10 could not be simulated because no AHS band had spectral overlap with the band 10 of Sentinel-2.

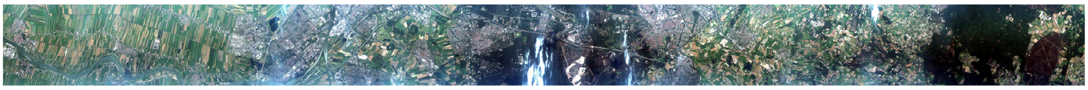

Figure 89. RGB image of Bands 4, 3 and 2 (665nm 560nm 490m) (spatial resolution is 10m)

Figure 90. FCC 8a, 12 and 5 (865nm 1610nm 705nm) (spatial resolution is 20m)

Figure 91. FCC image of Bands 9, 10, 1 (940nm, 1375nm, 443nm) (resolution is 60m resolution)

Conclusion and/or recommendation

We conclude that Sentinel-2 images were simulated successfully, except for bands 9-11. Sentinel band 10 could not be simulated as no AHS measurement has spectral overlap with this band. Sentinel-2 bands 9 and 10 are not simulated satisfactory because they are based the quality of their “parent” AHS bands (18 and 21) which was low.

10.2 Biophysical products

Team responsible: Patrick van Laake

Team members: Zoltán Vekerdy (ITC), Remco Dost (ITC), Joris Timmermans (ITC), Erik Claassen (FUGRO-Inpark), Ron Rozema (FUGRO-Inpark).

Overview

In determining the surface-energy budget, the interaction of the vegetation with the atmospheric boundary layer has always been coarsely approximated because an accurate description of the canopy could not be made. Vegetation has been assumed to have a single measure of roughness, an assumption that is particularly weak for natural forests. A good description of the forest canopy structure is necessary for the estimation of radiation absorption and emission by the canopy and its associated processes of photosynthesis and evapotranspiration. In this research we present the results of an analysis of a highly accurate laser scanning data of a needle-leaf forest in The Netherlands in combination with an object-oriented classification of tree crowns from airborne high-resolution optical imagery. The laser scanning data is applied to parameterize a mathematical description of tree crowns, which has required the development of a novel technique to distinguish between the signals emanating from nearby or interlocking tree crowns. The local, spatially and structurally accurate description of the canopy can then be combined with the object-oriented classification of the canopy over a larger area. These results combined with further variables (e.g. LAI) provide a basis for a more accurate description of the canopy and vegetation related parameters, such as surface roughness, biomass and directional backscatter, leading to more detailed modeling of radiation-governed processes.

Input data used

Terrestrial laser scan point cloud of a 0.1 ha Douglas fir stand next to the Speulderbos observation tower. The measurements were taken from several different view angles to minimize the obstruction of details.

A Leica HDS2500 laser scanner was used for the data acquisition, operated by FUGRO-Inpark B.V. (Fig. 92).

Figure 92. The Leica HDS2500 laser scanner in operation at Speulderbos.

Processing and/or analysis done

In the first step, the row scans were co-referenced and merged into one point cloud (Fig. 93). A subset of the point cloud was created then, making sure that both the top and the structure of the canopy is properly represented. Biometric characteristics of the stand and its canopy were analyzed.

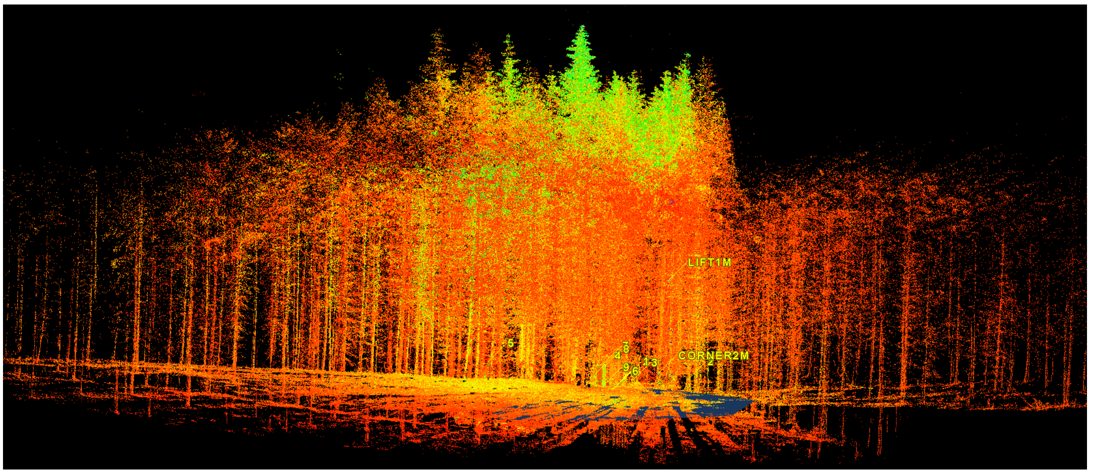

Figure 93. The co-referenced and merged point cloud of the Speulderbos forest site.

The analysis focused on two issues: the structure of the canopy, and the modeling of the forest.

Forest stands have an effect on the surface energy balance by, among others, representing increased aerodynamic roughness, which is a function of the stand and canopy structure. A variogram analysis was carried out to get an insight into the spatial variability of the canopy top.

Wind obstruction is a function of the density of the stand. It varies according to the structure of the forest: close to the ground it depends on the stem density and the understory, whilst close to the top it depends on the density of the branches and leaves. This was characterized with a voxel-based statistical method.

Using the maximum elevation in a fine grid superimposed on the point cloud, it is also possible to extract the shape of the crown (Fig. 94). When contours are drawn around the points, these contours can be used to derive a close envelope of the canopy or an approximate geometrical form (a cone in this case of pine trees). These abstract representations can be extremely useful in forest growth models (including carbon balance) because they allow for the statistical description of mixed forest stands. This line of investigation still requires additional research.

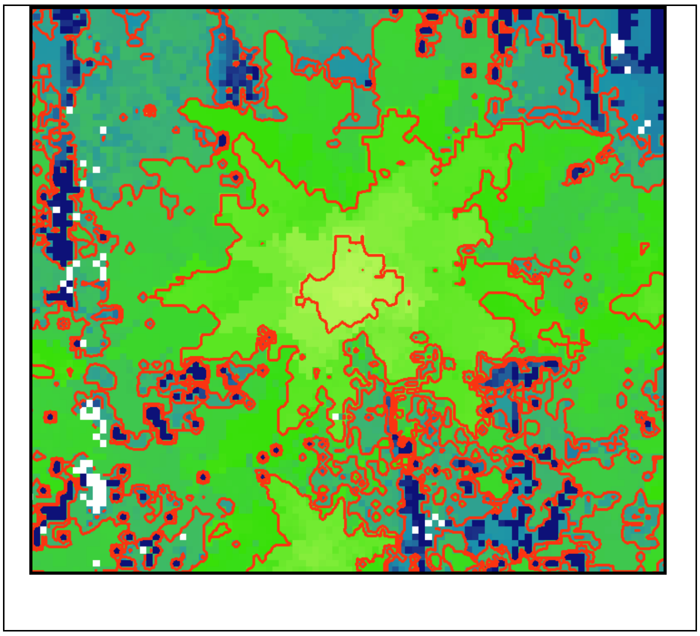

Figure 94. Canopy contouring (10 cm pixel spacing)

Results/Output description

The spatial variability of the surface is represented by the empirical (semi-)variograms (Fig. 95). The range depends on the average stem distance, in our case it is about 5 m.

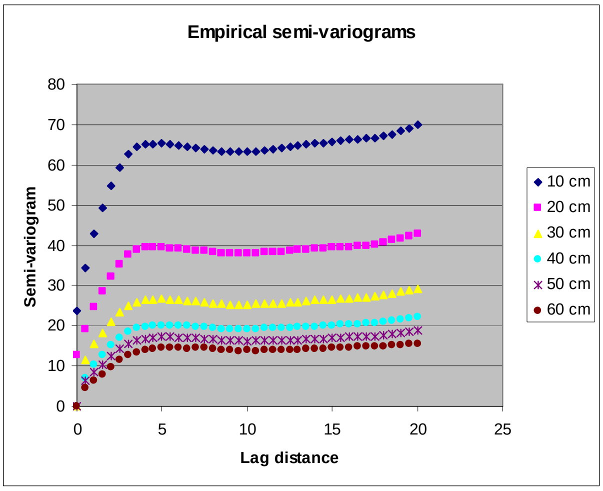

Figure 32. Dependence of the semi-variograms on the voxel size.

Horizontal sections taken at different altitudes from the ground were created (Fig. 96). Spatial analysis of point clustering proves the thickness of branches and leaves. In case of highly clustered points, like in the figure, the returns are mostly from stems, i.e. there is practically no undergrowth present.

The structure of the whole stand is characterized by the vertical distribution of the point density (Fig. 97).

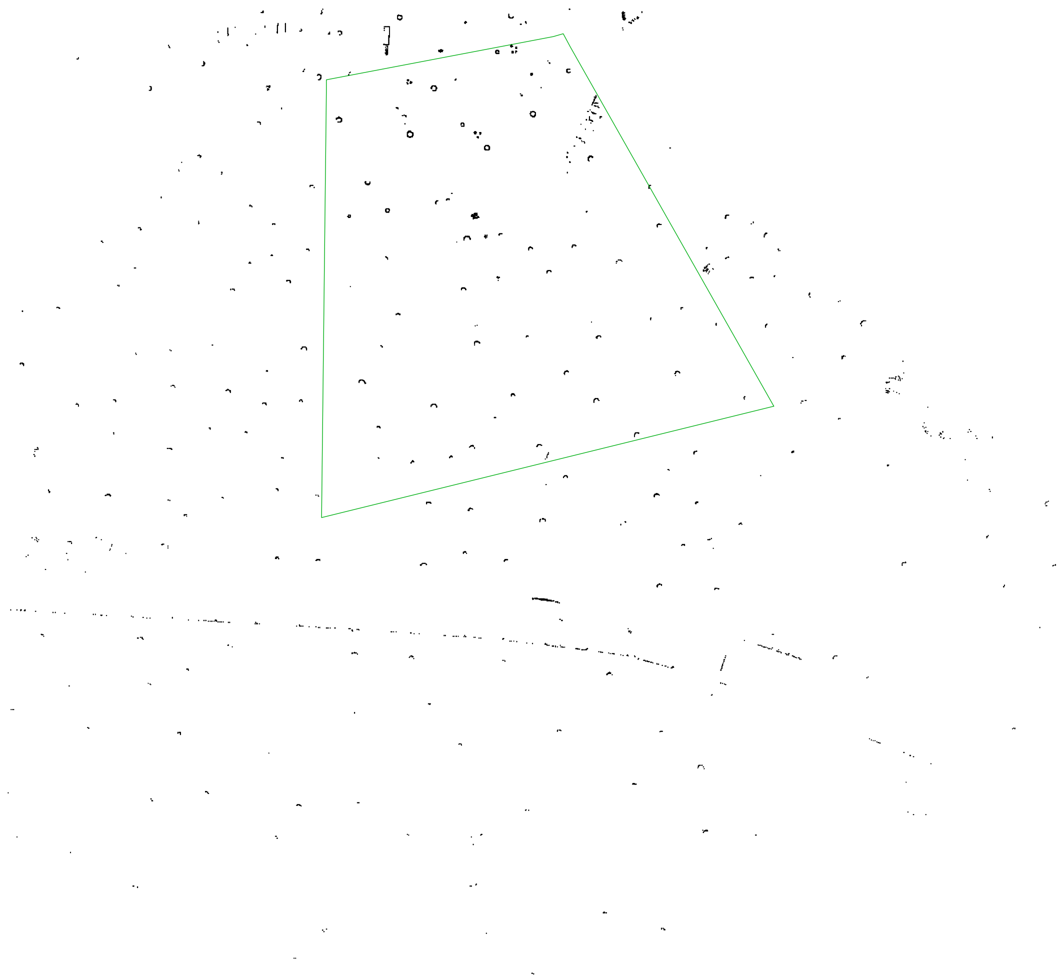

Figure 96. Horizontal section of the scanned area taken at breast height (1.3 m above ground level). The trapezoid shows the stand which was analyzed in detail.

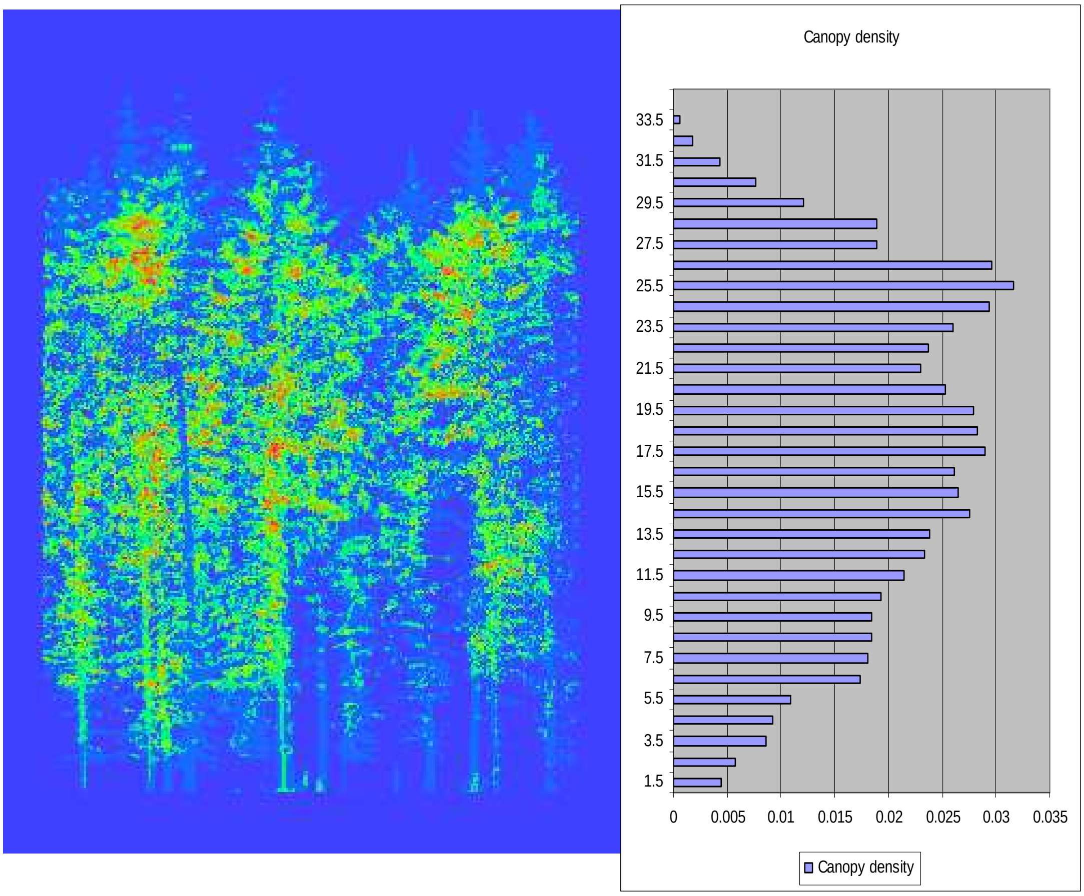

Figure 97. Vertical section of the forest (on the left) and the statistics of laser return counts per 1 m thick horizontal layers (on the right).

Conclusion and/or recommendation

The results of the analysis serve the first steps towards the complex modeling of forests. On the one hand, the structural analysis forms the basis of further investigations to a physically-based determination of aerodynamic roughness parameters (roughness length and height). Direct measurements of wind will be needed at different levels in and above the forest for describing the wind profile and relating it to the forest density profiles. This type of results has not been published widely in the international literature yet, so this is a promising field in surface energy balance related research. The second line of research, canopy structural modeling, is promising for developing new models of forest growth driven by current observation techniques.

10.3 Advanced products

10.3.1 Net ecosystem exchange and footprint analysis above forest and grassland

Team responsible: Massimo Menenti

Team members: Marco Esposito; Vicenzo Magliulo

Overview
The Sky Arrow ERA is small low flying research aircraft equipped with up-to- date instrumentation suitable for the determination of mass and energy exchange of terrestrial ecosystems, via airborne eddy covariance (AEC). AEC differs from ground-based eddy covariance for the algorithms used to establish the running mean to compute statistical moments, since a spatial average is used to avoid uneven sampling of turbulent structures. Turbulent fluxes measured by AEC refers to the landscape scale, thus allowing for studying the response of entire ecosystems to environmental drivers. In this work carbon dioxide, latent and sensible heat as well as momentum fluxes were calculated on both a grassland (Cabauw) and a forest site (Speulderbos) in the Netherlands, in the context of the EAGLE 2006 campaign. Results were compared with flux data of conventional eddy covariance towers. A total three mission flights were performed, two on the 13th of June 2006 and one on the 14th. The first flight was performed at the same time as the INTA CASA aircraft mission, to match in time in situ airborne measurements with hyperspectral data. The difference between the two different land use was significant even at the spatial scale of the area-averaged airborne measurements. These spatial averages of the airborne measurements were in good agreement with the time-averaged ground measurements. The mission was flown also at different altitudes to quantify the vertical divergence of the fluxes. A preliminary analysis of the measurements at different elevations showed an interesting vertical variability of fluxes, particularly for the Speulderbos site. Weather conditions and wind direction were very different on the 13th respectively 14th of June, suggesting significant differences in the flux densities. Since the wind direction changed from NE to SW, the footprint of the airborne measurements at a given location changed significantly from the first to the second flight and, with that, the observed flux densities. An approximate analytical model was applied to estimate the scalar flux footprint to clarify the differences in the flux values between the two days.

10.3.2 Temperature and evapotranspiration from AHS data

Team responsible: José Antonio Sobrino

Team members: Juan C. Jiménez-Muñoz, Guillem Sòria, Victoria Hidalgo, Belén Franch, M. Romaguera.

Overview
Land surface temperature and emissivity have been retrieved from the Airborne Hyperspectral Scanner (AHS) in the framework of the EAGLE2006 field campaign. Different plots were selected as a test points to compare results extracted from the airborne imagery against in-situ measurements. Differently to previous ESA/EU funded campaigns, EAGLE2006 offered for the first time the opportunity to test emissivity results over non-agricultural sites. Particularly, a plot of sand was considered in the study, which has a high spectral contrast and it is of special interest on the analysis of the emissivity spectrum. Other plots included grassland and forest, the last one continuously measured using a thermal camera. Surface temperature and emissivities have been used as input to solve the energy balance equation, from which evapotranspiration was finally estimated.

1) Land surface temperature

Input data used

The input data for the Land Surface Temperature product is composed by Airborne Hyperspectral Scanner (AHS) imagery (Level 1b product, at-sensor radiances plus IGM files for geometric correction).
Data included in the atmospheric soundings has been also used for atmospheric correction.

Processing and/or analysis done

Land Surface Temperature has been retrieved using the Temperature and Emissivity Separation (TES) algorithm (Gillespie et al., 1998). It is composed of 3 modules: NEM, RATIO and MMD. The NEM module is an iterative procedure that provides a first guess for temperature and emissivity. The RATIO module normalizes the surface emissivities, providing the so called beta spectrum. Finally, the MMD module uses a semi-empirical relationship between the minimum emissivity and the spectral contrast MMD: $\varepsilon_{min} = a + b\ MMD^{c}$. This method requires multispectral TIR data, with at least 4 or 5 thermal bands. From the 10 AHS TIR bands, we have selected bands 71,72,73,76 and 77, since they are located in optimal atmospheric regions and they are also similar to the five ASTER thermal bands, for which the TES algorithm was originally designed.

Results/Output description

Land Surface Temperature products correspond to AHS imagery geometrically corrected and acquired on 13-June-2006 (a complete description of AHS acquisitions can be found in the report provided by INTA). Temperature values are given in Kelvin (floating point format).

Land Surface Temperature retrievals have been validated against ground measurements collected in the top of the Speulderbos tower, using CIMEL and Thermal Camera instruments. Root Mean Square Errors of 1.1 K and 2.0 K were obtained when validating data acquired with Thermal Camera or CIMEL, respectively (see Fig. 98). An example of Land Surface Temperature maps is presented in Fig. 99.

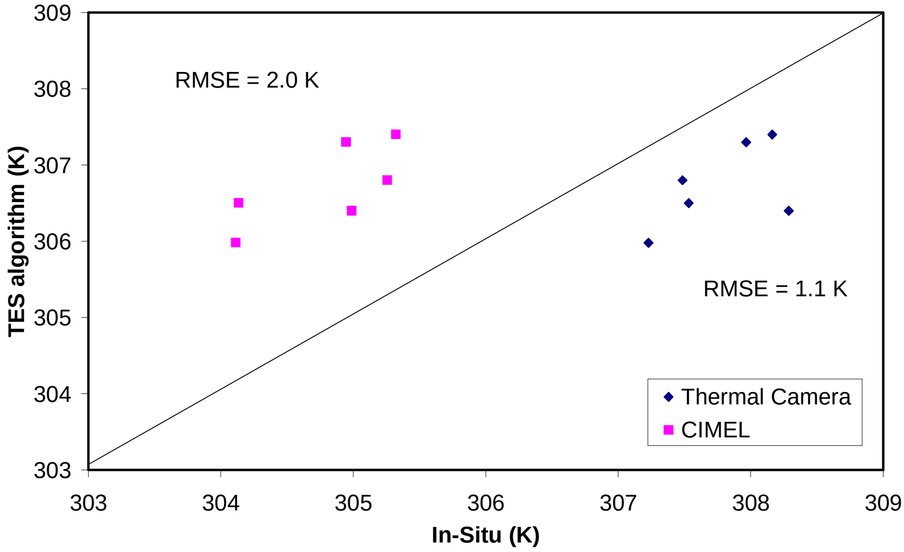

Figure 97. Comparison between Land Surface Temperature values extracted from AHS data after applying the TES algorithm and the ones measured in situ.

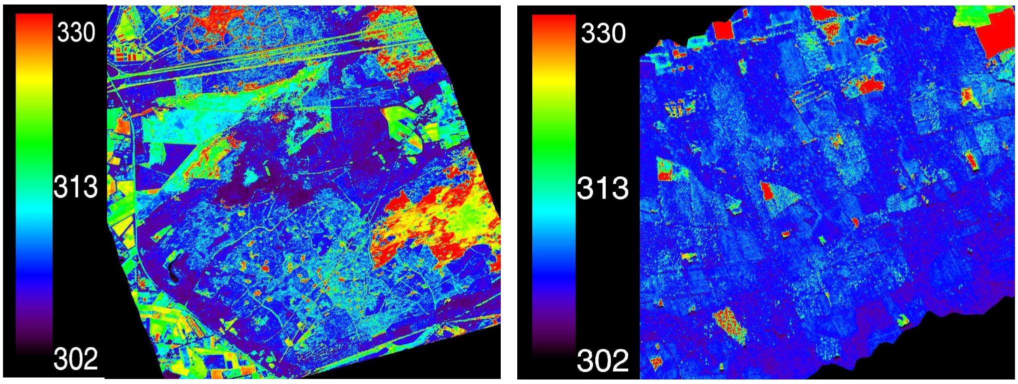

Figure 98. Examples of Land Surface Temperature maps obtained from AHS data.

Conclusion and/or recommendation

Land Surface Temperature products from AHS imagery have been obtained using the TES algorithm applied to AHS bands 71, 72, 73, 76 and 77. Validation against in-situ measurements provided a RMSE between 1 and 2 K.

2) Evapotranspiration from AHS data

Team responsible: José A. Sobrino (Global Change Unit)

Team members: Juan C. Jiménez-Muñoz, Guillem Sòria, Victoria Hidalgo, Belén Franch, M. Romaguera.

Input data used

The input data for the evapotranspiration (ET) product is AHS level 1b data and the Land Surface Temperature product.

Meteorological data as incoming longwave and shortwave radiation is also used.

Processing and/or analysis done

The method used for instantaneous and daily ET estimation is based on the Simplified Surface Balance Index (S-SEBI) model and the evaporative fraction concept proposed by Roerink et al. (2000). The evaporative fraction is obtained from the scatterplot between surface temperature and albedo, where albedo is calculated using AHS bands 9 and 12. Level 1b data has been transformed into reflectances and atmospherically corrected using the simple method proposed by Chavez (1996).

The soil heat flux has been obtained from the Modifield Soil Ajusted Vegetation Index (MSAVI).

For the calculation of ET we have assumed a value of 0.98 for emissivity and a value of 0.3 for the ratio between daily and instantaneous net radiation ($C_{di} = R_{nd}/R_{ni}$).

Results/Output description

Evapotranspiration products correspond to AHS imagery geometrically corrected and acquired on 13-June-2006 (a complete description of AHS acquisitions can be found in the report provided by INTA). Evapotranspiration values are given in mmd^{-1}.
Table 43 shows some of evapotranspiration values obtained for the Speulderbos area.
An example of ET maps is presented in Fig. 99.

Table 43. Values of daily ET (ETd) and instantaneous ET (ETi) obtained from AHS data in the Speulderbos area.

Local time	Flight Altitude	ETd (mm)	ETi (mmd^{-1})
12:51	1021 m	4	8
13:34	2789 m	4	9
13:50	2789 m	4	9
14:24	1021 m	4	10
14:32	1021 m	4	10
14:41	1021 m	6	12

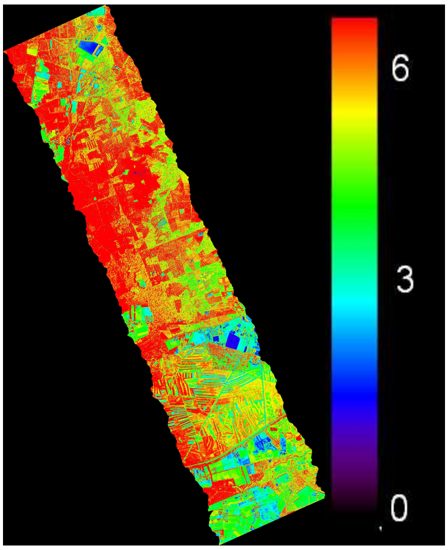

Figure 99. Example of evaspotranspiration map (in mmd^{-1}) obtained from AHS data.

Conclusion and/or recommendation

Evaporanspiration products from AHS imagery have been obtained using a method based on the S-SEBI model. At this moment this is a very experimental product, which needs a complete validation from in-situ measurements and also comparison with more sophisticated models.

10.3.3 Modeling fluxes of energy, water and carbon dioxide above the Speulderbos

Team responsible: Christiaan van der Tol

Team members: Christiaan van der Tol, Joris Timmermans, Wout Verhoef, Bob Su, Kitsiri Weligepolage, Oscar Hartogensis.

Overview

It is important to be able to accurately estimate vertical fluxes of energy, water vapour and carbon dioxide. These fluxes play a vital role in disciplines like weather prediction, agriculture, hydrology and climate change studies. Remote sensing is a promising tool to monitor fluxes over larger areas. The problem is that sensors on satellites and most airplanes do not detect fluxes directly, but only emitted and reflected radiation. One of the aims of the EAGLE campaign is to extract as much information about fluxes as possible from measured radiation.

During the EAGLE campaign, fluxes of carbon dioxide, water vapour and heat were measured with eddy covariance instruments above a 30 m tall spruce forest (Speulderbos) in the Netherlands. In addition, standard meteorological data, vertical profiles in the canopy of air temperature and humidity, and component temperatures were measured. The objective of these measurements is to test and improve flux retrieval algorithms from remote sensing products, in particular multi-directional thermal measurements.

A model was developed that calculates not only the vertical fluxes of energy, water vapour and carbon dioxide of a forest, but also the top-of-canopy reflected and emitted radiation. This model is a combination of a radiative transfer model (SAIL) and a 1D turbulent flux model. The combined model simulates the fluxes and the reflected spectrum simultaneously. Multi-angular remote sensing can be used to constrain the probability density of parameters in the model to improve estimates of fluxes.

Fluxes are calculated, first using a-priori parameter values only, and second using additional contact temperatures of needles to constrain the parameters of the model. A Bayesian approach was used, accounting for the accuracy of a-priori parameter estimates and the accuracy of measurements. The calculation was repeated for directional measurements of thermal infrared radiation above the canopy instead of contact temperatures. In both cases, using both a-priori parameters and measurements gives better estimates of the fluxes than using only a-priori information or only measurements.

Input data used

Measurements were carried out on a scaffolding tower with the highest platform at 46 m height, operated by the National Institute for Public Health and Environment (RIVM). Table 44 shows which data were measured at which height. All meteorological measurements except eddy covariance were carried out and data stored at 1 minute intervals on dataloggers (Campbell Scientific). Eddy covariance measurements were carried out and data stored at 20 Hz.

Table 45 shows how the data are organised in the database. The Excel file in directory 'meteo' contains only the raw, unprocessed meteorological data. The text files contain the processed data. Each directory contains a readme file.

Table 44. Micro-meteorological measurements carried out at the Speulder forest during the EAGLE campaign.

Measurement	Instrument	Height
Eddy covariance	CSAT3 (Campbell Sci., USA) LI7500 (Campbell Sci.)	47 m
Sensible heat flux	Large Aperture Scintillometer between Speuld and Drie (3 km) (Kipp and Zonen)	47 m
Radiation	CNR1 (Kipp and Zonen, Delft, The Netherlands)	35 m
Temperature and humidity	HMP45C-L (Campbell Sci.)	1, 27, 35 m
Wind speed and direction	Cup anemometer and wind vane (Vector Instruments Ltd., UK)	35 m
Vegetation contact temperatures	9 NTC resistances	17-30 m
Soil contact temperatures	8 NTC resistances	0 m
Soil moisture content	CS616 TDR (Campbell Sci.)	-5, -30, -55 cm
Soil temperature	107-L sensors (Campbell Sci.)	-1, -3, -8, -90 cm
Soil heat flux	3 HFP01SC-L Huxeflux (Cambell Sci.)	-0.5 cm

Table 45. Organization of the database

Directory	Sub-directory	Description
Meteo		Meteorological variables
Turbulence	LAS	Sensible heat flux with LAS
	EC	Eddy covariance measurements

Processing and/or analysis done

Processing of the raw data

Half-hourly averages of all meteorological data were calculated and stored in text files in directory meteo. A text file ‘t.s06’ denotes the local time (GMT +2) in decimal day corresponding to the meteo data files.

Radiation measured with the CNR1 was re-calculated after recalibration of the instrument in January 2007. The recalculated values are stored in the text file Rn.s06.

Soil moisture content is uncalibrated: the data represent the raw output signal of the CS616 in Θs. Conversion to volume fraction of soil moisture can only be carried out after calibration for the soil. This calibration is currently been carried out in the field, but results are not yet available. Alternatively, soil moisture content Θ can be calculated from the raw signal *S* with a standard as an approximation:

$$\theta = 0.007S^2 - 0.063S - 0.0663$$

Contact temperatures (^{o}C) were calculated from the raw signal of the NTC thermistors *S* (Ohms) using the relationship between resistance and temperature of the sensors:

$$T = -1.77 \cdot 10^{-6} S^3 + 1.7 \cdot 10^{-3} S^2 - 0.55\, S + 62.03$$

Eddy covariance fluxes were calculated with the software ECpack (http://www.met.wau.nl/projects/jep/index.html). The data were corrected for a linear trend, sonic temperature was corrected for humidity, the wind vector was turned such that the mean v = 0, and a Webb correction was carried out. The options used in the program ECpack are listed in the file ‘data/turbulence/ec/Spec_EC.dat’.

Sensible heat flux was calculated from Large Aperture Scintillometer data following Meijninger and De Bruin (2000), J. Hydrol., 229(42-49). The data base contains both the raw data and the calculated sensible heat flux.

Advanced analyses

The following advanced analyses were carried out:
(1) a study of the energy balance of the surface: incoming and outgoing radiation, sensible and latent heat flux and soil heat flux;
(2) a comparison between sensible heat flux calculated from eddy covariance data and from Large Aperture Scintillometer data;
(3) a study of the roughness of the surface from eddy covariance and wind measurements;
(4) a model study of the fluxes and contact temperatures.

Results/Output description

This section presents a summary and a key graph of the results of each of the 4 advanced data analyses.

Energy balance

The slope of the regression line of turbulent fluxes (latent and sensible heat flux) versus net radiation less soil heat flux and is 0.74 (Fig. 100). The fact that the energy balance does not close, is most likely caused by a combination of factors: overestimate of net radiation, underestimate of soil heat flux, and an underestimate of eddy covariance fluxes. The CNR1 radiation sensor was re-calibrated by the manufacturer in January 2007, and the calibration factors were significantly different. The error in the calibration of the CNR1 can be 10 percent of radiation, which is not enough to explain the error in the energy balance. Measured soil heat flux was only a few percent of net radiation, which is low compared to literature values. Even in a forest, soil heat flux can be a third of net radiation (Ogee et al., Agric. For. Met. (2001) 106(3) 173-186).

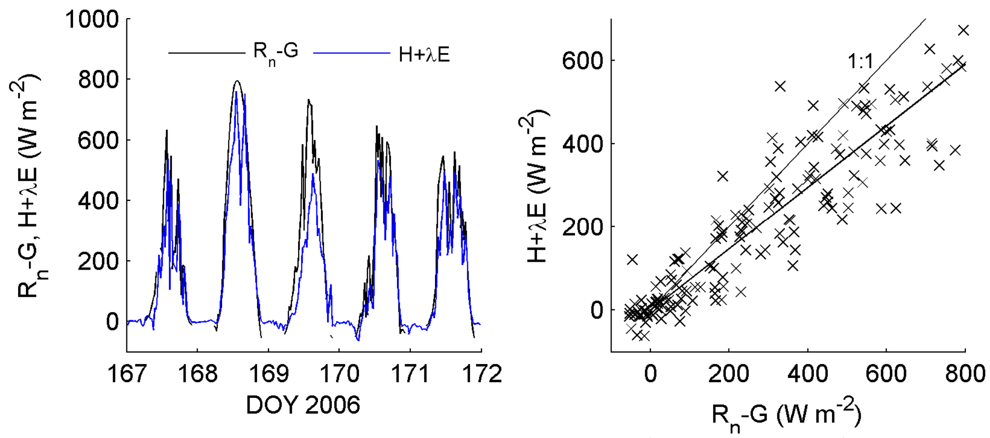

Figure 100. Comparison between net radiation minus soil heat flux and the sum of latent and sensible heat flux measured in the Speulder forest during the EAGLE campaign

Comparison between eddy covariance and scintillometer

Eddy covariance and large aperture scintillometer (LAS) measurements of sensible heat flux agree well, despite the fact that LAS measures over a larger area (Fig. 101). The two methods are not entirely independent, since in the calculation of sensible heat flux from the raw signal of the LAS, local roughness and stability estimates were used.

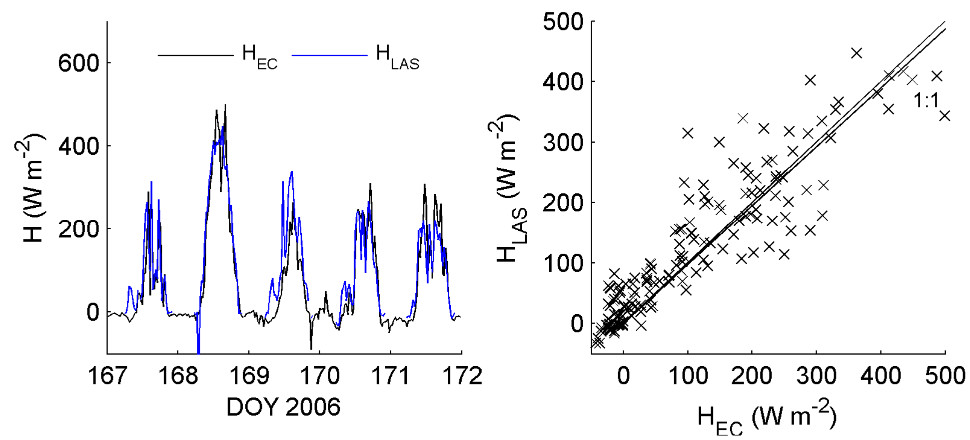

Figure 101. Comparison between eddy covariance and large aperture scintillometer measurements of sensible heat flux at the Speulder forest during the EAGLE campaign

Roughness

Roughness height for momentum z_{0m} and zero plane displacement height d for the Speulderbos site were derived from eddy covariance measurements at 47 m height and cup anemometer wind measurements at 35 m height using Monin Obukhov theory. The resulting values of z_{0m} = 0.54 m and d = 16.2 m are lower than expected based on values commonly found in literature (Fig. 102).

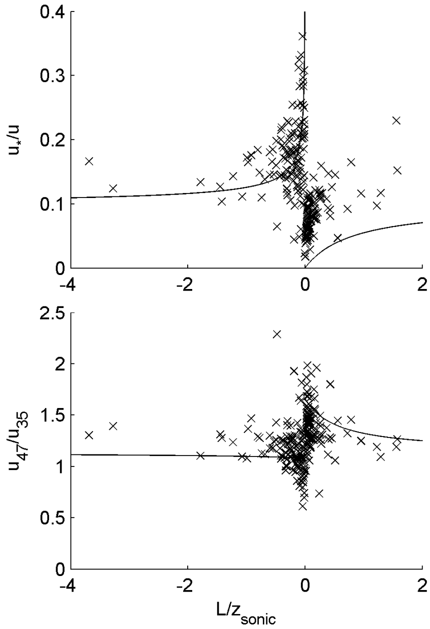

Figure 102. Left: measured (x) and modeled ratio of friction velocity over horizontal wind speed calculated from sonic anemometer data versus L/z_{sonic} (upper graph), and idem for u_{47}/u_{35} versus L/z_{sonic} (lower graph).

Modelling

A model was developed to calculate simultaneously radiative transfer and the fluxes of energy, water and carbon dioxide for a vegetation-soil combination. The model is applied to data measured during the EAGLE2006 campaign at the Speulder forest in the Netherlands between 16 and 20 June 2006. The model satisfactorily calculates the diurnal cycle of latent and sensible heat and carbon dioxide fluxes, vegetation and soil temperatures and reflected and emitted radiation. Modelled soil heat flux is higher than measured (Figs. 103-104). In the future, the model can be used to improve estimates of fluxes by means of parameter retrieval via model inversion.

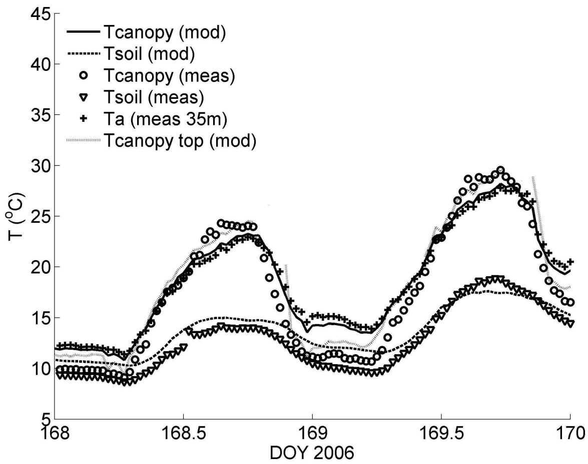

Figure 103. Modelled and measured mean canopy and soil temperature, measured air temperature at 35 m height and modelled temperature of the upper needle layer for 17 and 18 June 2006

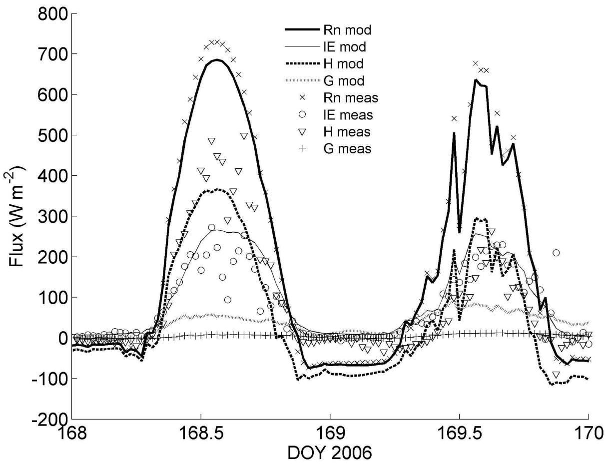

Figure 104. Modelled and measured energy fluxes of the canopy and soil together: net radiation (R_n), latent heat (*LE*), sensible heat (*H*) and soil heat (*G*) for 17 and 18 June 2006

Conclusion and/or recommendation

An extensive data set is available for micro-meteorological studies of surface exchange processes over a forest, and for calibration of and comparison with remote sensing products.

Although measuring the energy balance of a forest is inherently difficult, the large energy balance closure error in the measurements is unsatisfactory. For continuous measurements at the Speulder forest we recommend to duplicate radiation measurements, preferably with sensors of different manufacturers. Eddy covariance and large aperture scintillometer estimates of sensible heat flux correlate well. It would be preferable to measure eddy correlation fluxes at two different heights to evaluate the effect of the footprint. This can help explain the large energy balance closure error. It is also recommended that soil heat flux is estimated using measurements of soil temperature profiles and soil thermal properties.

Eddy covariance measurements are valuable to estimate surface roughness. They have the potential to be explored further. For the future it is recommended to measure wind speed at more heights, and use a second eddy covariance system lower above the canopy to estimate whether friction velocity changes with height. The data can be combined with estimates of the vertical distribution of needles and branches, based on a laser scans carried out during the EAGLE2006 campaign.

Contact temperatures are valuable measurements to test micrometeorological models which discriminate between soil and layers in the vegetation. They can help to study the relationship between actual surface temperatures and brightness temperature of the vegetation. A combined radiative transfer- energy balance model has been developed and applied to the data. The model reproduced measured surface temperatures and sensible and latent heat fluxes satisfactorily. Model inversion is required to study how much information about the fluxes can be extracted from brightness temperature measurements.

10.3.4 BRDF's acquired by directional radiative measurements

Team responsible: Joris Timmermans

Team members: Joris Timmermans, C. van der Tol, K. Weligepolage, L. Jia, Z. Su
E-mail: ***j_timmermans@itc.nl***

Overview

The understanding of bio-geophysical parameters of vegetated surfaces, like forest and grassland, is essential in the development of Earth system models for the prediction of global change. The potential of multi-directional observations for bio-geophysical retrieval algorithms is very high. The lack of appropriate observations restricts development of these algorithms. The objective of this research is to acquire and assess the directional radiative measurements over different types of vegetation. Two methods were used to acquire directional measurements: for low vegetation a goniometric setup was used, for high vegetation a tower setup was used. A goniometric setup measures from different directions the same area, the tower setup measures for different angles different areas. The measured radiation is used to calculate the BRDFs and directional temperatures. In the period from 10 June - 18 June 2006 directional radiative measurements were performed at two sites in the Netherlands: Speulderbos (forest), Cabauw (grassland and maize). The sensors covered the spectrum from the optical to the thermal domain. Concurrently to the radiative directional measurements contact temperature measurements were performed. The contact and radiative measurements are used to calculate the BRDFs or directional temperatures. This contribution describes the measurements and calculation of the BRDFs over the different crops during the Eagle 2006 fieldcampaign. Optical BRDFs have been acquired for grassland, maize and forest. Thermal angular signatures are acquired for grassland and maize.

Input data used

Directional measurements were performed using a goniometric setup and a tower setup. A goniometric setup is able to perform hemispherical measurements of the same target. A tower setup measures for different angles different targets. As the forest was homogeneous the error created by this is small.
The ASD and GER hyperspectral spectrometers were used to perform radiative measurements in the spectral range of 400 nm – 2500 nm. The Everest 3000 Radiometer and the Irisys 1011 thermal imager were used to perform radiative measurements in the spectral range of 8 μm – 12 μm.

Processing and/or analysis done

The most stable spectrum acquired over the several VNIR measurements for a single angle was used. The BRDF is produced from the splice corrected spectrum.
As for thermal radiative measurements no unique BRDF can be created, the thermal directional signature is created from the measurements. The post-processing of the data dealt with the directional behaviour of the acquired BRDFs and thermal signatures.
A normalized reflectance ratio is introduced to emphasize the directional behaviour of the measured reflectances.

$$Ratio = \frac{R_{\theta} - R_{nadir}}{R_{\theta} + R_{nadir}}$$

The standard deviation of this ratio per angle gives us a single parameter describing the directional behaviour of the BRDFs.

For the thermal images, the ratio of the standard deviation of the temperatures and the mean temperatures are used to acquire a single parameter for the directional behaviour. In the calculation of this thermal directional behaviour of the radiometer the measured values are used without processing. In the calculation of this thermal directional behaviour of the thermal imager the average temperatures per image are used.

Also the standard deviation of the temperature per image is used to derive a separation parameter. This separation parameter is used to give an indication if further processing to retrieve the canopy component temperatures would be successful.

Results/Output description

Final output only contains the BRDFs and the thermal signatures. In Table 46 the maximum standard deviation of the reflectance ratio is shown and in Table 47 the thermal directional signatures and the separation parameter of all the measured vegetation is given.

Table 46. Maximum standard deviation of the reflectance ratio per view angle.

Vegetation	Max(STD) VIS	max(STD) NIR	max(STD) MWIR
Forest	9.18	10.79	14.53
Pine tree	9.17	09.22	09.54
Grass (tall)	20.98	09.76	16.56
Young Corn	13.63	12.29	11.58

Table 47. Thermal directional signatures and component temperature separation parameter.

	Directional signatures		Separation parameter
Vegetation	Everest	Irisys	Irisys
Grass (tall)	97.0	48.7	04.17
Young Corn	179.0	69.6	09.30

Conclusion and/or recommendation

The tall grass displays the largest directional behaviour in the VIS and MWIR regions, young corn displays the largest directional behaviour in the NIR region. The overall directionality of the forest in the complete VNIR region seems low. This is because of the smoothing effect of the large FOV under low viewing angles.
Comparison between the directional signatures of the Everest measurements and the Irisys measurement show similar behaviour. With both instruments young corn shows the largest directional behaviour. The standard deviation of the temperatures per

image is highest at young corn. This implies that the component temperatures can be retrieved from the image in a later stadium.

10.3.5 Soil moisture field observations over the Cabauw grassland

Team responsible: Fouad Khaier

Team members: Jeniffer Kinoti Mutiga, Ali Abkar, Rahul Kanwar, Remco Dost, Mary Chiluba, Mustafa Gokmen, Meseret Teka Hunde, George Ndhlovu, Mayson Saila, Hosea Sanga, Madi Sarr, Gabriel Parodi

Overview

An extensive set of ground-based measurements is carried out in the framework of the EAGLE2006 Campaign. Field observations were performed with basically two objectives in mind. First of all they were used as radiometric reference measurements of different surface types for calibration and validation of remotely sensed air-borne and space-borne observations and as such they were performed simultaneously to the image acquisitions. Secondly, the field observations were carried out for the retrieval of bio-geophysical parameters. Depending on surface type and surface characteristic the measurements took place from towers or on the ground. Soil moisture was measured in the field for calibration and validation of soil moisture measurements through remotely sensed data, which have been acquired during the campaign. The measurements were carried out at the Cabauw grassland site and took place during the entire day on 8, 12, 13, 14, and 15th of June 2006. Basically two different measurement techniques were employed. The Hydra Probe (Stevens Water Monitoring Systems Inc.) performs high frequency electrical measurements which are directly related to simultaneous measurement of soil moisture. Hydra Probe provides output of data in water fraction by volume. More information on this device is available on: http://www.stevenswater.com/catalog/ In addition gravimetric measurements were done by taking soil samples by augering in soil rings. Then, the samples were taken to the laboratory to carry out the measurements. In the laboratory, soil moisture was first measured gravimetrically by weighing the wet volume of soil, oven drying at 105 ºC, and then re-weighing. The difference in mass corresponds to the mass of water then gravimetric water content of the soil can be determined. Using known soil bulk density, volumetric water can also be determined. The points of measurements were distributed in the four fields and marked with numbered sticks to repeat the measurements in the same position every time. The exact locations of the points were taken via the GPS station so as to reference them to the satellite images and airborne data. Sampling took place once a day, where the approximate distance between the points was 20-30 meters. The sampling was carried out at two depths; one at 5 cm and another one at 10 cm depth. There is no need for processing the soil moisture measurements from the hydra probe, since they are straight forward and ready to use. The gravimetric method needs some laboratory work which already has been done and the results are ready to use for calibrating the image data.

Input data used

Soil moisture field measurements.

Processing and/or analysis done

There is no need for processing the soil moisture measurements from the hydra probe, since they are straight forward and ready to use. However the gravimetric method needs some laboratory work which already has been done and the results are ready to use for calibrating the image data.

Results/Output description

An extensive set of ground-based measurements in Cabauw grassland site:

- In four fields
- At two depths 5 and 10 cm
- For five days: 8, 12, 13, 14 and 15 June 2006

A sample of the database (Table 48) and an example of a soil moisture map are given (Fig. 105).

Table 48. Sample of the database

				8_06_2006 by Jeniffer, Ali and Fouad					12_06_2006 by Jeniffer, Rahul and Fo				
ID	X	Y	Z	Time	sm1	sm2	T1	T2	Time	sm1	sm2	T1	T
A01	123288.478	442585.850	-0.889	0.12	0.34	0.38	30.30	30.20	11.25	0.23	0.31	25.00	26.
A02	123280.017	442605.950	-1.003	0.13	0.30	0.40	27.50	28.60	11.33	0.34	0.38	27.00	27.
A03	123271.494	442630.795	-0.929		0.36	0.39	26.70	27.20	11.37	0.33	0.37	27.40	28.
A04	123265.523	442658.237	-0.904	0.14	0.40	0.47	27.20	27.50	11.44	0.38	0.42	25.00	28.
A05	123238.075	442655.804	-0.967	0.15	0.45	0.50	26.30	26.70	11.47	0.37	0.39	28.00	28.
A06	123223.743	442647.376	-0.986	0.15	0.43	1.00	26.40	26.90	11.52	0.41	0.46	28.30	28.
A07	123202.754	442639.054	-0.918	0.16	0.42	1.00	27.50	28.20	11.57	0.38	0.44	28.50	29.
A08	123190.811	442658.157	-0.826	0.16	0.26	0.35	28.80	29.00	12.01	0.22	0.27	29.00	29.
A09	123184.265	442679.747	-0.796		0.29	0.24	29.90	30.00	12.07	0.24	0.37	29.00	29.
A10	123172.748	442702.516	-0.845		0.43	0.44	29.00	29.20	12.14	0.40	0.41	28.60	28.
A11	123168.223	442705.765	-0.795		0.41	0.46	27.80	28.40					
A12	123150.809	442747.501	-0.871		0.34	0.34	28.00	28.80	12.24	0.23	0.32	27.00	27.
A13	123169.935	442749.756	-0.782		0.37	0.40	29.10	29.30	12.30	0.32	0.34	27.70	28.
A14	123188.360	442763.050			0.38	0.39	28.90	29.00					
A15	123214.530	442766.280			0.37	0.37	28.00	28.80					
A16	123222.590	442743.980		0.71	0.35	0.43	28.80	28.60					
A17	123234.090	442720.420		0.71	0.39	0.44	28.00	28.10					
A18	123244.270	442700.570		0.71	0.45	0.50	27.00	27.20					
A19	123270.360	442691.440		0.71	0.67	0.89	26.90	27.60					
A20	123296.500	442689.120		0.72	0.52	1.00	27.60	28.01					
B01	123207.700	442622.822	-0.873						1.03	0.21	0.29	27.70	28.
B02	123225.081	442583.369	-0.879						1.08	0.18	0.30	28.50	29.
B03	123240.309	442550.404	-0.863						1.12	0.25	0.30	29.50	29.
B04	123257.037	442507.075	-0.790						1.17	0.27	0.29	28.90	29.

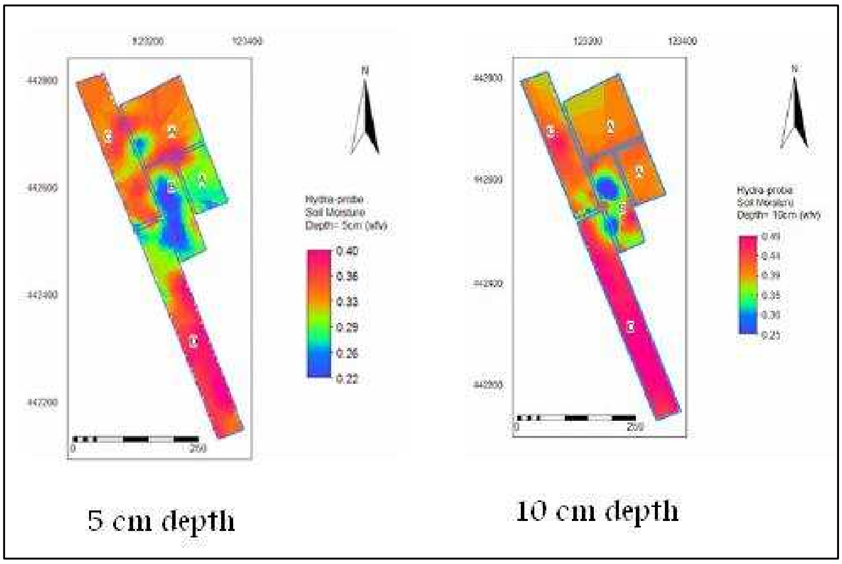

Figure 105. Soil moisture map

10.3.6 A Technique for validating remote sensing products of water quality

Team responsible: Suhyb Salama

Team members: Suhyb Salama: Processing, analysis, correction, atmosphere/water radiative transfer simulations, uncertainty analysis, twins' experiments, non linear fitting and retrievals of water quality parameters.
Wouter Verhoef: atmospheric radiative transfer simulation for Sentinel-2.
Joris Timmermans: Sentinel-2 simulation for inland waters based on water leaving reflectance.
Zoltan Vekerdy: supplied the raw in-situ measurements and some comments.

Overview

Remote sensing of water quality is initiated as an additional part of the on going activities of the EAGLE2006 project. Within this context intensive in-situ and airborne measurement campaigns were carried out over the Wolderwijd and the Veluwemeer (in the neighbourhood of Harderwijk) natural waters. However, in-situ measurements and image acquisitions were not simultaneous. This poses some constraints on validating air/space-borne remote sensing products of water quality. Nevertheless, the detailed in-situ measurements and hydro-optical model simulations provide a bench mark for validating remote sensing products. That is realized through developing a stochastic technique to quantify the uncertainties on the retrieved aquatic inherent optical properties (IOP). The output of the proposed technique is applied to validate remote sensing products of water quality. In this processing phase, simulations of the radiative transfer in the coupled atmosphere-water system are performed to generate spectra at-sensor-level. The upper and the lower boundaries of perturbations, around each recorded spectrum, are then modelled as function of residuals between simulated and measured spectra. The perturbations are parameterized as a function of model approximations/inversion, sensor-noise and atmospheric residual signal. All error sources are treated as being of stochastic nature. Three scenarios are considered: spectrally correlated (i.e. wavelength dependent) perturbations, spectrally uncorrelated perturbations and a mixed scenario of the previous two with equal probability of occurrence. Uncertainties on the retrieved IOP are quantified with the relative contribution of each perturbation component to the total error budget of the IOP. This technique can be used to validate earth observation products of water quality in remote areas where few or no in–situ measurements are available.

Input data used

Field measurements of water leaving reflectance, turbidity and Chlorophyll-a of the Wolderwijd and Veluwemeer (52º19'12.0"N, 05º36'12.0"E.) natural waters were available from EALGE2006 campaign for the 4th of July 2006. This filed campaign was also associated with hyperspectral airborne measurements form the Airborne Hyperspectral Spectrometer (AHS). MEdium Resolution Imaging Spectrometer (MERIS) and Advanced Space borne Thermal Emission and Reflection Radiometer (ASTER) observations were also available during the EAGLE2006 campaign. For more details on EO data availabilities and specifications the reader is encouraged to consult the EAGLE2006 data acquisition report,. Table 49 summarized the used dataset in this work.

Table 49. Summary of the subset from Eagle2006 dataset used in this study.

Acquisition	Sensor	Description	Date
Space borne	MERIS	MER-FR-PNEPA20060608_101603_000000502048_00237_22335_1597.N1	08-06-2006
	ASTER	AST_L1B_00306082006104429_20060706063029_30252.hdf	08-06-2006
Airborne	AHS	AHS_060613 level L1b	13-06-2006
Field measurements	ASD	9 Spectra: corrected for sky reflectance using the NIR spectrum	04-07-2006

Processing and/or analysis done

Available images are geo-referenced, corrected for smile effects and converted to top of atmosphere reflectance. Atmospheric path correction is then preformed using radiative transfer computation. Gaseous transmittances of ozone, oxygen, carbon dioxide, methane and nitrous oxide are assumed constant over a sub region of all images. Two aerosol models with 40 km visibility are used, namely maritime aerosol for MERIS and urban aerosol for AHS and ASTER. The adjacency effects from the surrounding lands is accounted for in the computation.

Non-linear fitting is used for simultaneous retrieval of the water IOP. This method is applied on MERIS and AHS spectra. The spectral characteristics of ASTER constrain the application of such non-linear fit method. Instead, matrix inversion method is applied on ASTER’s two visible bands. In consequence only two variables were retrieved form ASTER image.

An inter-comparison between retrieved values of SPM backscattering and Chl-a and DOM absorptions are performed for two cross sections over the Veluwemeer (start {52.38307, 5.63710}, end {52.3681, 5.65516}) and the Wolderwijd (start {52.34515, 5.60731}, end {52.3579, 5.59198}).

Results/Output description

In situ remote sensing measurements: In-situ measurements are fitted to model’s predictions (Fig. 106a). Stochastic formulation is developed to estimate the relative contribution of each fluctuation component to the total uncertainties on the retrieved IOP (Fig. 106b).

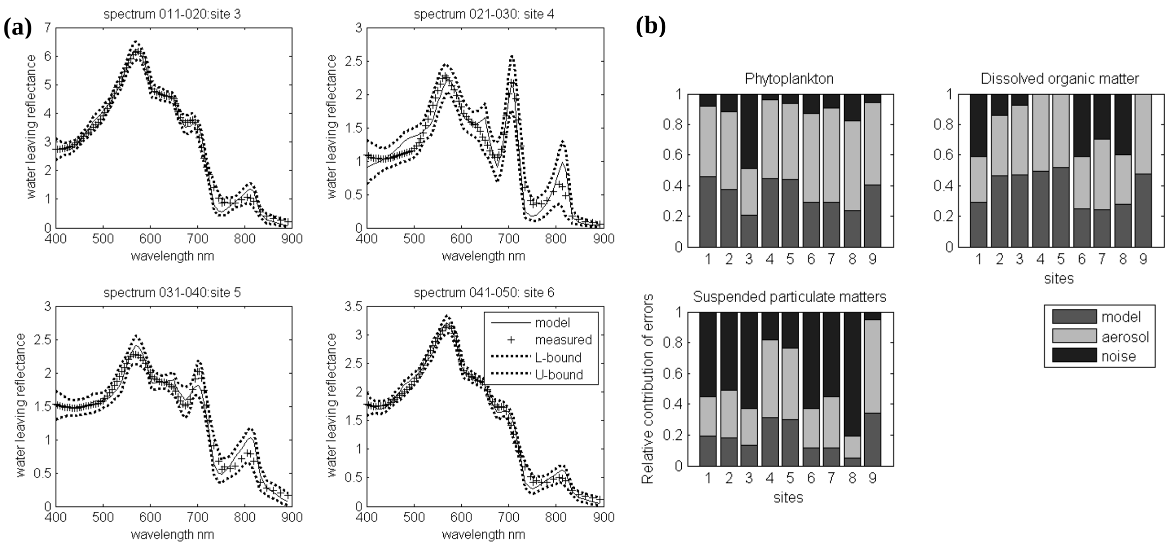

Figure 106. (a) Modeled versus ASD water leaving reflectance with 99% of confidence with upper bound (U-) and lower bound (L-); (b) The relative contribution of the different errors to the total uncertainties on the IOP.

AHS

A subset of the original image is processed - Spectral subset for the VIS bands (400nm –900nm); spatial subset for the water targets.

AHS image is geo-referenced using automatic image registration with supplied level L1C images. The image is then atmospherically corrected using 6S. Image spectra are then inverted using non-linear least squares fit technique. The results are water inherent optical properties and the associated uncertainties expressed as the standard deviation at 95% of confidence (see Fig. 107).

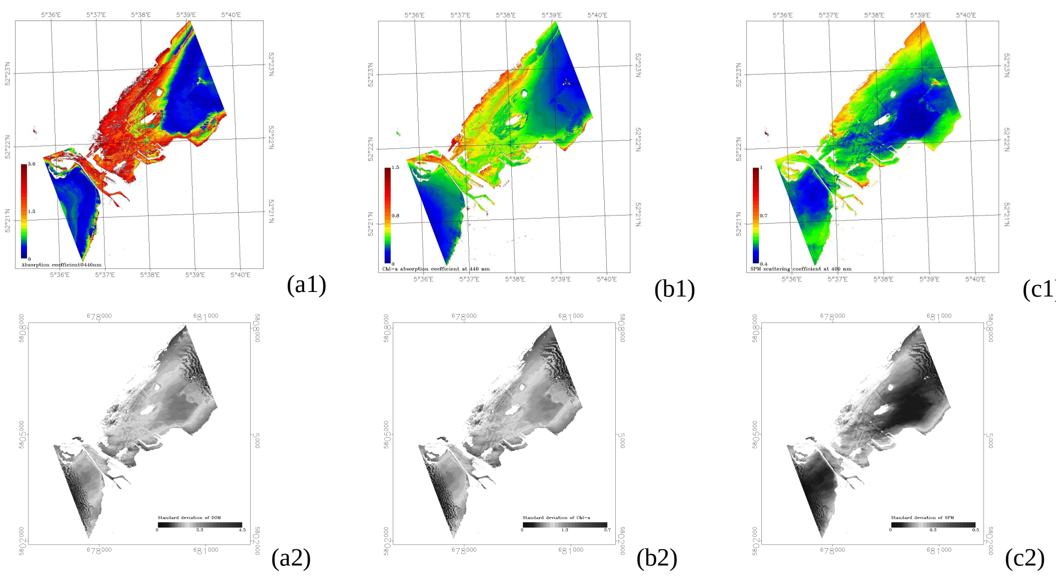

Figure 107. Upper panel shows the retrieved IOP from AHS (a1: DOM, b1: Chl-a and c1: SPM); the associated uncertainty maps are shown in the lower panel.

ASTER

The image is georeferenced using standard ASTER-module in ENVI 4.3. ASTER image is atmospherically corrected using MODTRAN 4.0. Urban model with initial visibility of 40 km was used in the simulation. The absorption coefficient of dissolved organic matter is set to a constant value of 0.25 m-1. The IOP are estimated using singular value decomposition of ASETR's two bands 556 nm and 661nm (Fig. 108).

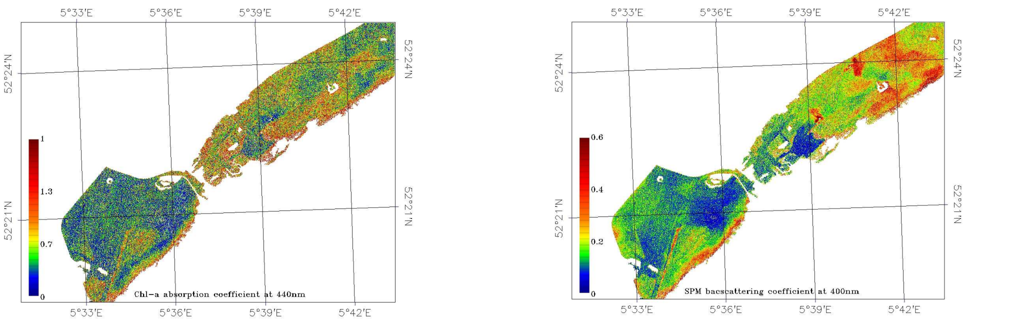

(a) (b)

Figure 108. IOP retrieved from ASTER image: (a) Absorption coefficients of chlorophyll-a at 440nm; (b) Backscattering coefficient of SPM at 400nm

MERIS

The image is georeferenced, corrected for smile effects and converted to TOA reflectance using standard MERIS-modules in Beam 4.1. The image is atmospherically corrected using 6S and maritime model with initial visibility of 40 km. Gradient-expansion algorithm is employed to compute a non-linear least squares fit between MERIS spectra and model simulated spectra. Poisson weighting was used during the fitting (Fig. 109).

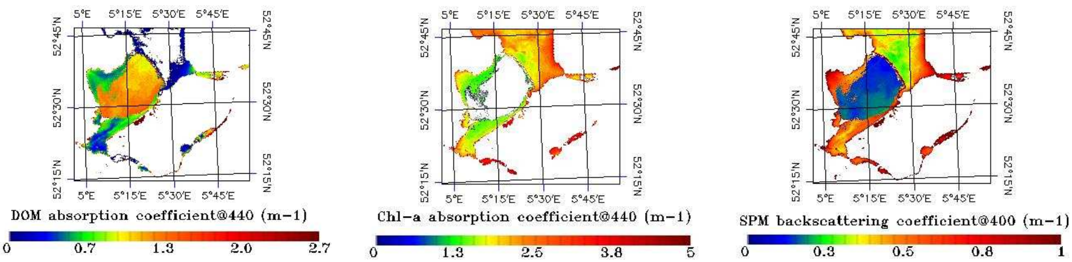

(a) (b) (c)

Figure 109. Retrieved water quality parameters from a subset of MERIS. (a) DOM absorption coefficient at 440nm, (b) Chl-a absorption coefficient at 440nm, (c) SPM backscattering coefficient at 400nm

New approach is suggested to improve the atmospheric correction of MERIS using NIR band and priori knowledge about SPM backscattering. The results are shown in Fig. 110.

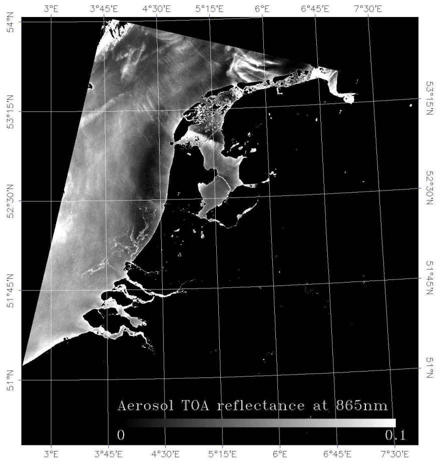

(a)

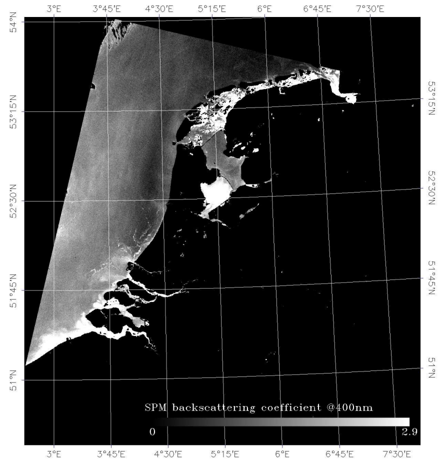

(b)

Figure 110. The results of a new algorithm for simultaneous retrieval of (a) atmospheric reflectance at 865nm and (b) SPM backscattering ate 400nm.

Conclusion and/or recommendation

The inversion might fail in predicting the blue and the red absorption bands of DOM and chlorophyll-a. This is because the spectral slope of the DOM was assumed constant. The variation of the chlorophyll-a absorption coefficient with phytoplankton species is not considered in this study.
Moreover the inversion will only be able to separate the absorption of chlorophyll-a from that of DOM at the blue and the red bands (centered at 440nm and 675 nm respectively). Fluctuation in these two bands, will therefore, result in degenerated concentrations of chlorophyll-a and DOM. On the other hand the resulting concentrations of SPM are expected to be biased proportional to the residuals at the NIR.

Erroneous estimation of aerosol optical thickness and model inversion are the major source of errors. They contribute about 55% for SPM to 86% for DOM to the total error. While noise contribution ranges from 14% for Dom to 43% for SPM. These observations are valid for the adapted inversion technique, non absorbing aerosol and the used noise spectral variation.

ASTER results are very patchy and their values are generally higher than those retrieved from MERIS and AHS.
There is a very good match between MERIS and AHS retrieved values of SPM backscattering and Chl-a absorption. Retrieved values of DOM absorptions coefficient from MERIS and AHS have large discrepancy. This can be attributed to the absence of the green absorption band from AHS spectra band and imperfect atmospheric correction. These two factors can contribute up to 86% of errors in the retrieved value of DOM.
Uncertainty maps are simultaneously estimated for each retrieved IOP. This information forms a benchmark for validation and fusion of remote sensing products of water quality parameters.

11 Conclusions and Recommendations

The EAGLE2006 campaign was initially conceived as a combination of activities to cover several objectives and as such, the objectives of the EAGLE2006 Campaign were closely related to the objectives of other ESA campaigns (SPARC2004, SEN2FLEX2005 and especially AGRISAR2006), being: (a) to build up a database for the investigation and validation of bio-geophysical parameters obtained from different radar frequencies (X-, C-, and L-band) and at hyperspectral optical and thermal bands over vegetated natural areas, (b) development and validation of models and inversion algorithms for quantitative surface parameter estimation and process studies in forests and grasslands, (c) to simulate Sentinel-1 and Sentinel-2 image data and image products over the land (forest and grassland) in order to help in the definition of requirements and performances for the GMES/Sentinel-1 and -2 missions and (d) to derive useful indicators and tools to be used to monitor land-atmosphere (turbulent) flux exchanges. In addition to these main objectives, the EAGLE2006 campaign also considered the validation of satellite data and derived products, particularly from MERIS and ASTER. This chapter summarizes the main derived conclusions and provides recommendations for future activities, both for future campaigns and for the proper exploitation of the large amount of dada collected in the EAGLE2006 campaign.

Planning a campaign with several objectives and different elements is always a difficult task. However, such multi-objective activity has the advantage of optimization of the available resources to get a maximum profit from the combination of activities by different teams with varying background and expertise. In this respect, the EAGLE2006 “opportunity” campaign is a good example of how different objectives from different projects can be realized. The results obtained for the main components of the EAGLE2006 activities can be considered rather complete, and the overall activity has been quite a success. However, the main task remains now to fully exploit the available dataset (and also those from SPARC2004, SEN2FLEX2005 and especially AGRISAR2006), with many perspectives for future exploitation of the data collected in this campaign. The dataset provides in-situ data for calibration and validation of airborne and spaceborne sensor observations, input parameters and validation data for modelling activities from multi-directional soil/canopy reflectance and emittance studies, land surface processes and land-atmosphere interactions including energy, water and carbon fluxes, ecological models and water quality models. This unique dataset covers a wide spectral range from visible to microwave domain and a wide range of bio-geophysical parameters and processes over different landscapes – grassland, agricultural land, forest, desert, water and atmosphere. A key issue is to keep the data properly archived to allow the use by external researchers not involved in the campaign. A review of main results and conclusions, together with some recommendations for future activities, is given below.

11.1 EAGLE2006 Campaign Conclusions

A unique dataset has been acquired, including (quasi)simultaneous SAR and optical (hyperspectral, visible and thermal) and atmospheric turbulence airborne datasets as well as ground measurements. Atmospheric data from different ground based sensors has been gathered in combination with in-situ atmospheric soundings to characterize the atmospheric conditions during airborne and satellite acquisitions. The SAR data are of high quality at different frequencies (with relevance to Sentinel-1 simulation) and the optical data are of high quality as well (for Sentinel-2 simulation). In addition, the turbulence acquisitions and ground data are of also good quality.

Analysis showed a high potential of the data for use in further studies as well as a high potential for new product development. With respect to SAR, a combination of L- and C-band is preferred for classification purposes and the optical CASI and AHS system specifications are all together optimal for bio-physical parameter retrieval. With respect to the atmosphere, validation and sensitivity of water and heat (energy) balance has been performed, where thermal data has been found an essential input to the models.

11.2 EAGLE2006 Campaign Recommendations

With respect to potential products for the Sentinel-1 and Sentinel-2 missions, land cover classification maps currently can be considered as in a pre-operational phase. For soil moisture maps, surface roughness, biomass, fractional vegetation cover and LAI products, the algorithm are in an experimental stage, whereas maps of actual evapotranspiration can be considered as a potential level 3 experimental product as well (providing the thermal input).

Furthermore, we have observed the need for a continuous agricultural data acquisition to cover a bigger variability. With respect to that, a higher crop diversity and variability in surface conditions is needed for future field campaigns. In addition, multi-temporal, as well as simultaneous observations with both SAR and optical sensors are desirable.

With respect to ground observations, a higher data acquisition frequency might be needed, in combination with the need for investigation of the separation between bio-physiological (vegetation growth) and natural (wind, rain) effects.

All in all, the strongly multi-disciplinary character of the EAGLE2006 field campaign is considered a very strong aspect. Hence, an intensive analysis by the (very) different teams, and external users, with the collected data should be supported.

12 EAGLE 2006 Database

All data as acquired in and during the EAGLE2006 Field Campaign are available via the Field Campaign ftp site (ftp.itc.nl/pub/eagle06/EAGLE2006 Database/), where access is acquired through a username and password.

The structure of the database is along the lines of the structure of this report, that is:

1. General
   1.1. Data
      1.1.1. Topographic data
      1.1.2. DEM (AHN)
      1.1.3. National data
   1.2. Documents
2. Space-borne data
   2.1. MERIS
   2.2. MODIS
   2.3. AATSR
   2.4. ASTER
   2.5. ASAR
   2.6. SEVIRI
3. Air-borne data
   3.1. AHS-INTA
   3.2. CASI-ITRES
   3.3. ESAR-DLR
   3.4. ISAFoM-SkyeArrow
4. Atmospheric data
   4.1. CESAR data
   4.2. In-situ data
5. Ground-based data
   5.1. Ground radiometric data
      5.1.1. Solar range data
      5.1.2. Thermal range data
   5.2. Surface Energy Budget data
      5.2.1. Micro-meteorological data
      5.2.2. Goniometric data
   5.3. Ground Bio-physical data
      5.3.1. Biomass data
      5.3.2. PAR data
      5.3.3. Soil moisture data
      5.3.4. Water data
      5.3.5. LAI data
      5.3.6. Roughness data
      5.3.7. Emissivity data
      5.3.8. Laser scan data
      5.3.9. DGPS data
   5.4. Reference meteorological
      5.4.1. Cabauw-KNMI data
      5.4.2. Loobos-ALTERRA data
6. Data analysis and Results
   6.1. Simulation products
      6.1.1. Sentinel-1
      6.1.2. Sentinel-2
   6.2. Biophysical products
   6.3. Advanced products
      6.3.1. Net ecosystem exchange and footprint analysis above forest and grassland
      6.3.2. Temperature and emissivity form AHS data
      6.3.3. Modeling fluxes of energy, water and carbon dioxide above the Speulderbos
      6.3.4. MBRDF’s acquired by directional radiative measurements
      6.3.5. Soil moisture field observations over the Cabauw grassland
      6.3.6. Technique for validating remote sensing products of water quality

13 References

Anderson M. C. (1964) Studies of the woodland light climate I. The photographic computation of light conditions. Journal of Ecology 52, 27-41.

Anderson M. C. (1981) The geometry of leaf distributions in some south-eastern Australian forests. Agricultural Meteorology 25, 195 - 205.
ASD-Inc. (2002) Analytical Spectral Devices. FieldSpec Pro User's Guide. Boulder, USA, 148.

Beljaars A. C. M. & Bosveld F. C. (1997) Cabauw data for the validation of land surface parametrization schemes. Journal of Climate 10, 1172 - 1193

Bonhomme R. & Chartier P. (1972) The interpretation and automatic measurement of hemisperical photographs to obtain sunlit foliage area and gap frequency. Israel Journal of Agricultural Research 22, 53 - 61.

Coll C., Caselles V., Valor E. & Rubio E. (2003) Validation of temperature-emissivity separation and split-window methods from TIMS data and ground measurements. Remote Sensing Environment 85, 232-242.

Dana R. W. (1969) Measurement of 8-14 micron emissivity of igneous rocks and mineral surfaces. NASA Science Report NSG-632. Goddard Space Flight Center, Greenbelt, MD, USA.

Domínguez Barroso A., Amaro Cormenzana A., de Miguel Llanes, E., (2005) Perfil de metadatos del Servicio de Teledetección de INTA. XI Congreso Nacional de Teledetección; Tenerife.

Esposito M., Magliulo V. & Menenti M. (2007) CNR ISAFoM Data Acquisition Report Missions on 13th and 14th of June 2006 over Speulderbos, Loobos and Cabauw. ERALab CNR ISAFoM Instituto per i sistemi Agricoli e Forestali del Mediterraneo, January 2007, S. Sebastiano al Ves.

Fernández-Renau, A.; Gómez, J. A.; de Miguel, E. (2005) The INTA AHS system. Sensors, Systems, and Next-Generation Satellites IX. Edited by Meynart, Roland; Neeck, Steven P.; Shimoda, Haruhisa. Proceedings of the SPIE, Volume 5978, pp. 471-478.

Gillespie, A., S. Rokugawa, T. Matsunaga, J. S. Cothern, S. Hook, and A. B. Kahle, (1998)A temperature and emissivity separation algorithm for advanced spaceborne thermal emission and reflection radiometer (ASTER) images," IEEE Transactions on Geoscience and Remote Sensing, vol. 36, pp. 1113-1126.

Hajnsek, I. et al., (2008) "AGRISAR 2007- Airborne SAR and Optics Campaigns for an improved monitoring of agricultural process and practices". In AgriSAR/EAGEL2006 proceedings.

Jager C. J., Nakken T. C. & Palland C. L. (1976) Bodemkundig onderzoek van twee graslandpercelen nabij Cabauw (In Dutch). N.V.Heidemaatschappij beheer, Arnhem.

Martimort. P., (2008) Sentinel-2 Overview. In AgriSAR/EAGEL2006 proceedings.

Moncrieff J. B., Masshedera J. M., Bruin H. d., Elbers J., Friborg T., Heusinkveld B., Kabat P., Scott S., Soegaard H. & Verhoef A. (1997) A system to measure surface fluxes of momentum, sensible heat, water vapour and carbon dioxide. Journal of Hydrology 188-189, 589-611.

Richter R., and Schläpfer D., (2002) Geo-atmospheric processing of airborne imaging spectrometry data. Part 2: Atmospheric/Topographic Correction. International Journal of Remote Sensing, 23(13):2631-2649.

Rubio E., Caselles V. & Badenas C. (1997) Emissivity measurements of several soils and vegetation types in the 8-14 min waveband: Analysis of two field methods. Remote Sensing Environment 59, 490-521.

Saugier B. & Ripley E. A. (1978) Evaluation of the aerodynamic methid of determining fluxes over natural grassland. Quarterly Journal Royal Meteorological Society 104, 257 - 270.

Schläpfer D. and Richter R., (2002) Geo-atmospheric Processing of Airborne Imaging Spectrometry Data Part 1: Parametric Orthorectification. International Journal of Remote Sensing, 23(13):2609-2630.

Sluiter R. J., Kwast H. V. d. & Santen P. V. (2007) NESCAFE - Near Sensing Camera Field Equipment for high resolution, quantitative assessment of field variables. (In Prep.).

Steege ter H. (1996) WINPHOT. Nationaal Herbarium Nederland.
Ulden A. P. V. & Wieringa J. (1996) Atmospheric boundary layer research at Cabauw. Boundary-Layer Meteorology 78, 39-69.

Su, Z., et al., 2008, EAGLE 2006 – Multi-purpose, multi-angle and multi-sensor in-situ and airborne campaigns over grassland and forest. In AgriSAR/EAGEL2006 proceedings.

Wösten J. H. M., Veerman G. J. & Stolte J. (1994) Waterretentie- en doorlatendheidskarakteristieken van boven- en ondergronden in Nederland (In Dutch). Staringreeks. Vernieuwde uitgave 1994. Technisch Document 18, Wageningen.

Zanoni, V. et al, (2002) Remote Sensing requirements development: a simulation-based approach. ISPRS Commission I Symposium. Denver, November 2002.